UNIVERSITY OF CAPE TOWN
IYUNIVESITHI YASEKAPA • UNIVERSITEIT VAN KAAPSTAD

EXAMINATION OF FLEXURAL CRACK WIDTH PREDICTION IN CONCRETE: COMPARISON OF ANALYTICAL AND NUMERICAL MODELS

By

Brandon Fredericks

FRDBRA002

Thesis presented for the degree:

Masters in Engineering (Structural Engineering and Materials)

In the Department of Civil Engineering

Faculty of Engineering and the Built Environment

Date of submission: February 2019

"I know the meaning of plagiarism and declare that all the work in the document, save for that which is properly acknowledged, is my own. This thesis/dissertation has been submitted to the Turnitin module and I confirm that my supervisor has seen my report and any concerns revealed by such have been resolved with my supervisor."

Signed by candidate

Signature: ……

Date: 26/02/2019……

Abstract

The reliability of crack prediction methods in concrete design plays a role in the degree of confidence with which durability can be ensured. Bond failure between concrete and the embedded reinforcing steel exposes the steel surface within a crack path. This relative slip results from differential tensile strain between concrete and steel that allows harmful ions to reach and then react along the rebar length. A reliable prediction method should therefore account for the loss of bond in crack propagation.

Researchers question the significance of the role played by surface cracks in structural deterioration, therefore casting doubt on the need for exhaustive crack analysis. The applicable fundamental theory of cracking, namely non-slip or slip determines the steel exposure and therefore the likelihood of reduced structural service life attributable to crack behaviour. However, while cracks originate at the surface of reinforcement through bond failure, simultaneously a cover distance away no cracks could appear on the concrete tension surface or they could be twice to ten times the crack width at the rebar level. Due to the heterogeneous composition of concrete, some commentaries state it impossible to accurately predict crack widths. Design standards therefore provide estimates of maximum crack widths to a degree of probability.

This study examines the methods available for predicting cracks on the tension surface and the degree to which this is indicative of weakened bond between concrete and reinforcement. In this examination, it will be seen that concrete has ductility due to tension softening behaviour. The addition of steel to the tension area transforms the fracture process zone problem to the definition of a bond-slip relationship. Bond stresses generated at the rebar perimeter define the analytical relationships in design codes. These stresses control crack width at the tension surface.

Results from the analytical code-based models are compared for increasing section depths, bar sizes and maximum spacings in the tension zone. A significant variation in the predicted maximum crack width is observed for deeper members. For very large concrete sections, the analytical models appear to provide unreasonable crack width values.

The analytical equations in design codes focus on the bond relationship and ignore the size effect of concrete inherent in its microstructure. The concentration of flaws increases in larger members; hence size effect would play a greater role. Numerical modelling for crack prediction is therefore recommended for crack analysis in larger concrete members.

TABLE OF CONTENTS

TABLE OF FIGURES

1. INTRODUCTION

It is well documented in literature by Alexander, Ballim and Beushausen (Owens & Fulton, 2009) that the movement of aggressive ions and molecules into the microstructure of concrete is related to its penetrability. Penetrability is the degree to which concrete allows gases, liquids and ions to move through its pore structure and is quantified in terms of the transport parameters. The formation of cracks modifies these parameters.

Properties such as crack width, shape, frequency and degree of connectivity as well as the origin dictate the characteristics of macroscopic transport in concrete members. Mehta & Monteiro, in their review on the microstructure of concrete (Mehta & Monteiro, 2014), states the primary consideration in design, when deformation is considered, is the extent to which the applied stresses will cause detrimental crack behaviour.

Crack analysis is important in the evaluation of overall damage and corrosion resistance of reinforced concrete structures, significantly influencing aspects of strength, stiffness and durability (Xu, et al., 2017). Durability considerations address the potential for reduced service life in a structure due to steel corrosion (Borosnyoi & Snobli, 2010).

Concrete will crack in areas where the accumulation of tension stresses is greater than its tensile strength. When tensile capacity is exceeded, localised fracture damage results, i.e. cracking. Fracture begins locally and spreads to the rest of the matrix under sustained applied stress. The stress can originate from direct and indirect actions. Indirect actions include imposed deformation (differential settlement, shrinkage and swelling) and restrained movement (thermal movements). The effect of indirect actions is evaluated by the serviceability limit states. Direct actions form stresses under the action of applied forces. The effect of direct actions is evaluated first by the ultimate limit states, linked to failure, then by serviceability.

The hardened cement paste obtained from Portland cement is brittle in nature and susceptible to cracking. Portland cement concrete is a heterogeneous composite with a multiphase microstructure. The multiphase nature of its microstructure results in irregular cracking behaviour under load. This property presents a challenge in attempting to predict crack patterns and sizes with reasonable accuracy.

Nevertheless, with this inherent complexity, durability requirements must be met, and concrete design codes set limits on maximum surface design widths related to conditions of exposure. The aim is to limit the ingress of deleterious substances. The materials within a concrete mix have various elastic ranges. The differential strains that occur under load cause microcracking within the hardened concrete body.

When a load is applied perpendicular to a beam's longitudinal axis, the furthest face undergoes tension according to normal beam theory. The tensile stresses cause cracks on this surface. This local tension failure of the concrete is necessary to transfer the tensile stresses to the steel, which provides the element with its load capacity under flexure. The behaviour of the tensile cracks is controlled by the layout of the reinforcement at the tension face.

Crack analysis models to predict the expected surface crack width under applied flexure are available. The methods focus on modelling the interface relationships of the different phases within the microstructure:

- Numerical methods – These are based on fracture theory and material physics. The energy available within the microstructure to resist fracture is estimated by modelling empirically obtained relationships between constituents.
- Analytical methods – The methods focus on the stresses in the member's tensile zone to predict surface crack width. The tension zone of the flexural member is considered as a reinforced axial tie. The relative movement between the concrete and the reinforcement determines the crack width at the surface.

These crack models all account for physical variables using different assumptions on material behaviour.

1.1 The research problem

The crack models proposed by concrete design codes differ in formulation. Consequently, when the different codes are applied to the same problem, different crack estimates are obtained.

In South Africa, the methods proposed by local design codes have been based on the British Standards. The British Standards have been superseded by the Eurocodes since 1 April 2010 (Wescott, 2010), and the South African codes are gradually being aligned with Eurocodes. Since more new structures will require adherence to Eurocode principles, the traditional methods of crack analysis need reconsideration.

When results from Eurocode have been compared with those from other international codes, crack width values varied (Allam, et al., 2012).

Since different codes would potentially provide different crack estimates, a situation could arise where one model may indicate acceptable design and the other failure for the same crack problem. The assessment of design adequacy especially in the repair of older structures could be problematic. Concrete elements designed adequately to previous codes could be concluded as being inadequately designed when applying new methods.

The following questions arise:

- What is the variation in the estimated maximum crack width values across commonly used design codes?
- When considering the basis of their formulation, which models are likely to be more suited for durability design?

1.2 Purpose of study

This research investigates the formulation of crack prediction theory through examination of theorems and models available for crack analysis. Comparisons are done between local and international codes and methods.

1.3 Objectives of study

The study aims to identify the differences in application of the crack models examined and the variances of crack width estimates. This is done by simultaneously applying the methods to various beam configurations and noting the differences in estimated maximum crack width.

1.4 Scope of research

The study investigates load-induced cracking on the tension face of reinforced concrete members. The deformation of one-way spanning elements is compared. The comparisons are based on tensile strains resulting from characteristic applied loads, where the formulas available for direct calculation of crack values are computed. The origins for determining concrete crack width values are examined to identify the analytical basis.

Cracks resulting from chemical effects (ASR cracking), imposed deformations, restrained movement and shear cracking are not examined. Delayed fracture, fatigue fracture and tensile stresses resulting from cyclic loads are not included. The fracture process is described with reference to the fundamental principles of solid body mechanics.

Corrosion bond models are available in the fib code and formulas for the provision of secondary reinforcement have been published by Chairns and Holly. The investigation of corrosion bond models and the influence of secondary reinforcement on crack width models falls outside the scope of this report.

.

2. LITERATURE STUDY

Concrete has a highly heterogeneous and complex microstructure. This presents a challenge in creating realistic models to reliably predict its behaviour. Knowledge of the properties of its constituents and the nature of their interaction in the matrix, particularly at interfaces, is required (Mehta & Monteiro, 2014).

2.1 Composition of reinforced concrete

Concrete is a two-phase construction material comprised of a heterogeneous mixture of core ingredients. The two phases are the fresh plastic state and hardened elastic form. The core ingredients are water, cement (ordinary Portland cement or blended cement) and aggregate (coarse stone and fine sand). In normal concrete, the largest portion of the total volume of concrete yield is comprised of aggregate. The aggregate volume is bound together by the cement paste to form the hardened composite solid.

Due to its heterogenous nature, concrete consists of many internal flaws. Initial cracking originates from stress concentrations around these flaws.

Literature points toward three levels of observation within reinforced concrete by which the fracture behaviour is evaluated (Mier, 1997). These are listed in Table 2-1 according to the numerical level of observation of reinforced concrete, adapted from Mier and Wittman.

Table 2-1: Levels of observation to evaluate fracture behaviour (Mier, 1997) (Wittmann, 1983)

Level	Property	Origin of characteristics
Micro-level	Interfacial transition zone	W :C ratio, admixtures, fines content
Meso-level	Aggregate interface	Course aggregate properties
Macro-level	Bond relationship between reinforcement and concrete	Analytical models

When concrete is considered from a meso-mechanical perspective, it can be considered a three-phase composite material consisting of aggregate, hardened cement paste and the interface of these two (Neville, 1997).

2.1.1 Concrete matrix

The cement paste in its hardened form, i.e. the hardened cement paste (HCP), has high strength with low elasticity, making it very brittle. HCP is transformed from a brittle to a more elastic material through the addition of coarse aggregate (Tasdemir & Karihaloo, 2001). Aggregates on its own are known to have linear elastic brittle behaviour, like hardened cement paste. Figure 2-1 shows the deformation response to failure of the concrete constituents

separately. It can be noted how concrete displays softening behaviour with more ductility than the separate constituents.

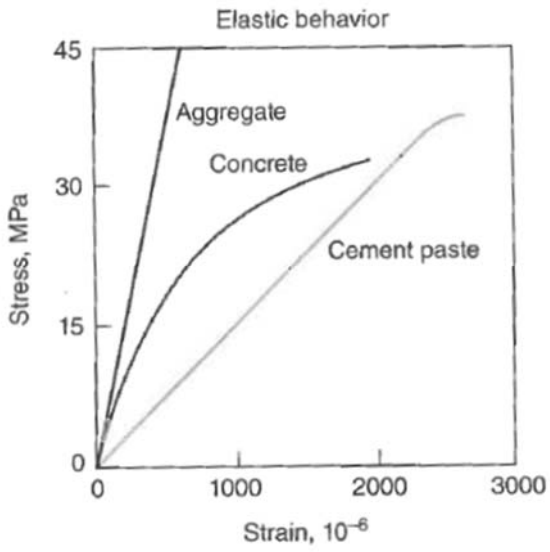

Figure 2-1: Illustration of typical deformation behaviour of inclusions and the composite (Mehta & Monteiro, 2014)

This illustrates how a brittle matrix is transformed progressively into a ductile composite by the addition of a brittle inclusion, i.e. aggregate. The aggregate and HCP on its own can absorb more stress but is weaker in combination. The interaction of these constituents affects deformation response, and in turn fracture behaviour. The source of this interaction is identified at the levels of observation.

a) *Meso level - Aggregates*

The aggregate selected has a substantial influence on the fracture characteristics of the concrete mix (Mehta & Monteiro, 2014).

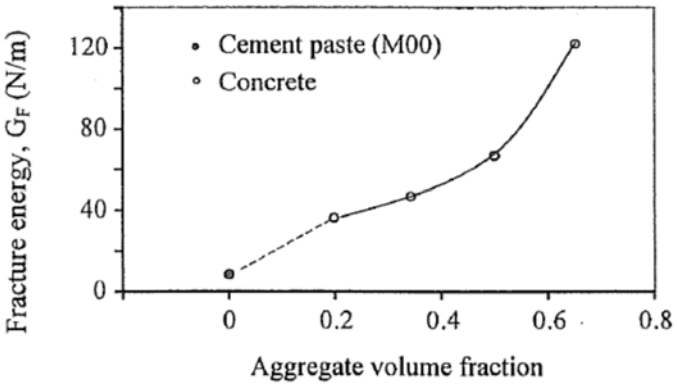

Figure 2-2: Influence of aggregate volume on fracture energy (Tasdemir & Karihaloo, 2001)

Aggregate particles in a concrete matrix cause crack initiation at a lower stress, while increasing ductility and toughness (Tasdemir & Karihaloo, 2001).

Experimental testing found compressive strength decreased with an increase in aggregate volume up to 50% of the total batch volume. Strength remained constant with increasing aggregate volume past 50% (Tasdemir & Karihaloo, 2001). The same testing showed increased aggregate volume improved deformation characteristics, including Young's modulus, splitting tensile strength and the fracture energy. This occurred when high strength aggregate was used in high strength mixes and lower strength aggregate in normal strength mixes. In normal strength concretes cracks propagate by following the path of the weaker cement paste between the aggregates. The aggregates resist crack widening and growth by deflecting crack growth paths. The volume of fine sand had no significant influence (Tasdemir & Karihaloo, 2001).

Further to this, testing showed fracture energy for normal and high strength mixes is higher with stronger aggregate. The aggregates compared were basalt and limestone. Mixes with basalt exhibited higher bond strength with reinforcement than mixes with limestone (Darwin, et al., 1985).

El-Sayed, et al. found the effect of the maximum aggregate size on the fracture energy is dependent on the shape of the aggregate. The shape determines the mechanical bond between the matrix and the aggregates (El-Sayed, et al., 1998).

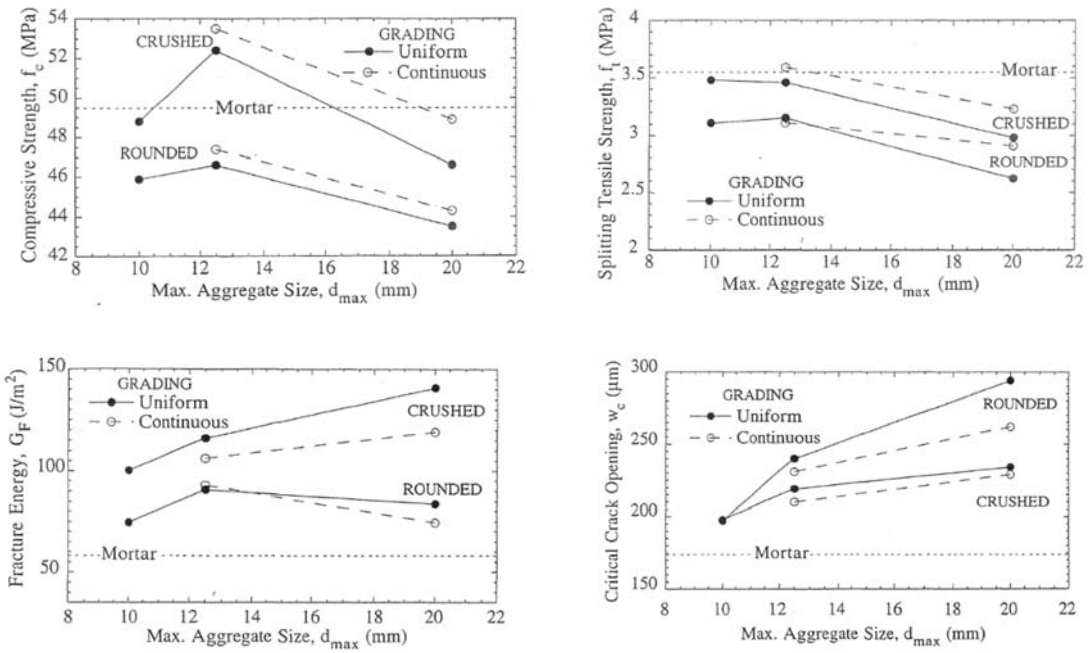

Figure 2-3: Influence of aggregate shape on fracture behaviour (El-Sayed, et al., 1998)

b) *Microlevel - Interfacial transition zone (ITZ)*

The interface between the cementitious paste and the diluted aggregate is the weakest region in the concrete. Here the bond strength depends on mechanical interlock, physical attraction and direct chemical bonding (Mehta & Monteiro, 2014).

In freshly compacted concrete, films of water enclose the course aggregate particles creating a higher water: cement ratio closer to aggregate. This forms a porous network in the matrix around the aggregate. The weak zone around the aggregate is improved by the addition of fines and a higher cement content, where unhydrated cement particles are deposited (Mehta & Monteiro, 2014).

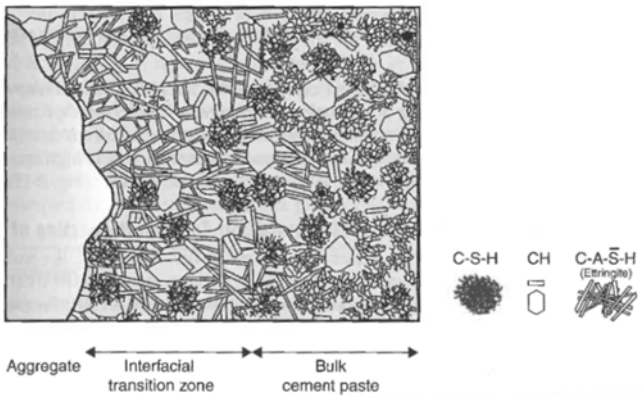

Figure 2-4: Diagrammatic representation of the interfacial transition zone and bulk cement paste in concrete (Mehta & Monteiro, 2014)

Due to the characteristics discussed here, the fracture process in hardened concrete normally begins in the pores of the hydrated binder, and the interfacial transition zone of cement paste (Hassanzadeh, 1998).

2.1.2 Steel reinforcement – Meso level observation

Steel reinforcement under applied stress exhibits a ductile material response and its inclusion compensates for concretes weakness in tension. The interface relationship between the steel surface and concrete matrix is defined by the stress transfer along the length of the bars. This relationship increases the ductility of the concrete section. The reinforcement provides additional stable deformation capacity to the concrete member under stress (Mehta & Monteiro, 2014).

The crack width in flexural concrete is proportional to the steel stress (Han, et al., 2011). In elastic theory, the stress at which reinforcement yields is a critical variable as irreversible plastic deformation in the concrete member follows (Regan & Yu, 1973).The texture of the rebar perimeter determines the type of bond action resisting movement between the reinforcement and concrete (slip).

Plain bars rely on surface friction for bond capacity. Deformed bars rely on friction and mechanical interlock. Poor surface conditions are caused by residues that have a greasing effect on the steel surface. Ignoring any intentional coating of the reinforcement, residue as well as surface degradation is commonly caused by corrosion (Regan & Yu, 1973).

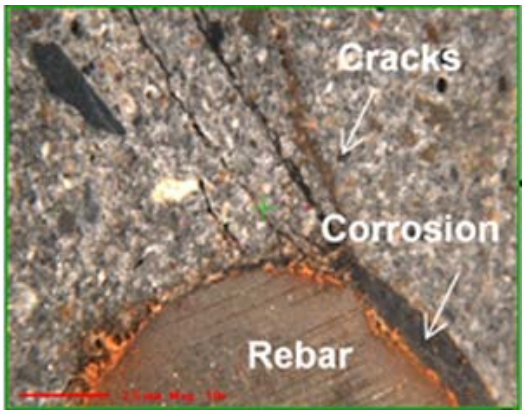

Figure 2-5: Mesolevel observation of steel-concrete interface subject to corrosion (Applied Petrography Group)

2.2 Mechanism of cracking in reinforced concrete

This discussion shows the importance of the strain compatibility relationship in deformation analysis. The compatibility is disrupted by tensile strain and elastic differences between steel and concrete. Flexural crack analysis requires the modelling of this. Strain compatibility is maintained by the appearance of cracks in the tension region of the member (McCormac & Brown, 2009).

2.2.1 Crack formation and beam theory

Under flexural loading, response phases occur up to eventual failure. The phases considered for crack analysis fall in the period before the reinforcement yields under tensile stress. The rectangular beam response at various stages are here summarised (Regan & Yu, 1973).

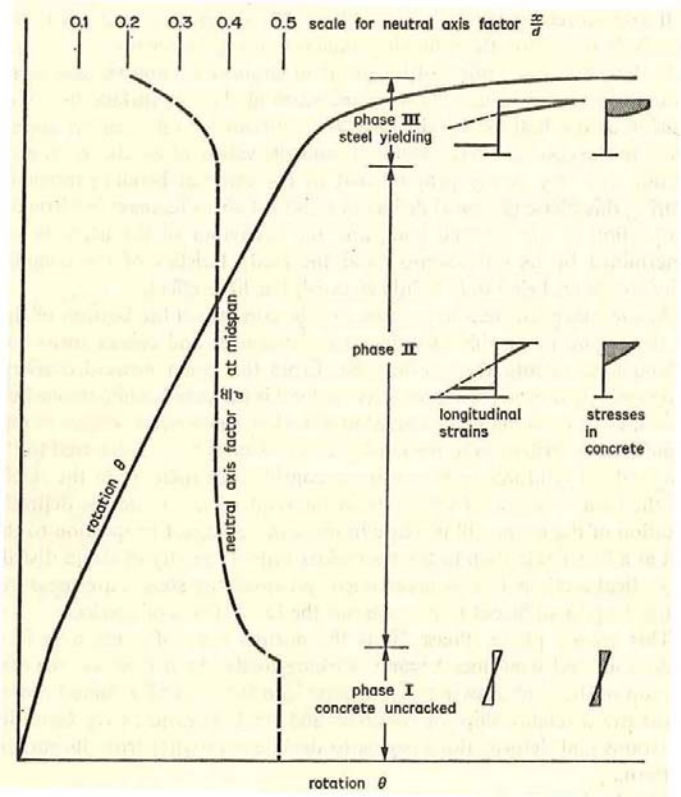

Figure 2-6: Typical deformation of rectangular beam under flexural load (Regan & Yu, 1973)

1. Phase I : Uncracked phase - Reinforcement not stressed
   - Tensile capacity at tension face not exceeded.
   - Beam acts as a homogenous body.
   - Neutral axis at midheight of the section
2. Phase II : Crack initiation and stabilised growth – Stressing of reinforcement.
   - Cracks form and rebar is loaded with tension force.
   - Beam no longer homogeneous
   - Neutral axis moves upward reducing the compression area. The neutral axis remains in this position, with increasing force in the rebar, until yield strain is reached.
3. Phase III : Reinforcement yields

Phase 2 describes the normal state of beam in its service condition. During phases I & II a concrete beam adheres to elastic behaviour and the theory of classical elastic theory is relevant. The basic elastic theory of a body has the following relationship: (Hughes, 1976).

$$\boldsymbol{M = \int Z \times 10^{-6}} \quad (1)$$

where:

$M = \text{the bending moment at the section} \quad (kN.m)$

$\int = \text{the stress in the extreme fibre at the furthest edge from load application} \quad (N/mm^2)$

$Z = section\ modulus$

The main assumptions of the elastic beam theory are summarised here: (Hughes, 1976)

- Rebar and concrete deform relative over the full length (strain compatibility). Adequate bond between the reinforcement and concrete needs to be present.
- In bending Euler - Bernoulli's beam theorem is adhered to (plane sections remain plane).
- Elasticity of concrete and the rebar. The quasi-brittle nature of concrete where tension softening is possible allows compatibility in this relationship.
- Concrete resists no flexural tensile stresses and is ignored in bending.
- Stresses occurring due to restraint from thermal and shrinkage variations are ignored.
- The cross-sectional area of the reinforcement is small in comparison with that of the concrete.

According to Euler - Bernoulli's beam theorem, the strain at any point in the height of the section is proportional to its distance from the position of zero strain.

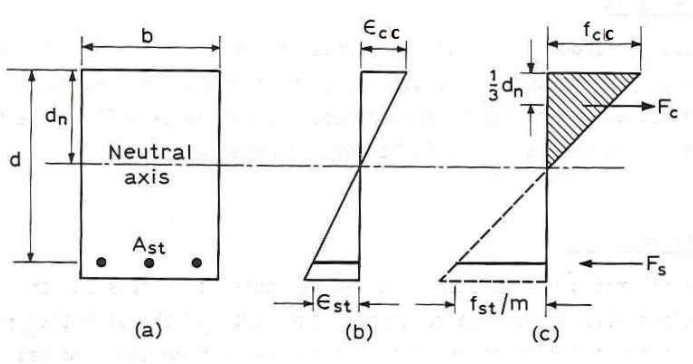

Figure 2-7: Elastic stress and strain distribution (Hughes, 1976)

From the linear stress diagram in Figure 2-7 the distance between the two forces are given by: $\mathbf{z = d - {d_n}/{3}}$ **(lever arm)**. (2)

The stresses in the concrete and steel are determined from the relationships of elastic beam theory shown here:

- Concrete (Phase II - Rebar in elastic range)

$$\boldsymbol{M = \tfrac{1}{2}\, f_{cc} b d_n \left(d - {d_n}/{3}\right)} \quad (3)$$

$$\boldsymbol{f_{cc} = \frac{2M}{b d_n \left(d - {d_n}/{3}\right)}} \quad (4)$$

- Steel (Phase II - Rebar in elastic range)

$$\boldsymbol{M = f_{st} \rho b d \left(d - {d_n}/{3}\right)} \quad (5)$$

$$f_{st} = \frac{M}{\rho b d\left(d - {}^{d_n}/_{3}\right)} \qquad (6)$$

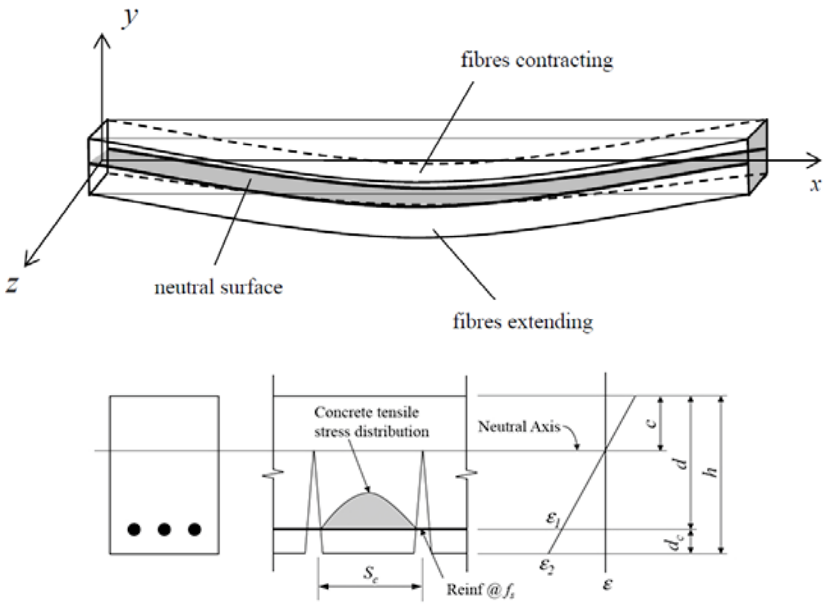

Figure 2-8: Flexural beam cracking model (Frosch, 2014)

With increasing stress, and proportional increase in strain, a peak stress is reached (cylinder strength) at a strain of approximately 0.002. With further strain increase the stress reduces until failure occurs at a strain of about 0.0035. (Reynolds, et al., 2008).

2.2.2 Causes and mechanisms

Under applied tension strain, concrete undergoes an increase in length. With increasing moment, the limiting tension strain of a beam section is eventually reached and the tension region cracks.

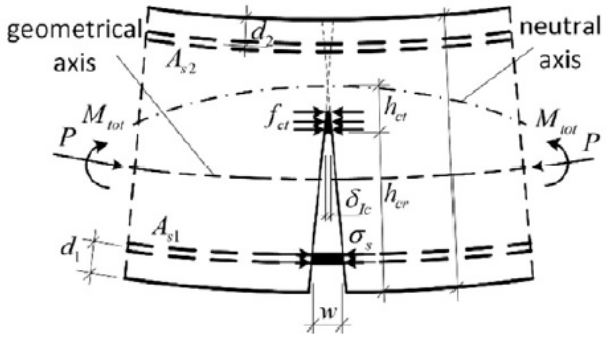

Figure 2-9: Typical model for normal crack development (Jokubaitis, et al., 2013)

A typical model for crack development is based on the rules provided by the fracture mechanics of solids. The theory permits the two extreme ends of each crack to be determined, where one

end propagates towards the neutral axis and the other coincides with the level of tensile reinforcement. All the tensile stresses occurring at the crack locations are transferred to this reinforcement (Jokubaitis, et al., 2013). A clear width is added to the length (crack width) of the member as it deforms. The accumulation of these distances along the length equals the tensile strain (Mosley, et al., 2012).

Crack widening is resisted by the bond forces at the rebar level, these forces control the width of the crack (Jokubaitis, et al., 2013).

Crack development is considered to occur in two phases (Lapi, et al., 2018):

- Crack formation phase (crack initiation)
- Stabilised crack growth phase (crack propagation)

During formation, cracks initiate in weaker regions, according to the random distribution of local tensile stresses. Adjacent to the cracks, the concrete tensile stress starts increasing from zero as the bond forces transfers tension. In this way, the tension in the rebar at the cracks, gradually transfer back to the concrete between cracks. A certain distance from the crack the tensile stresses again reach the limiting concrete tensile stress, and a new crack is created. This distance over which the transfer of forces occurs is called the transfer length (Lapi, et al., 2018). The distance between adjacent cracks (2 x the transfer length) is the total length over which tensile force transfer takes place.

When the distance between all adjacent transfer lengths are zero, no new cracks can initiate, and the stabilised crack growth phase begins. The cracks formed during formation begin to widen under further load (Leonhardt, 1988).

A tensile force difference exists between the exposed bar length in the cracks and that embedded over the transfer length. A strain difference exists, where the strain of the embedded

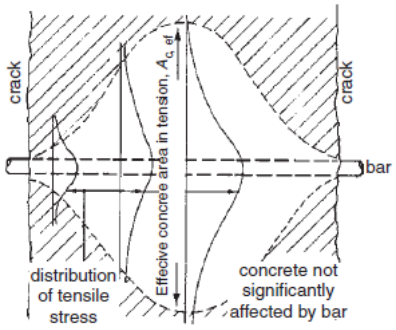

bars ($\epsilon_{s1} = at\ zero\ slip$) is less than in the crack ($\epsilon_{s2} = maximum\ slip$). The force transfer between cracks result in strain incompatibility between the concrete and rebar.

Figure 2-10: Illustration of effective concrete area in tension (Borosnyoi & Balazs, 2005)

The release of stress by the rebar to the concrete causes an increase in the Young's modulus of the steel (Borosnyoi & Balazs, 2005). The concrete between the cracks thereby increases the stiffness of the tension reinforcement, known as tension stiffening.

The crack width at rebar and concrete interface is determined by their relative displacement (slip). (Borosnyoi & Balazs, 2005).

Two theories in RC design account for the incompatibility of strains across the transfer length (Lapi, et al., 2018).

- No slip theory – No slip occurs at the interface. An engineering rule is assumed where the transfer length is proportional to the available cover. The theory accounts for shear deformations over the cover distance.
- Slip theory – Due to the action of bond stresses formed from the tensile strains, a physical slip occurs at the concrete and reinforcement interface. This theory does not account for the existence of shear deformations over the cover distance.

In addition to the bond-slip mechanism and the fracture mechanics of concrete, the shear deformability of concrete cannot be neglected when evaluating the profile of a main crack (Fantilli, et al., 2007). The main cause of different widths along a main crack is the tensile stress distribution in the concrete cover (Fantilli, et al., 2007).

Early research quoted by Borosnyoi showed the surface crack width can considerably differ from the primary crack at reinforcement level (Borosnyoi & Snobli, 2010). Despite cracks

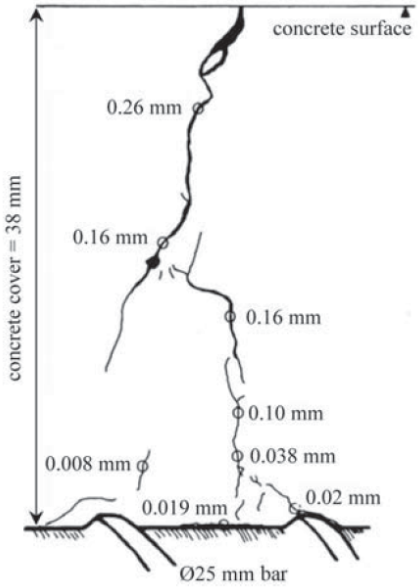

Figure 2-11: Variation of crack width in a concrete cover according to Beeby (Borosnyoi & Snobli, 2010)

originating at the surface of reinforcement, widths can drop to almost zero near concrete

surface. In some instances, surface crack widths have also been found to be twice to 10 times the crack widths at the rebar level (Borosnyoi & Snobli, 2010).

Research has shown the crack width (slip) at the rebar level is independent of the thickness of the cover, however the surface crack widths are proportional to the thickness of the cover (Borosnyoi & Snobli, 2010). The surface crack width is linearly proportional to the tensile stress in the steel reinforcement, with the influence reducing to zero closer to the reinforcement (Borosnyoi & Snobli, 2010).

Experimental work showed different concrete covers result in varying local stiffnesses of the tensile member. Higher regions of stiffness collect the deformations resulting in larger crack widths. Observed crack widths at 20mm from the reinforcement of 0.11mm, 0.15mm, 0.2mm and 0.32mm were noted for covers of 20mm, 40mm, 60mm and 80mm respectively. In these situations the crack width at rebar level were found to be independent of the cover (Borosnyoi & Snobli, 2010). The variation within this depth depends on the bond between the rebar and concrete as well as the deformations within the cover itself. At low tensile forces, crack widths across the cover depth are similar. With increasing load crack widths are narrower at the reinforcement.

The cracks formed up to this point, where distance between the cracks are twice the transfer lengths are called primary cracks. Their average spacing, in a region of constant moment, has been shown experimentally to be $1.67\,(member\ depth - \text{neutral axis depth})$ (Mosley & Bungey, 1990). The spacing of primary cracks is not influenced by the arrangement of reinforcement (Mosley, et al., 2012). It is a function of the strain in the rebar as well as the rebar type (ribbed or plain).

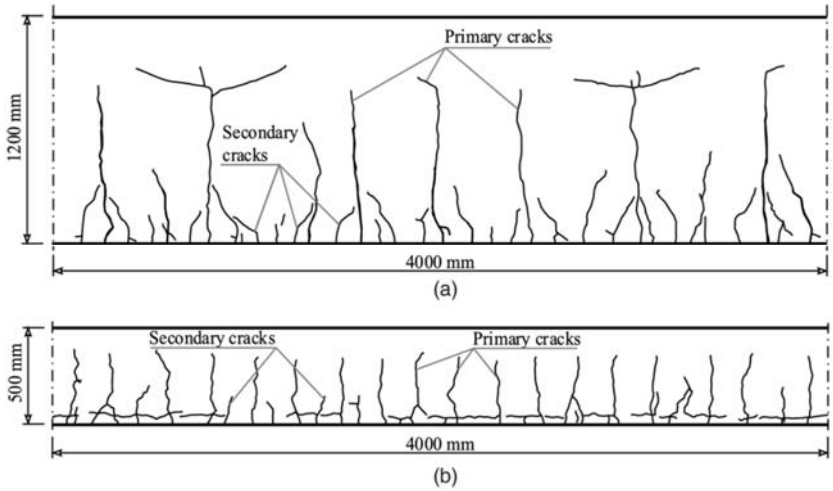

Figure 2-12: Typical primary and secondary crack distribution on a simply supported beam face (Kaklauskas, 2017)

With increasing moment passed this point, crack development is controlled by the reinforcement arrangement. Primary cracks grow over the height of the beam towards the neutral axis (Kaklauskas, 2017).

Bond stress increase over the transfer lengths result in further cracks (secondary cracks) away from the primary (main) cracks. The spacing of these secondary cracks is determined by the spacing of the reinforcement. Their existence is a result of the tensile stresses from the bars. If the rebar is closely spaced, adjacent influence zones overlap, resulting in secondary cracks joining across the member. Where bars are far apart, they will form only next to each individual bar (Mosley, et al., 2012).

Cracks on the surface of concrete are noticeable while internal cracks are referred to as micro-cracks. Microcracks occur between constituents in the concrete matrix, but also develop around reinforcing steel due to internal breakage under tension.

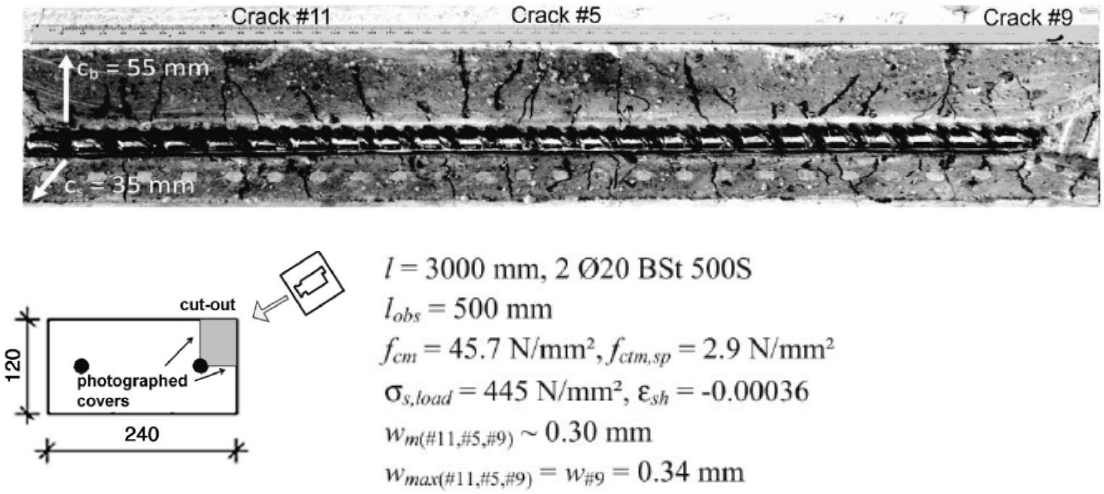

l	= length of element	$\sigma_{s,load}$	= applied steel stress
l_{obs}	= steel anchor length	ε_{sh}	= free shrinkage strain
f_{cm}	= mean 28 day compressive strength	w_m	= mean crack width
$f_{ctm,sp}$	= mean tensile splitting strength	w_{max}	= max. crack width (crack 9)

Figure 2-13: Internal micro-cracks around reinforcement (Balazs, 2013)

Figure 2-13 shows the results of testing proving the existence of internal microcracks in concrete around stressed rebar. The existence of internal micro-cracks around the rebar was discovered by Goto and Otsuka (Goto & Otsuka, 1971) through the injection of ink along embedded reinforcement. Other investigations have shown the extent of the existence of these cracks (Balazs, 2013). Goto described the crack formation around reinforcement as follows:

- Shortly after the primary cracks form, small internal cracks form around the deformed bars. The internal cracks started at a stress level lower than 96 MPa
- Initially no secondary cracks appear at the concrete surface.

- Internal cracks on both sides of the primary cracks form cones with apexes near the rebar lugs and bases directed toward the primary crack.
- At the interface where cracks occur, there is zero adhesion between steel and concrete. Bond is dependent on the bearing of the concrete cones against the lugs.
- When the applied tension force is released after the formation of the internal cracks, the stress of the embedded reinforcement does not return to zero.

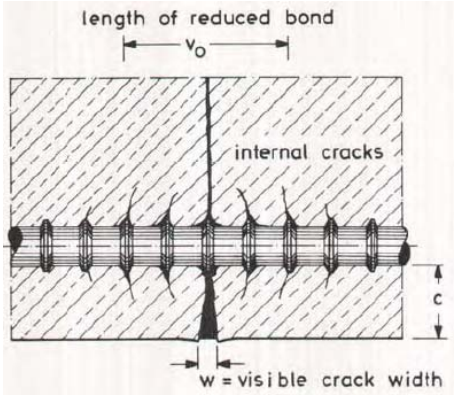

Figure 2-14: Depiction of internal cracks forming on rebar lugs (Leonhardt, 1988)

The effects of internal breakage are a loss of bond over the reinforcement length and widening of cracks across the cover distance at the tension edge. Salinger and Billing (McCormac & Brown, 2009) estimated the steel stress just before cracking to be in the order of magnitude of 42 to 49 MPa, resulting in an initial crack width at the most extreme concrete edge in tension of about 0.025mm.

2.2.3 Consequences of cracking and fracture

Aggressive agents travel across the concrete cover distance through slow transport mechanisms such as diffusion (Owens & Fulton, 2009). Cracks in the cover immediately around the steel, are preferred channels for chloride transport (Sagues & Kranc, 2001). The cracks allow direct paths to the embedded reinforcement (corrosion initiation). These flow paths reduce the time to corrosion initiation, compared to diffusion transport. A shorter corrosion initiation period can drastically reduce structural design life (Sagues & Kranc, 2001). Corrosion modelling has an initiation and propagation period, with consequences for serviceability and structural failures.

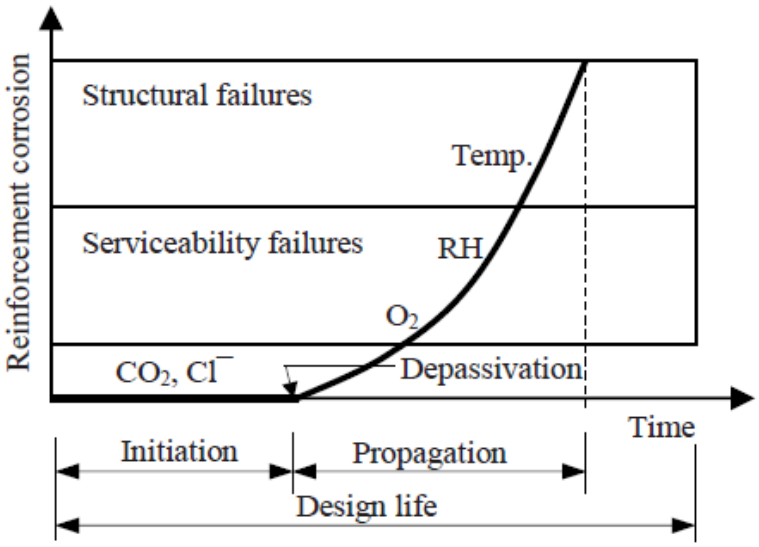

Figure 2-15: Typical deterioration model of service life due to reinforcement corrosion (Holly & Bilcik, 2013)

The electromechanical potentials to form the corrosion cells are generated when differences in the concentration of dissolved ions, such as alkalis and chlorides, occur in the immediate vicinity of steel bars (Mehta & Monteiro, 2014). Some sections of the metal become anodic and the other cathodic. The fundamental chemical changes occurring in these areas are shown in Figure 2-16.

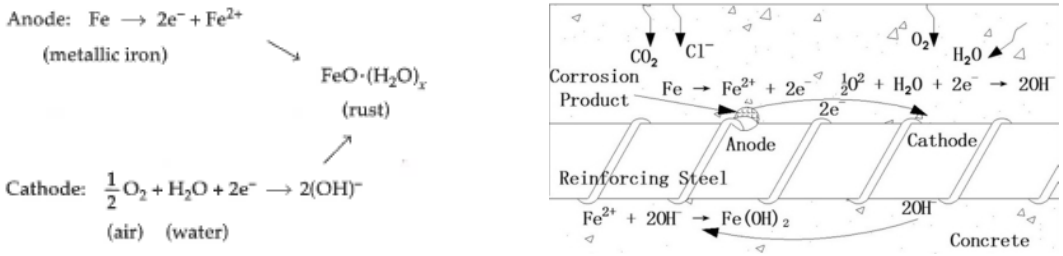

Figure 2-16: Chemical changes at anodic and cathodic areas (Mehta & Monteiro, 2014)

Concrete embedment forms a protective passive film on the steel surface. A double-layered oxide film is formed consisting of an inner iron layer (Fe_3O_4) and an outer iron oxide layer (Fe_2O_3). Anodic reaction (iron removal) will not fully progress unless the electron flow to the cathode (oxygen reduction) is maintained by electron consumption. The presence of both air and water at the surface of the cathode is necessary. The metallic iron is not available for the anodic reaction until the passivity is destroyed. This occurs below a PH level of 11.5. Once fully degraded corrosion can commence (corrosion propagation). In highly permeable concrete, the PH in the steel vicinity will drop when the alkalis and most of the calcium hydroxide have been carbonated or leached away. (Mehta & Monteiro, 2014).

Reinforcement corrosion at crack positions involves a macro-cell where steel exposed at the crack tip becomes an anode and actively corrodes when the critical chloride concentration is exceeded. Adjacent passive rebar serves as the cathode for oxygen consumption. To maintain the charge conservation, the anodic corrosion reaction can occur only as rapidly as oxygen can be consumed at the cathodic sites. Significant corrosion cannot occur until there is enough oxygen to transfer along at the steel surface. Oxygen will not be available if the steel-cement interfacial zone remains impermeable. Microcracking in this zone forms a pathway for oxygen, creating conditions that allow significant corrosion. The concretes inherent microcracks, the initial size influenced by the mix design, widen by the four points listed in the diagram of Figure 2-17. The widening of microcracks increases permeability, allowing seawater and air to initiate corrosion of the steel. Surface corrosion increases the steel volume, splitting the concrete and thereby widening the cracks and further increasing the permeability.

This crack widening and corrosion interaction follows the cycle depicted in Figure 2-17.

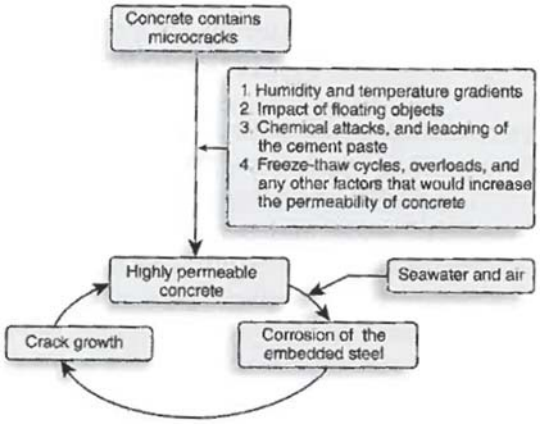

Figure 2-17: Concrete deterioration cycle due to corrosion (Mehta & Monteiro, 2014)

Microcracking around the steel can therefore initiate an escalating cycle of cracking, corrosion and crack propagation, that progressively increases the rate of structural deterioration (Mehta & Monteiro, 2014). A theoretical comparison of localised corrosion found that localised corrosion rates (cracked concrete) can be one order of magnitude greater than under uniform ingress (sound concrete). The analysis showed that corrosion at localised active spots can result in significant greater damage shortly after corrosion initiation (Sagues & Kranc, 2001).

Schiessl and Raupach (Schiessl & Raupach, 1997) tested cracked reinforced concrete beams to identify the corrosion mechanism and the influence of crack width. Mechanically cracked specimens with crack widths ranging 0.1mm to 0.5mm were studied. After the local depassivation of rebar by chlorides entering the cracks, the crack zone acted as an anode and the steel between the cracks as a cathode. The corrosion rate in the crack zone was greatly

influenced by the conditions between the cracks. While corrosion initiated earlier in wider cracks, steel corrosion at the crack decreased with time. In the long term (2 years) this activity was independent of crack width difference. Researchers concluded the quality (impermeability) and thickness of cover around the rebar influences the corrosion rate more significantly than crack width.

An investigation of corrosion on eight reinforced concrete coastal bridges was conducted in Florida, to determine how the rate of chlorine penetration may be affected by pre-existing stress cracks.

Existing cracks on the structures were identified. A pair of cores were taken, one directly on a crack and the second immediately adjacent in sound concrete between cracks. A value for chloride concentration in the concrete microstructure was obtained by the ratio of concentration in the sound concrete and the concentration in the cracked concrete. In analysing the data, it was assumed the chloride concentration that reached the crack tip is the indicator for potential of reinforcement corrosion at the crack. Figure 2-18 was produced where the chloride concentration ratio was plotted against the crack width. At a few bridge locations, the concentration ratios obtained were similar for narrower cracks and wider cracks. The investigations concluded that even in thin cracks, substantial chloride penetration occurred immediately around the cracks compared with the surrounding sound concrete.

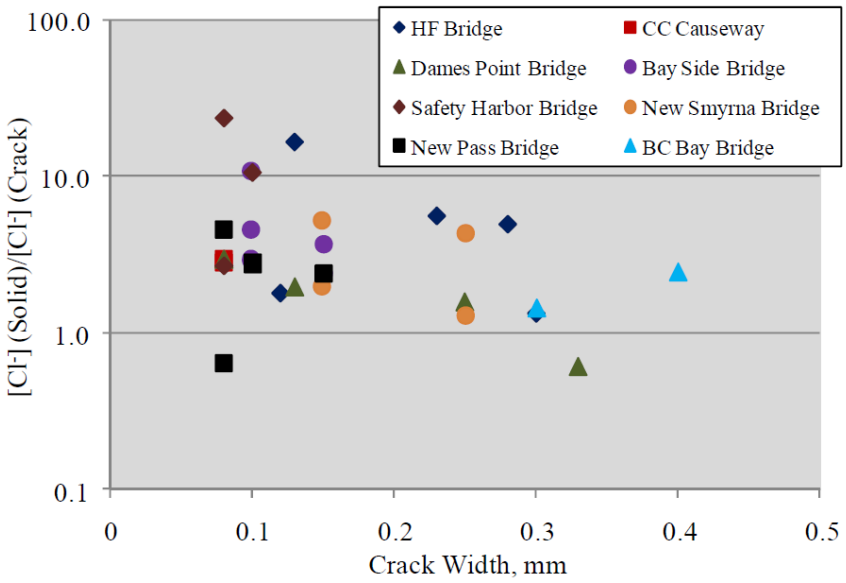

Figure 2-18: Chloride concentration versus crack width (University of South Florida, Tampa; Florida Department of Transportation; Federal Highway Administration, 2001)

It was further noted that in higher quality impermeable concrete, chlorides remained closer to the crack than in lower quality concrete, where the chloride diffusion was more widespread.

Despite the concentration at the cracks being greater than the thresholds for corrosion initiation, corrosion was not noted. Narrower cracks provided less of a pathway for chlorides while deep cracks provided increased wall area for lateral transport to adjacent concrete (University of South Florida, Tampa; Florida Department of Transportation; Federal Highway Administration, 2001).

Several papers also discussed the impact of crack width on the corrosion of steel embedded in concrete. It was demonstrated the tendency for corrosion as well as the rate of corrosion of embedded steel are independent from surface crack widths (Borosnyoi & Snobli, 2010).

Earlier commentary on the relevance of crack width calculations in designing for durability were numerous:

- Beeby stated there is no link between the level of flexural cracking and corrosion (Beeby, 1979).
- Leonhardt stated crack widths up to 0,4mm do not significantly harm the corrosion protection of reinforced concrete when thick dense cover is implemented (Leonhardt, 1988).
- Hognestad referred to experiments on loaded concrete beams that were monitored over 25 years. The results failed to prove a correlation between crack width and the extent of deterioration (Darwin, et al., 1985).
- The American concrete institute issued commentary quoting research where a clear correlation between corrosion and surface crack widths in normal service stress ranges could not be found (ACI318, Committee, 2014).

Committee 224 formalised the following viewpoints on crack influence (ACI committee 224, 2001):

- Cracks reduce the service life of structures by allowing deleterious substances to reach the rebar more rapidly.
- Cracks accelerate the onset of corrosion; this corrosion is however localised. Overtime uncracked concrete, due to inherent porosity, inevitably permits the penetration of deleterious substance initiating corrosion propagation.

The last point implies corrosion protection is mainly a function of cover and concrete quality with crack width playing a lessor role. ACI committee 224 recommend limiting crack widths for exposure conditions, noting that in specifying the limits, with time a large portion of widths will exceed the design values. The committee confirmed the values are not indicative of expected corrosion or deterioration since larger covers would provide better durability even with wider crack widths. (ACI committee 224, 2001).

Table 4.1—Guide to reasonable* crack widths, reinforced concrete under service loads

Exposure condition	Crack width	
	in.	mm
Dry air or protective membrane	0.016	0.41
Humidity, moist air, soil	0.012	0.30
Deicing chemicals	0.007	0.18
Seawater and seawater spray, wetting and drying	0.006	0.15
Water-retaining structures†	0.004	0.10

* It should be expected that a portion of the cracks in the structure will exceed these values. With time, a significant portion can exceed these values. These are general guidelines for design to be used in conjunction with sound engineering judgement.
†Exclusing nonpressure pipes.

Figure 2-19: Reasonable design crack widths for conditions (ACI committee 224, 2001)

Microcracking in hardened concrete has been reported by Mehta as being a typical cause of insufficient water tightness. Halvorsen (1987) made a case that crack widths ranging from 0.15mm to 0.3mm could be considered unacceptable for aesthetic reasons as these are visible to the naked eye, providing a sense of insecurity. Leonhardt (Leonhardt, 1988) commented that crack widths should be limited to 0,2mm on surfaces seen at close distance to avoid concern from casual observers.

2.3 Review of material and concrete fracture

Fracture energy (G_F) is used to assess the toughness and brittleness of concrete. The larger the value of G_F (toughness), the less brittle and the more work required to cause failure (Young, et al., 1998).

Fracture is defined as the fragmentation of a solid under the action of applied stresses (Hertzberg, 1996). It may be either partial or complete (ultimate failure). Partial fracture normally includes microcracking and localised damage. The process of fracture ~~i~~involves crack initiation followed by crack propagation.

The stress-strain behaviour of most materials under incrementally increasing load is divided into elastic and plastic deformation.

- Elastic strain – The strain is initially proportional to the applied stress and is reversible when the load is removed.
- Plastic or inelastic strain – Under higher applied stress levels the strain is no longer proportional to this stress.

The ductility of a material is a measure of the amount of inelastic strain that can occur before ultimate failure. The descriptive term for ductility is material toughness and measured by the energy required for ultimate failure (fracture energy) (Karihaloo & Huang, 1991).

In a plot of the stress-strain curve, the total fracture energy equals the area under the curve.

A tough material is ductile and possesses strength. The measure of strength of ductile material is less the brittle material. Kumar therefore commented when the strength of the material goes up, generally the ductility and toughness reduces (Karihaloo & Huang, 1991).

2.3.1 Ductile fracture

When a ductile body deforms under applied load, the Young's modulus relationship is linearly proportional (Hooke's law), indicative of constant material stiffness (Teo, et al., 2014). In this condition, it behaves purely elastic. As the stress increases, the proportional limit is reached, and the stiffness is no longer constant. From this point a slight increase in load will cross the elastic limit (yield limit), ending the elastic stress range (Teo, et al., 2014). Applied stress beyond this limit will result in permanent deformation. The typical profiles of the stress strain diagram for steels in tension is shown in Figure 2-20 and Figure 2-21.

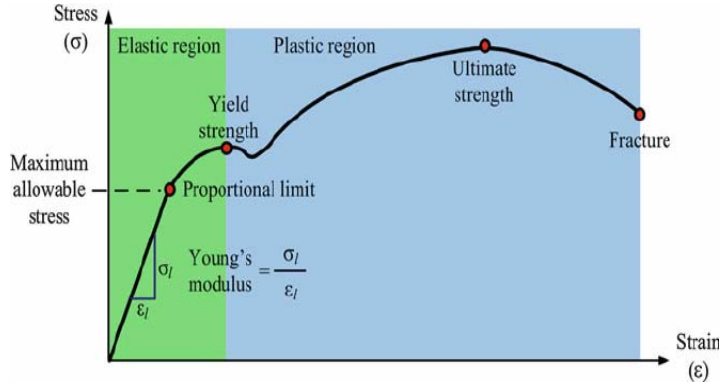

Figure 2-20: Engineering stress strain curve (Teo, et al., 2014)

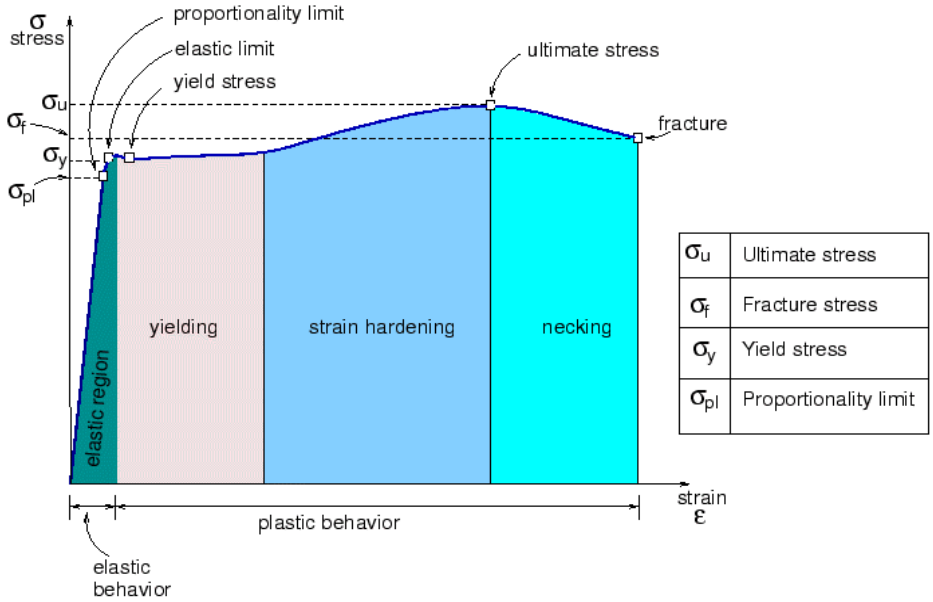

Figure 2-21: Illustration of material behaviour at critical points according to the Material Science Network (Maleque & Salit, 2013)

The Figure 2-21 has a steeper elastic region and therefore less ductile steel than Figure 2-20. The critical points are when the material undergoes changes in property under increasing strain.

2.3.2 Brittle fracture

Deformation in a brittle body, follows the ductile response till the proportionality limit. An increase in stress beyond this point shows no noticeable yield behaviour. (Teo, et al., 2014) At the initiation of plastic deformation, a longitudinal crack propagates perpendicular to the applied stress. This halts any plastic response. In a perfectly brittle material final failure occurs with no plastic deformation. The material fails prior to exhibiting any significant yielding. There is no partial fracture and no development of a crack growth phase (Karihaloo & Huang, 1991). A comparison of the typical stress-strain curves for typical brittle and ductile material in tension is compared in Figure 2-22 and Figure 2-23.

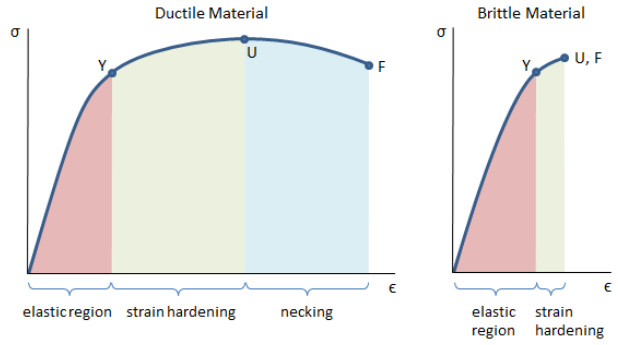

Figure 2-22: Response comparison for deformation curves 1 (Karihaloo & Huang, 1991)

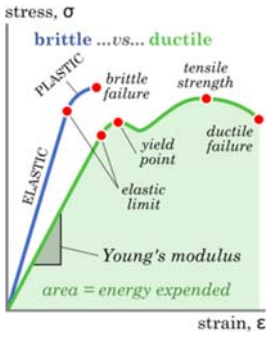

Figure 2-23: Response comparison for deformation curves 2 (Karihaloo & Huang, 1991)

2.3.3 Quasi-brittle fracture

A variety of brittle materials exhibit more nonlinear stress strain behaviour than the expected brittle response. Both elastic and plastic zones are present in the volume and the fracture behaviour is termed quasi-brittle (Karihaloo & Huang, 1991). When the limit of proportionality is reached, the existing flaws start to grow, and new flaws are added.

Like brittle materials, a small amount of strain hardening occurs prior to reaching the ultimate stress (partial fracture). Where true brittle materials fail at the ultimate stress level, quasi-brittle materials show increased deformation and energy absorption with decreasing tensile transfer past ultimate. The higher the ultimate stress on the response curve, the lower the potential strain. The decrease in tensile transfer is attributable to tension softening (strain softening) due to localised damage (strain localisation). The tension softening effect can be described as the decreasing process of concrete stress along with the release of fracture energy (Xu, et al., 2017). During the softening branch of the stress-strain relationship, stable crack growth prior to final failure occurs. Typical profiles of the stress strain diagram for quasi-brittle materials is illustrated in Figure 2-24 and Figure 2-25. Figure 2-24 illustrates the critical points and the different concrete cube deformation properties under increasing tensile load. Point A and B is the yield and ultimate stress respectively. Point C and is the safe tensile stress where partial crack (wδ) is formed. Point D is a complete crack (w_c)at failure stress.

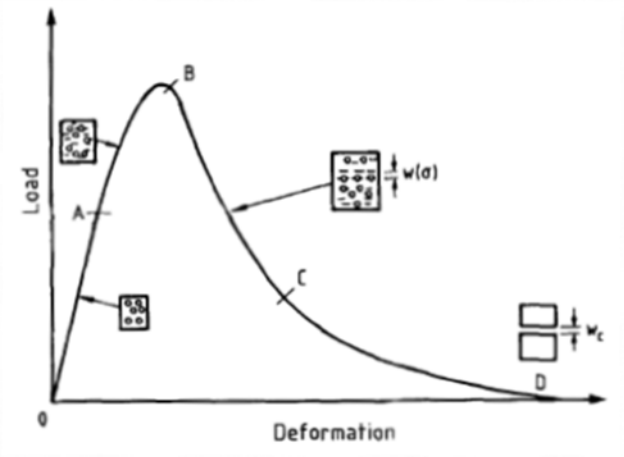

Figure 2-24: Typical stress strain curve for quasi-brittle materials 1 (Xu, et al., 2017)

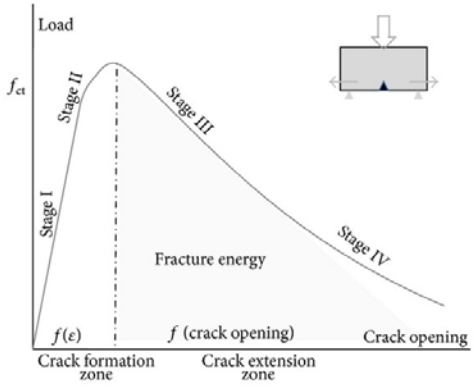

Figure 2-25: Typical stress strain curve for quasi-brittle materials 2 (Xu, et al., 2017)

Table 2-2 provides a summary of the deformation responses discussed as well as typical materials in which they occur.

Table 2-2: Fracture types and typical materials with their behaviour (Mier, 1997)

Fracture Type	Material	Cause of fracture	Result before Ult. (σu)	Result after Ult. (σu)
Ductile	Steels	Slip of dislocations	Elastic/Yielding/strain hardening	Necking till complete failure.
Brittle	Hardened cement paste (HCP), glass, cast iron	Densification of dislocations	Elastic/strain hardening	Immediate complete failure.
Quasi-brittle	Portland cement concrete	Growth in existing flaws and creation of new flaws	Elastic/strain hardening	Tension softening (strain softening) till complete failure.

In quasibrittle materials, at the microscopic level ahead of a crack (at the crack tip) a plastic zone is formed, as in the ductile response, which blunts the crack while strain hardening occurs near the crack surface. Microcracks in concrete originate from strain localization and develop ahead of the crack tip creating a fracture process zone (FPZ) (Mehta & Monteiro, 2014).

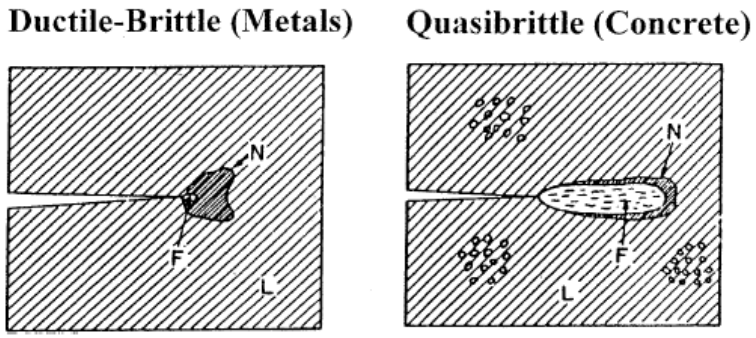

N	= Plastic concrete zone
L	= Elastic concrete zone
F	= Fracture process zone

Figure 2-26: Model of plastic behaviour and fracture zone for materials (Bažant, 2002)

2.3.4 Fracture characteristics of concrete

The behaviour of concrete under loading is related to Young's modulus E and Poisons ratio (Bangash, 2001). In homogeneous materials, the elastic modulus is a measure of the interatomic bonding forces and is unaffected by changes in microstructure. In the heterogeneous case, such as concrete, the effect of the multiple phases and the resultant variable internal forces, are exhibited by the elastic modulus varying with varying compressive strength.

Portland cement (PC) concrete mixtures are termed particulate composite materials. It consists of a single continuous phase (i.e. HCP) and a single discontinuous particulate phase (i.e. aggregate). The characteristic behaviour of a composite is usually that of the continuous phase (Young, et al., 1998). Portland cement concrete would be expected to be a true brittle but research has shown this not to be the case.

Size effect plays an important role in the behaviour of quasi-brittle bodies. Larger bodies have been noted to behave more brittle while smaller samples more ductile (Karihaloo & Huang, 1991). Quasi-brittle materials generally exhibit measurable deformation prior to failure.

The crack behaviour of PC concrete has been described by many authors (Mindness, et al., 2003).

Prior to any loading being applied, concrete members contain many defects and microcracks (Francois, 1991). The microcracks are mostly concentrated in the porous regions of the mix. The porosity of the concrete increases significantly in the interfacial region at the aggregate surface (DiTommaso, 1984), and therefore more microcracks exist in the interfacial transition zone (Mehta & Monteiro, 2014).

Longer cracks are present on the aggregate surface than elsewhere in the mix. The microcracks influence the deformation behaviour under applied stress, exhibited by the tension softening curve of the stress-strain response.

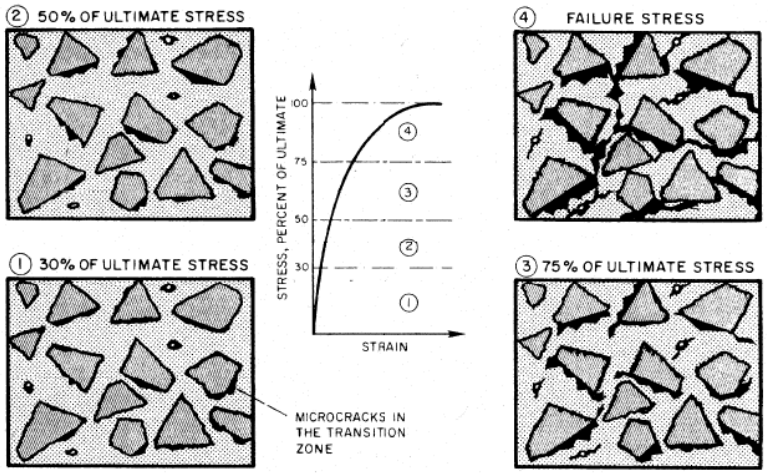

Figure 2-27: Progressive failure in concrete microstructure (Glucklich, 1968)

When a load is applied to a concrete element, at critical stress the cracks at the interface of the aggregate and cement paste begin to grow. The cracks spread through the mortar until reaching an adjacent aggregate, where it deflects. The change in growth direction causes the crack to lose energy, and in this manner eventually contained. With further applied load, crack extension within the solid concrete body resumes. This two-stage propagation process lowers the brittleness of hardened concrete in comparison to the cement paste (Francois, 1991). The process produces diffuse type cracking that allows the element to absorb energy, providing toughness and the typical quasi-brittle response. This is the typical behaviour under compressive loading, illustrated in Figure 2-28.

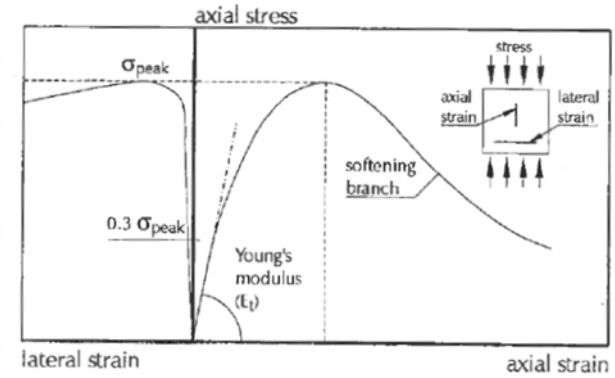

Figure 2-28: Stress-strain curve for concrete under uniaxial compression (Mier, 1997)

The stress strain curve for concrete under uniaxial compression shows linear elastic behaviour up to about 30% of the ultimate strength fc. The microcracks in the interfacial transition zone remaining undisturbed under short term loading at this intensity. With an increase in stresses the curve shows a gradual increase up to about 0,75 f_c to 0,9 f_c. From here it bends sharply, almost flattening at the top, and descends until the specimen fractures. Based on the curve

shape, at an intensity range between 0,30 f_c to 0,50 f_c, the microcracks in the interfacial transition zone show some extension. No cracking appears in the mortar matrix however. Up to this stress level crack propagation is assumed to be stable. When the stress intensity reaches a range between 0,50f_c to 0,75f_c, the cracks become more unstable as crack growth resumes in the interfacial zone. A gradual decline in the elastic modulus and the compressive strength occurs.

The unstable cracking occurs at the stress level of 0,75f_c (i.e critical stress), this also corresponds to the maximum value of volumetric strain. In stress range 0,75f_c and 0,90f_c, the cracks in the interfacial transition zone and mortar connect and complete failure can occur. Above 0,75f_c, concrete shows time dependant fracture, where under sustained stress the cracks formed to this point would cause failure at a stress lower than ultimate f_c. Price and Rush (Mehta & Monteiro, 2014) confirmed this through simulated testing. In the investigation when a sustained stress was 0,90f_c, failure occurred in an hour. When the sustained stress was 0,75f_c, failure was at 30 years. Ople and Hulsbos reported that repeated cyclic loading has an adverse effect on concrete strength at stress levels greater than 0,50f_c. This results from progressive microcracking in the interfacial transition zone and the matrix.

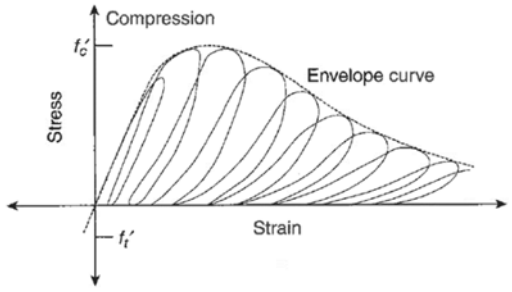

Figure 2-29 Concrete deformation response under repeated uniaxial loading (Mehta & Monteiro, 2014)

The behaviour under uniaxial tension is like uniaxial compression. Tension stresses however produce a more acute effect as crack propagation spreading from the aggregate interface is more rapid. The interval of stable crack propagation is therefore much shorter. The ability to contain cracks, by shielding and aggregate bridging, during growth is greatly reduced in the tension state. Decreased crack containment means failure in tension is caused by a few bridging cracks, whereas compressive failure is due to numerous cracks. These factors give concrete its weakness in tension.

Due to rapid crack propagation under applied tension stress, the descending branch of the stress strain curve has not been easily discernible during experimental testing (Mehta & Monteiro, 2014).

As the compressive strength increases the tensile strength also increases, at a decreasing rate. This means the higher the compressive strength, the lower the tensile to compressive ratio. There is no direct proportionality in the relationship. Testing has shown the ratio is approximately 10 to 11 percent for low-strength concrete, 8 to 9 percent for moderate-strength, and 7 percent for high-strength.

Strength of Concrete (MPa)			Ratio (%)		
Compressive	Modulus of Rupture	Tensile	Modulus of Rupture to Compressive Strength	Tensile Strength to Compressive Strength	Tensile Strength to Modulus of Rupture
7	2	1	23.0	11.0	48
14	3	1	18.8	10.0	53
21	3	2	16.2	9.2	57
28	4	2	14.5	8.5	59
34	5	3	13.5	8.0	59
41	5	3	12.8	7.7	60
48	6	4	12.2	7.4	61
55	6	4	11.6	7.2	62
62	7	4	11.2	7.0	63

Figure 2-30: Relationship between tension and compressive strength of concrete (Mehta & Monteiro, 2014)

A decrease in the porosity of the matrix and the interfacial transition zone results in an increase in compressive strength. Tension strength increase will remain small unless the strength of the hydration products of which the ITZ is comprised is simultaneously improved. This means a concrete with a low-porous ITZ will still be weak under tensile stress if large amounts of orientated crystals of calcium hydroxide are present in the zone. Here the size and concentration of calcium hydroxide crystals can be reduced by a pozzolanic admixture or a reactive aggregate (e.g. a calcareous aggregate) (Mehta & Monteiro, 2014).

Under applied loading a tension zone forms near the tip of a crack where complicated micro failure mechanisms take place. Here microcracking, deflection; crack branching, crack coalescence and debonding of the aggregate from the matrix occurs. These effects provide inelastic toughening mechanisms that coexist with a crack when it propagates. In quasi-brittle bodies, the larger portion can be in an elastic state while locally a crack can simultaneously be developing with a plastic zone at its tip.

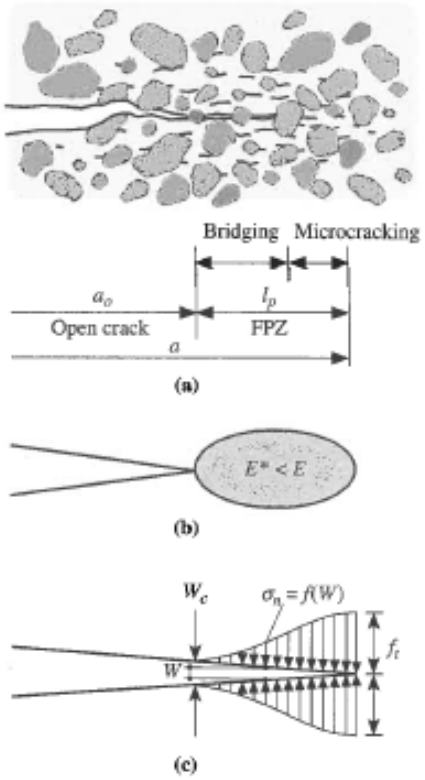

α_o	= actual crack length	f_t	= maximum closure stress at FPZ tip
l_p	= length of fracture process zone	w_c	= critical crack opening displacement
α	= effective crack length		
E*<E	= region of strain softening		

Figure 2-31: Concept of FPZ according to Shi: a) FPZ in front of open crack, b) reduced effective modulus of elasticity inside FPZ, and c) tension softening inside FPZ (Shi, 2009)

Fracture in concrete initiates in the FPZ ahead of an open crack. The FPZ is a partially damaged zone (neither continuous nor discontinuous) with some remaining stress-transferring capabilities through aggregate interlock and various microcracking activities. It is a transition zone between the open crack and intact material. Fracture energy is consumed in overcoming the resistance of various toughening mechanisms to form an open crack at the end of the FPZ. The amount of fracture energy required to break a unit area of concrete is regarded as a material property that determines the fracture behaviour. The relationship (tension softening law of concrete) between cohesive stress and the crack opening displacement determines this (Shi, 2009). The tension softening law, defined by the fracture energy, is the constitutive relationship for the material in the FPZ. As concrete fracture originates within the FPZ, the numerical analysis of cracks starts with deciding how to model the FPZ (Shi, 2009). The stress strain relation of concrete according to the tension softening law possesses two distinctive features:

- A steep descending slope – indicates rapid loss of tensile strength in the initial stage of softening.
- A long tail as the crack opening displacement increases – indicating stress transfer capability of aggregate interlock in the FPZ.

The improvement of ductility is illustrated, by the lengthening of the downward slope of the stress strain response curve (Shi, 2009).

Experimental work to propose numerical crack models has established tension softening law as the basis for fracture mechanics of concrete (Shi, 2009). Two concepts have been accepted in the development of computational theories:

- The discrete crack approach – The FPZ is modelled as a fictitious crack subject to external forces that are equal to the cohesive forces transferred through the FPZ to the elastic regions. This is an accurate mathematical description of the problem.
- The smeared crack approach – The local inelastic deformations in the FPZ are smeared over a band of certain width according to stress strain relations. The FPZ is therefore modelled in a continuous manner. This is an approximate approach to crack analysis.

The fictitious crack model (FCM) proposed by Hillerborg, Modeer and Peterson (1976) first introduced the concepts of fracture process zone and crack opening displacement to crack analysis. These concepts are now the basis of fracture mechanics of concrete. They were developed through Hillerborg's experimentation with uniaxial tension tests on concrete bars.

The studies showed that crack formation in concrete is an evolutionary two stage process:

- Strain build up in the pre-peak region
- Strain localisation and visible crack formation in the post peak region

This basic concept of crack formation is illustrated in Figure 2-32.

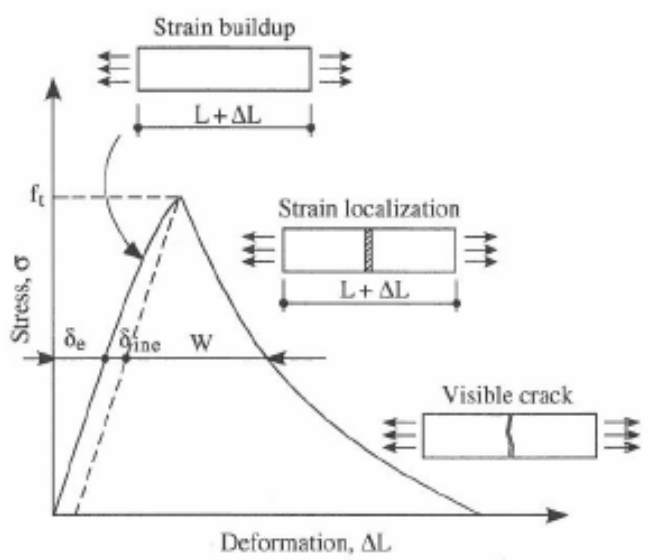

Figure 2-32: Illustration of the evolution of crack formation after Hillerborg, Modeer and Peterson (Shi, 2009)

2.4 Properties that affect flexural crack initiation and propagation

The important parameters for crack analysis are Young's modulus (concrete and rebar), surface pattern of bars, bar spacing, bar diameter, the cover and reinforcement ratio of the section (Borosnyoi & Balazs, 2005).

2.4.1 The Bond Slip relationship of concrete and reinforcement (Macro-level)

The stress transfer between tension bars and concrete is referred to as bond. The anchorage of the bars within a concrete member is dependent on the nature of bond (Mahran, 2013). Crack width and spacing is proportional to the bond stress, which is defined by the steel and concrete interaction. Bond stress is the equivalent unit shear stress acting parallel to the reinforcing bar at the concrete and bar interface. The force in the rebar varies along its length due to force transfer through bond stress development. Bond stress is related to the rate of change of steel stress (Mahran, 2013).

An adhesion surface exists between the concrete and rebar. Slip resistance is given by the shear strength of fine concrete particles that fill the indentations on the rebar surface (Bangash, 2001). When slip failure occurs the concrete surrounding the rebar is crushed and the value of the adhesion force is zero. Once slip failure occurs, bond generally relies on the friction at the failure surface. Larger slip lengths cause this friction resistance to become zero as well. (Bangash, 2001). The following meso-level contributions to bond-slip have been identified (Mier, 1997).

- Crack growth in the weak interface layer between concrete and steel
- Crack growth from the ribs of deformed rebar
- Frictional slip between steel and concrete after the cracks have developed

Ingraffea, et al and Mier (Mier, 1997) identified the following manifestations of bond slip action:

- Elastic deformation
- Crushing - Where concrete bears on ribs of rebar
- Secondary radial cracking – From the mechanical interlock of ribs causing wedging forces.
- Longitudinal splitting cracking

In regions of high stress at the rebar perimeter, bond behaviour is related to confining pressure and steel strain, in addition to the bond stress and slip. These are the main variables defining bond (Mahran, 2013). In bond experiments the following has been noted according to Mahran:

- When confinement is not provided, for example by closing rebar such as stirrups, bond stress disappears as soon as longitudinal cracks develop through the cover.

- The concrete cover also provides confinement through tensile hoop stresses prior to cracking.
- Bond stress is higher when bars are pushed rather than pulled.
- The ultimate resistance at large slips appear to be of the coulomb friction type.

The work of Rehm (Mahran, 2013) characterised the bond behaviour of deformed bars under increasing applied load:

1. Adhesion phase (chemical and physical) – This is present due to the cement fines and rough surface of the bar. Failure results in very small displacements.
2. Bearing phase – When the slip is mainly due to the compression of the concrete lodged between the rib.
3. Shearing phase - At higher loads the concrete between the ribs are sheared. If the ribs are closely spaced, $^{c}/_{a} < 7$, the fracture pattern extends over the full member length and the slip is increased by sliding at the fracture face. With widely spaced ribs, the fracture is limited to a wedge shape. This failure does not result in immediate change in slip when restraining rebar is present, and more load can be absorbed before complete shearing occurs.

The difference in rib spacing has the following influence:

- When the rib spaces are wide the initial fracture occurs at a lower load.
- The full resistance obtained with close ribs depends on the inclusion of lateral restraint to resist wedging action.

Mahran created a numerical bond behaviour model to illustrate the distribution of the various actions around a steel bar by using the shape and properties of a reinforcing bar and the properties of concrete. This is used here to illustrate the extent of the bond contribution actions along the bar length. It can be noted the radial stresses and longitudinal bond stresses are highest immediately adjacent to the load application, at the side of the high compressive stresses caused by bearing. The deformation strain (tensile strain) is highest away from the load application indicating the increase in tensile strength in the concrete away from the crack.

The surface condition of the reinforcement and the concrete composition can play an important role in the bond relationship (Holly & Bilcik, 2013).

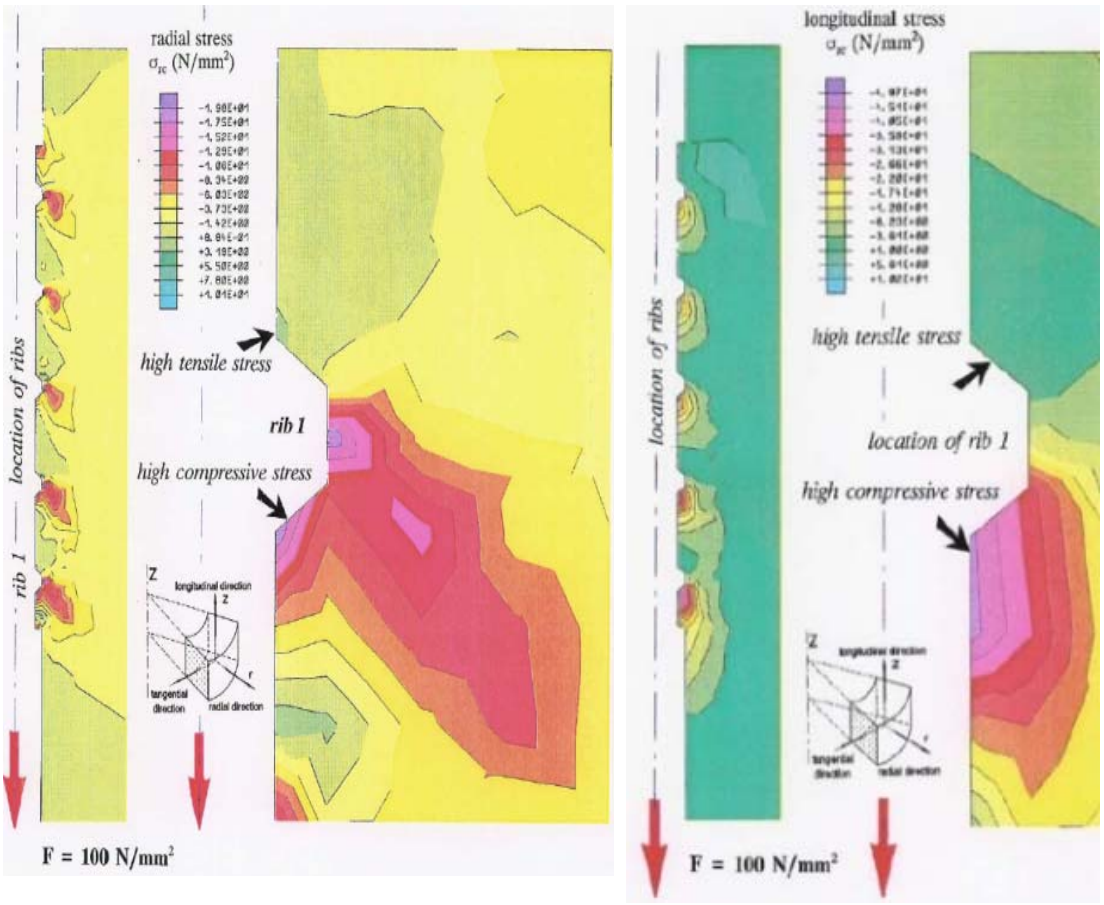

Radial bond stress *Longitudinal bond stress*

Figure 2-33: Results of numerical bond stress model within the embedment length by Mahran (Mahran, 2013)

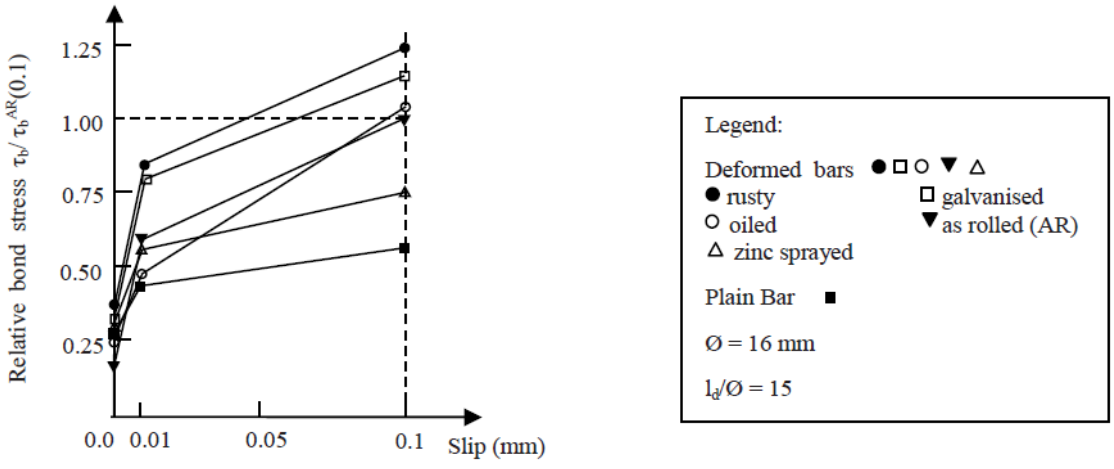

Figure 2-34: Effect of various surface conditions on bond stress (Holly & Bilcik, 2013)

The most common cause of a compromised steel surface is due to surface corrosion. Build-up of corrosion products at the interface between concrete and steel weakens the bond

between rebar and concrete (Holly & Bilcik, 2013). The difference of bond strength varies with corrosion build-ups between two opposing effects:

- A small increase under initial corrosion due to the expansive nature of ion-oxides
- A drastic reduction in the region of 50% or more due to the build-up of soft products at the interface.

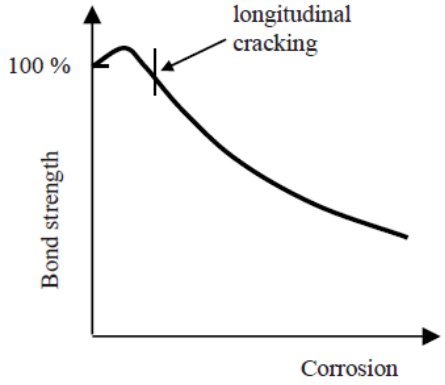

Figure 2-35: Variation in bond strength with corrosion (Holly & Bilcik, 2013)

Corrosion contributes to the loss of bond stress in the following ways (Holly & Bilcik, 2013):

- Loss of mechanical interlock between ribs due to degradation of the bar ribs and reduction of the cross-sectional area.
- The lubricating effect of the build-up material from the corrosion process and the adherence of this to the concrete.

Literature indicates the provision of confinement (secondary) reinforcement assists in retarding the loss of bond due to corrosion. Less brittle bond behaviour and a higher bond stiffness has been noticed in specimens tested. Studies were performed by Auyeem (Holly & Bilcik, 2013) that confirmed the inclusion of confinement rebar provides a means to counteract bond loss. An observation was noted that for low diameter loss a bond stress reduction of 80% could be avoided with the inclusion of confinement steel. Corrosion bond models are available in the fib code and formulas for the provision of secondary reinforcement have been published by Chairns and Holly.

2.4.2 Modulus of Elasticity and creep

The differences in the modulus of elasticity of concrete and steel and its role on crack formation has been noted in sections 2.2.1 and 2.2.2.

this report. The deformation response of the two materials are as follows:

- Concrete has quasi-brittle response – Displays a softening response with lower strain before failure.

- Steel has ductile response -Absorb more strain before failure.

In crack analysis, this relationship is represented by the modular ratio. The ratio of the steel modulus E_s and the concrete modulus E_c provides the unitless value:

$$\alpha = \frac{E_s}{E_c} = \frac{f_s}{f_c} \quad (7)$$

It by default refers to the stress relationship due to applied load (McCormac & Brown, 2009). The relationship exists due to the assumption of elastic beam theory where strain difference is zero (no slip). The ratio of the steel modulus E_s and the concrete modulus E_c is therefore proportional under increasing stress. The ratio indicates the degree of elastic mismatch where the higher the ratio, the sooner the material of lower elasticity will crack. The value points to the likelihood of differential cracks propagating around the reinforcement. The strain differences cause slips in the bond under tensile load. After a crack is formed, compatibility of strains is maintained at the crack vicinity only if relative displacements (slips) are accounted for in the intact concrete (load transfer lengths). This consideration forms the basis of crack width design and analytical formulations in design codes exist to account for this (Borosnyoi & Balazs, 2005).

2.4.3 Tension softening and stiffening effects

The stress in the cracking region will gradually decrease from maximum tensile stress f_t to zero as the crack width w develops from zero to the maximum width w_u. Based on tensile effects, a reinforced concrete member can be divided into two critical regions (Xu, et al., 2017).

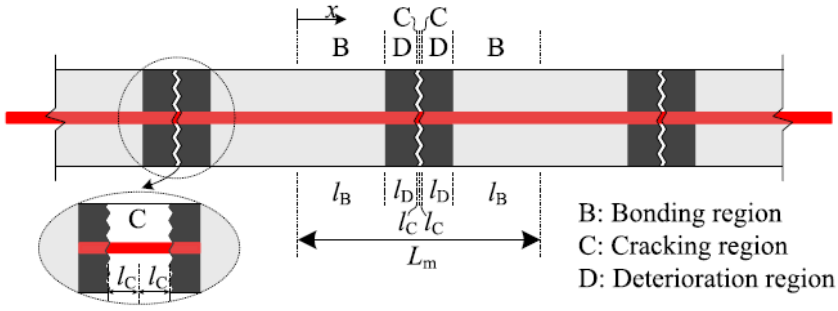

l_B	= length of tension stiffening region
l_C	= length of tension softening region
l_D	= length of bond deterioration
L_m	= average crack spacing

Figure 2-36: Regions of concrete member under tensile load (Xu, et al., 2017)

- The bonding region (region B) - the tension stiffening region where the bar is stiffened through bond-slip interaction.

- The cracking region (region C) - the tension softening region where the cracks form (the crack opening).

In region D, the bond relationship deteriorates. Bond action gradually diminishes as the crack width reaches a certain large value. Simultaneously the tension stiffening effect gradually decreases until vanishing completely (Xu, et al., 2017).

a) Tension softening

In elastic design, the tensile capacity of concrete is ignored since this value is much less in comparison to the compressive strength of the concrete. Theoretically plain concrete has some tension capacity, even after localised cracking due to tension softening (quasi-brittle behaviour). In quasi-brittle materials cracks are preceded by localised dispersed microcracking in a large fracture process zone ahead of the crack tip. Small amounts of strain energy are converted to create new crack surfaces and absorbed in this zone providing some ductility. (Alam, et al., 2010).

b) Tension stiffening

The decreasing bond stresses at the edge of a crack means this region takes up less load and therefore less strain. These regions therefore stiffen. The stiffening effect wears off incrementally further from the crack as more load is again transferred, and the steel in turn stiffens. The load reduction in the tension bars reduces tension strain and thereby the elastic strain value in a cracked section analysis.

The average rebar strain between two adjacent cracks is a function of the maximum strain in the crack (ϵ_{s2}) and the effect of this tension stiffening ($\Delta\epsilon_s$) on the steel. The expression representing this relationship is as follows: $\epsilon_{sm} = \epsilon_{s2} - \Delta\epsilon_s$.

The theory of tension stiffening allows concrete to have tension capacity after cracking. This effect increases the flexural stiffness of the member. In Figure 2-37 strain distributions of the reinforcement, the concrete and the bond stress distribution along the element are schematically represented. Tension stiffening reduces under sustained long-term loading or repeated loading (Balazs, 2013). This is linked to the loss of stiffness between cracks concrete experiences under long term repeated loading. After initial cracking, increasing load will lead to breakdown in the bond between the reinforcement and the concrete.

In the range of steel stress limitation 0.8fy, the tension stiffening effect is negligible, and it would appear reasonable to ignore tension stiffening in certain design applications (Clark, 1983). If ignored in cases where it was applicable, disregarding the effect could indicate structures that are behaving acceptably should be failing (Beeby, 1979). In Figure 2-38 the

effect of increasing load on increasing bar strain can be seen. The graph shows how the effect tapers off with increasing load.

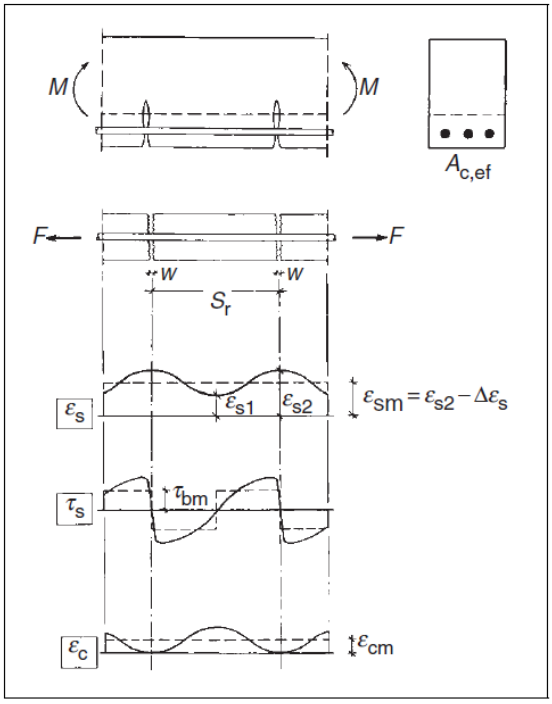

M	= moment	ε_{s1}	= minimum strain in steel
F	= axial force in tension steel	ε_{s2}	= maximum strain in steel
W	= crack width	τ_{bm}	= bond stress
S_r	= crack spacing	ε_{cm}	= average concrete strain
ε_{sm}	= average steel strain	$A_{c,ef}$	= effective tension area of concrete

Figure 2-37: Development of strain and bond stresses at bonded reinforcement (Borosnyoi & Balazs, 2005)

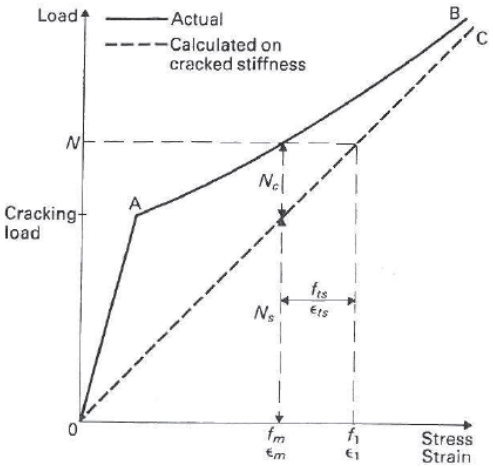

Figure 2-38: The effect of increasing load on deformation with and without tension stiffening (Clark, 1983)

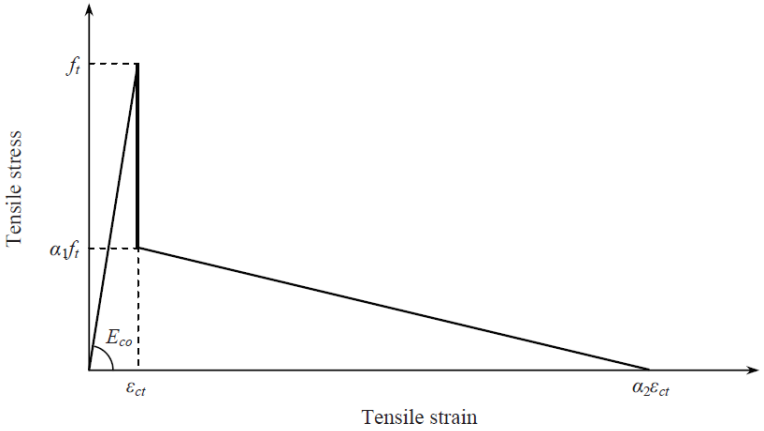

Figure 2-39: Proposed tension stress block by (NG, et al., 2011)

Various analytical formulas are available in design codes to estimate strain reduction. A method is proposed by Scott, Beeby and Lam (NG, et al., 2011) whereby the tension stiffening effect may be accounted for using a tensile stress block in the section analysis.

A stress block was derived by testing of beams (NG, et al., 2011). In the ascending branch, the tensile stress increases linearly to the tensile strength of the concrete at a gradient equal to the initial elastic modulus of elasticity of the concrete. In the descending branch, the tensile stress decreases linearly from a certain tensile stress to zero at the ultimate tension strain. The equations for the tensile stress block are shown here in Figure 2-40. The accuracy of the tensile stress block has been verified by section and member analysis carried out by Lam.

$$\sigma = E_{co}\varepsilon \qquad \text{for } \varepsilon \le \varepsilon_{ct}$$

$$\sigma = \frac{\alpha_1 f_t(\alpha_2\varepsilon_{ct} - \varepsilon)}{(\alpha_2\varepsilon_{ct} - \varepsilon_{ct})} \qquad \text{for } \varepsilon_{ct} < \varepsilon \le \alpha_2\varepsilon_{ct}$$

$$\sigma = 0 \qquad \text{for } \alpha_2\varepsilon_{ct} < \varepsilon$$

Figure 2-40: Equations for deriving tensile stress block (NG, et al., 2011)

2.4.4 The size effect

In larger structures, the energy absorbed in the fracture process zone is negligible in comparison with the energy absorbed to create new fractures (Bažant, 2002). Many flaws and discontinuities exist in a concrete's microstructure, acting as points of higher stress concentration. Due to the increased quantity of micro flaws a larger concrete body has lower nominal strength. Bazant and Planas identified the following relevant size effect (Bazant & Planas, 1997):

1. Statistical size effect – These results from the randomness of constituent material strength.
2. Fracture mechanics of size effect – This result from the release of stored energy of the structure into the front of the fracture.

In experimental research the analytical model of Eurocode 2 underestimated the crack width when comparing the results of three point bending tests on three rectangular beams of different sizes (Alam and Loukili 2009). The beams in the testing had the following properties:

- The tensile reinforcement ratio was kept constant
- Cover varied proportionately with the overall beam size.
- The concrete was made with cement PC52,5.

The measurement of crack opening displacement and crack spacing done by digital image correlation. The width obtained using digital image correlation was plotted against the calculated expected results from Eurocode as a function of the steel strain.

The conclusions from the experiments were as follows:

- At low strains and small beam sizes, measured values more or less agreed with the calculated values from Eurocode.
- When the strain is higher the difference between the measured and calculated values increases.
- There is therefore a significant size effect on the experimental crack width and spacing that is not incorporated in the Eurocode design formula.

2.5 Estimation of expected crack behaviour

Borosnyoi & Balazs (Lapi, et al., 2018) identified four methods for calculating crack width:

- Analytical methods by solving the differential equation of bond slip.
- Semi-analytical equations where the models include simplifications in either the bond stress or the strain values.
- Empirical relationships identified based on the comparison of a large amount of experimental data.
- Numerical modelling.

A model can be constructed in two forms, where it can be physically built or based on mathematical formulation (mathematical model). Mathematical models are used most extensively in modern engineering as these are more versatile. (Pinder & Herrera, 2012). Mathematical models integrate scientific and technological knowledge with the purpose of predicting system behaviour. (Pinder & Herrera, 2012). This knowledge is computational and can be written in computer code and spreadsheet format. When analysing a system, the general procedure used to predict its behaviour is by modelling the system. A model of a system is to be considered as a surrogate whose behaviour mimics that of the system. (Pinder & Herrera, 2012)

The earliest crack prediction methods were based on empirical relationships from regression analysis of large ranges of experimental data performed on physical concrete specimens (Beeby, 1979).

The results could vary dependant on the type of specimen, method of loading as well as type of reinforcement (Frosch, 2014).

Empirical methods were generally based on deformed bars being used in the concrete section. With new types of reinforcement in use in recent decades, estimates based on older empirical methods are not always applicable (Yamato, et al., 2008).

Crack width estimation involves modelling the variance in strain between reinforcement under tension and the surrounding concrete. Analytical models for this bond relationship have been investigated by various researchers, and numerous formulas have been presented (Lapi, et al., 2018).

2.5.1 Numerical models

Numerical models for the estimation of concrete crack behaviour are based on the theories of fracture mechanics. Fracture mechanics within the field of concrete is a developing field and

the use of the available models were accepted more recently than other crack determination approaches (Shi, 2009).

The contribution of the macroscopic interaction of the materials in the mixture to the behaviour of the composite is reliably modelled by classical linear, nonlinear and continuum approaches. Bazant has listed 5 reasons why numerical methods using the fracture mechanics approach should be considered in crack analysis (Bazant & Planas, 1997):

- The methods account for the energy required for cracks to form
- The objectivity required in analysing a structure
- The analysis must agree with the absence of a yield plateau from the load deflection diagram.
- The analysis must provide a means to compute the energy absorption capability and ductility.
- The analysis must capture the size effect

Fracture mechanics theories of failure determine cracking paths by energy criteria. It considers propagating cracking throughout the structure rather than focusing on a failure surface. An acceptable form of fracture mechanics to model the heterogeneous relationships in the concrete microstructure was introduced in the 1980's (Bazant & Planas, 1997). Numerical methods are used to model these relationships. The main advantage of these methods is it allows the inclusion of the size effect in concrete crack analysis (Alam, et al., 2010). As concrete exhibits tensions softening past the point of ultimate tensile stress researchers have postulated a design approach based on fracture theory being the most appropriate (Bažant, 2002).

Mathematical models based on numerical simulation permit the study of complex systems and natural phenomena that are very costly or impossible to study by direct experimentation (Bangash, 2001). There are two generally accepted computational theories in fracture analysis namely the smeared crack approach and the discrete crack approach (Shi, 2009). The methods apply finite element models to represent cracking in a structural concrete continuum.

2.5.2 Analytical formulations

When slip failure occurs, compatibility of strains over the transfer length is achieved when strain differentials are accounted for. This is done by considering the fundamental relationship of bond slip (Lapi, et al., 2018). A rigorous formulation of crack widths is obtained by the integration of the actual strains of reinforcement and concrete between cracks based on accumulated slips. The slip between rebar and concrete is defined by the following integral:

$$s(x) = \int_0^x [\,\epsilon_s(x) - \epsilon_c(x)]dx \qquad (8)$$

(Borosnyoi & Balazs, 2005)

With the variation of the slip along the rebar length x being given by the following:

$$\frac{ds(x)}{dx} = \epsilon_s(x) - \epsilon_c(x) \quad (9)$$

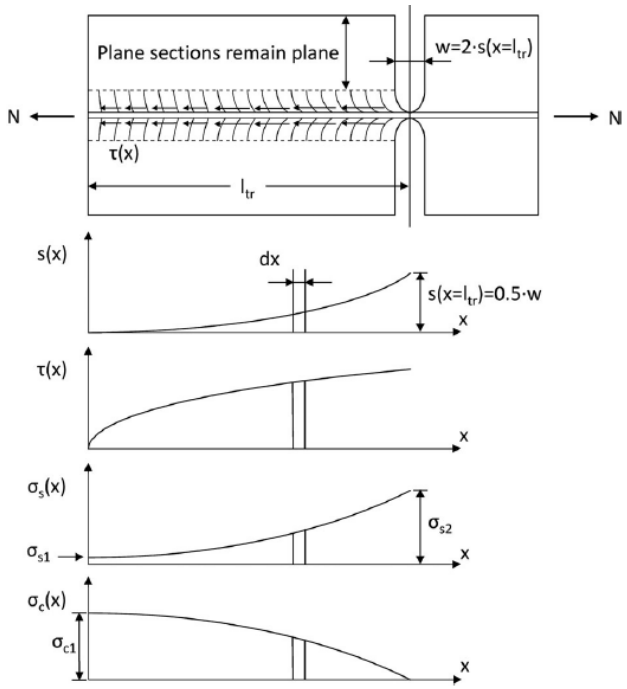

N	= axial force in tension steel	σ_{sX}	= steel stress
W	= crack width	σ_{cX}	= concrete stress
l_{tr}	= transfer length	dx	= relative slip distance
$S_{(x)}$	= slip between rebar and concrete		
$\tau_{(X)}$	= bond stress		

Figure 2-41: Distribution of stresses and slip near a crack according to non-linear bond-slip relationship (Lapi, et al., 2018)

2.6 Fundamental analytical theory

This section examines the fundamental theory leading to the semi-analytical formulas in design codes.

The basis of analytical theory dictates that the crack formed due to the extension of an axial tie, is fully contained in the crack (Beeby & Narayanan, 2005).

Pioneering crack theory was introduced by Salinger in 1936, where the spacing of cracks on the tension face of concrete adhered to defined boundary conditions as follows (Beeby, 1979):

- The minimum crack spacing is the distance (S_r) from zero stress (crack edge) to the point where stress reduction (tension stiffening) wears off.
- In regions outside the S_r length of adjacent cracks, tensile stresses can exceed concrete capacity and a new crack can form.
- When all cracks on the tension face have formed, the maximum spacing is the influence distance S_r of adjacent cracks.
- The crack pattern on the face therefore adheres to the boundary condition:

$$S_r < S < 2\,S_r \qquad (10)$$

This is based on assumptions of transfer lengths existing between cracks:

The compatibility relationship between average crack width, average final crack spacing, and strain thereby exists being in the form (Mosley, et al., 2012):

$$w_m = S_m\,\epsilon_m \qquad (11)$$

2.6.1 Average crack spacing

The value for average crack spacing was determined from the relative slip. The two fundamental bond assumptions at the steel-concrete interface was applied.

a) *Slip approach*

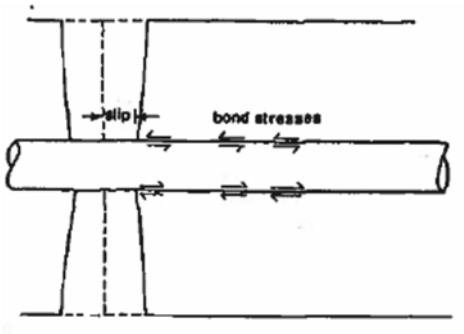

Figure 2-42: The slip approach (Beeby, 1979)

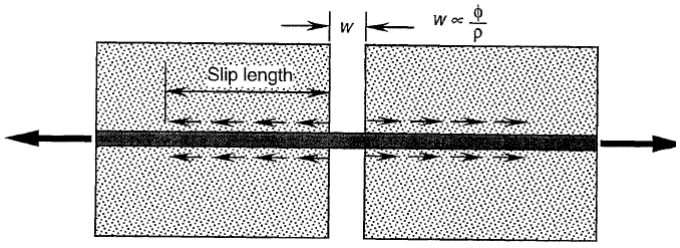

Figure 2-43: Bond slip model (Carino & Clifton, 1995)

The approach is based on the crack behaviour of an axial tie in pure tension, where plane sections remain plane and concrete stress is uniform across the entire section. It is assumed compatibility of strains between steel and concrete is not maintained, and bond failure through slip occurs at each crack location. Tensile force is transferred between the rebar and the concrete through bond stresses away from the crack. The distribution of bond stresses along the rebar between cracks is a function of ultimate bond strength (Beeby, 1979).

The following relationship for S_r (also referred to as S_o) was created by these assumptions:

$$S_o = k_1 \frac{\emptyset}{\rho} \frac{f_t}{\tau_{ult}} \quad (12)$$

- k_1: A constant dependant on the shape of bond stress distribution
- $\emptyset$: Bar diameter
- ρ : Reinforcement ratio
- $\frac{f_t}{\tau_{ult}}$: The ratio of tensile and ultimate bond strength of concrete.

Research found for a bar type, τ_{ult} was directly proportional to f_t, therefore the compatibility equation could be written as follows (Beeby, 1979).

$$w_m = K \frac{\emptyset}{\rho} \epsilon_m \quad (13)$$

The coefficient K was found experimentally in a manner that made assumptions on bond stress distribution, minimum, maximum and average crack widths and spacing irrelevant (Beeby, 1979).

b) *Non-slip approach*

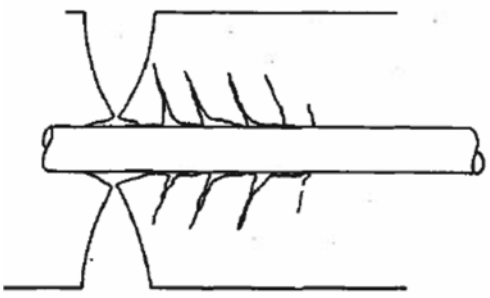

Figure 2-44: The non-slip approach (Beeby, 1979)

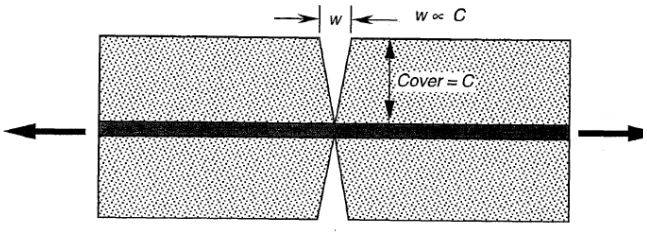

Figure 2-45: No slip model (Carino & Clifton, 1995)

This approach is more relevant to beam action than the slip approach. Plane sections do not remain plane and stresses are not uniform across the section. The estimation of stresses in the concrete is not as simple. No slip occurs at the crack locations, therefore no bond failure. The distance from the crack to the position where stresses are not influenced by the crack (S_r) equals the cover (Beeby, 1979).

These assumptions produced the following crack width equation:

$$w_m = K\, c\, \epsilon_m \quad (14)$$

c) *Combined theory*

The slip and non-slip approaches were considered different components of the same problem simultaneously applicable (Beeby, 1979).

- Non-slip approach always applied as locally close to a crack, plane surfaces would never remain plane. This will reduce stress in surface concrete close to the crack.
- When bond slip occurred, a further reduction of stress would result. This increases the value of S_r.

Crack spacing value was considered to consist of two components.

- S_{o1} – value derived from non-slip approach
- S_{o2} – value derived from bond failure approach

Ferry and Borges (Beeby, 1979) found the two components could be added together to obtain the fundamental theory for mean crack spacing.

$$S_m = K_1 c + K_2 \frac{\emptyset}{\rho} \quad (15)$$

(Ferry-Borges equation)

This formula was found to provide good predictions for axially reinforced square sections under pure tension.

The empirically obtained K coefficients accounted for the following:

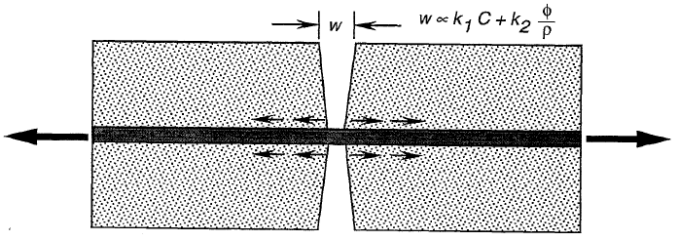

Figure 2-46: Combined approach (Carino & Clifton, 1995)

- K_1 = this factored the influence cover depth has on the surface stress influence distance determined by the probability of the average crack value being exceeded. (applicable to no bond failure)
- K_2 = this factored the influence of shape of bond distribution, bond strength, reinforcement ratio and bar diameter. (applicable to bond failure)

The estimation of reinforcement ratio is dependent on the type of stress:

- Pure tension members consider the full cross section for ρ.
- Flexural members consider an area around each bar where the centroid of area is the bar centre.

This formed the basis of the crack width model in CEB recommendation 1970, the model from which Eurocode 2 and fib codes were derived (Balazs, 2013).

Assuming the stress developed is proportional to the rate of development of internal failure, the crack spacing is given by the Ferry-Borges expression. The formula can therefore be applied generally and is independent of the form of internal breakage (Beeby, 1979).

2.6.2 Tension stiffening

The maximum value for tension strain equals the strain obtained by elastic analysis of a crack section. Since the concrete between the cracks carries considerable stress, stiffness is increased. Tension stiffness is allowed for by reducing the elastic strain with an appropriate tension stiffening allowance (Carino & Clifton, 1995).

A reasonable general formulation was found from the following (Beeby, 1979):

$$\Delta\boldsymbol{\varepsilon_s} = \boldsymbol{K}\frac{\boldsymbol{f_t f_{scr}}}{\boldsymbol{E_s \rho f_1}} \quad (16)$$

Where:

$\Delta\varepsilon_s = tension\ stiffening\ correction\ at\ the\ level\ of\ the\ reinforcement$

$f_t = tensile\ strength\ of\ the\ concrete$

$f_1 = steel\ stress\ under\ the\ load\ considered\ calculated\ on\ the\ basis\ of\ a\ cracked\ section$

$f_{scr} = is\ the\ steel\ stress\ at\ cracking\ calculated\ on\ the\ basis\ of\ a\ cracked\ section$

$E_s\rho = the\ Young's\ modulus\ of\ steel\ and\ the\ reinforcement\ ratio$

$K = Constant\ that\ depends\ on\ the\ bar\ type\ and\ the\ manner\ in\ which\ \rho\ is\ calculated$

Simplifications were made to the tension stiffening equation with the following approximations:

- $\frac{f_t f_{scr}}{E_s} was\ assumed\ equal\ to\ 0.7\ \text{x}\ 10^{-3}$
- $f_1\ (elastic\ steel\ stress\ in\ the\ cracked\ section) was\ taken\ as\ equal\ to\ 0.58 f_y$

Extending the strain to the level of the tension face gave the following relationship.

$$\Delta\boldsymbol{\varepsilon} = \frac{\boldsymbol{1.2bh}}{\boldsymbol{A_s f_y}}\ \mathbf{x}\ \mathbf{10^{-3}} \quad (17)$$

To reduce this value linearly to zero at the neutral axis, the formula adjusted to:

$$\boldsymbol{\epsilon_m} = \boldsymbol{\epsilon_1} - \frac{\boldsymbol{1.2\ b_t h\ (\alpha' - x)}}{\boldsymbol{A_s f_y (h - x)}}\mathbf{x}\ \mathbf{10^{-3}} \quad (18)$$

$\alpha' = distance\ to\ the\ crack\ position\ from\ the\ compression\ face$

3. EXAMINATION OF ANALYTICAL MODELS IN CONCRETE CODES

The analytical equations in concrete codes provide semi-analytical solutions to the bond slip relationship. The methods proposed by the following codes are investigated in this section:

- Eurocode 2 – European standard for the design of concrete structures
- Fib model code – The set of documents is intended to be used as a model code for the development of future national codes. The present Eurocodes were based on earlier versions of this document.
- ACI 318:14 - Technical standards document issued by the American concrete institute.
- British Standards BS8110 & BS5400 – In 2010 these codes were superseded by the Eurocode 2 with the relevant clauses included in the British National Annex.
- South African National standard 0100-1 (SABS 0100-1) – Technical standard for the design of reinforced concrete. Currently still the official national standard but to be replaced by Eurocode 2.

The Eurocode, fib and ACI codes are modern codes based on more recent research and design technology. The ACI codes is revised every 6 years.

The design methods in the concrete codes model the relative slip between concrete and rebar under tensile strain. The stress gradient between the tension zones and the concrete surface is also considered.

The actual variation in crack widths in reinforced concrete elements are quite wide and cannot be calculated to a precise level (Mosley & Bungey, 1990). Crack scatter, resulting in varying widths over the surface, are inherent due to heterogeneity.

Due to inherent randomness, the values for crack widths and crack spacing are scattered. The frequency distribution of crack widths is roughly log-normal (Lapi, et al., 2018), therefore the maximum crack width is associated with a specified probability of being exceeded.

The calculated widths are maximum values that will not be exceeded by a percentage of cracks over the surface of the tension region, termed probability of exceedance. The probability of the cracks widths not being exceeded are as tabulated in Table 3-1.

Table 3-1: Probability of crack widths not being exceeded

Code	PROBABILITY OF EXCEEDANCE
British standards	80%
Eurocode/FIB	95%
American	90%

In cracked sections compression and tension stress limits are placed on the concrete and steel respectively.

Table 3-2: Table of limits from the code provisions

PROPERTY	BS8110/ BS8007	BS5400	SABS 0100-1	Fib MC2010	Eurocode 2	ACI 318
Compressive stress in triangular block	$0.45f_{cu}$ (BS8007-Appendix B2)	$0.5f_{cu}$ Table 2	$0.45f_{cu}$ Stress-strain design graph	$0.6f_{ck}$ Clause 7.6.3.3	$0.6f_{ck}$ Clause 7.2	$0.45f_{c'}$ Stress-strain design graph
Stress in rebar	$0.8f_y$ (BS8110-2 Clause 3.8.3	$0.75f_y$ Table 2	$0.8f_y$ Appendix A3.2.1	$0.8f_{yk}$ Clause 7.6.3.3	$0.8f_{yk}$ Clause 7.2	$0.6f_y$ Clause 7.2

Where
f_{cu} = characteristic compressive cube strength of concrete at 28 days
f_{ck} = characteristic compressive cylinder strength of concrete at 28 days
$f_{c'}$ = compressive cylinder strength of concrete at 28 days
f_y = yield strength of reinforcement
f_{yk} = characteristic yield strength of reinforcement

The codes specify characteristic loads to be used in the serviceability analysis of crack width. The British standards (BS8110/BS8007) indicates the full live load to be applied, referring to this as conservative. Later codes require a quasi-permanent portion of the live load to be differentiated from short term live load.

In deriving the basic relationships of fundamental analytical theory, the conditions in the tension zone of a flexural member were assumed to be identical to those of a pure tie. This was found experimentally not always to be true. The codes have their own unique methods of accounting for beam action.

3.1 British Standards

The British codes refer to serviceability crack analysis as a non-critical design case, where characteristic loads are used (BS8110-2: clauses 2.3.2 and 3.6).

3.1.1 Estimating crack spacing

Beam action is considered by the behaviour of an unreinforced concrete column under an eccentric load (Beeby, 1979). The height of the resulting crack forming on the tension face was experimentally found to be equal to the influence distance over which the surface stress is reduced away from the crack.

The spacing of the crack pattern is thereby limited as follows (Beeby, 1979):

$$h_{cr} < S < 2\,h_{cr}$$; where h_{cr} is the crack height.

This showed a stable crack pattern was possible without the inclusion of rebar.

The crack width for the case of the unreinforced section was found to be given by the formula (Beeby, 1979):

$$\boldsymbol{w} = \boldsymbol{K_1\, h_{cr}\, \epsilon_m} \quad (19)$$

K_1 is the same coefficient as in the fundamental theory for no bond failure.

When reinforcement is added, the unreinforced model is added to the pure tension Ferry-Borges formula.

The interaction was studied, and two scenarios were found (Beeby, 1979):

- With a small h_{cr} and reinforcement ratio, the spacing or width calculated from Ferry-Borges was larger than the formula considering crack height.
- With a large h_{cr} the Ferry-Borges equation gives a width smaller than the equation considering crack height.

The Ferry-Borges expression for pure tension had to include an allowance for crack height:

- For the minimum crack width (w_o), the height h_{cr} equals the cover c.

The crack width then equals $K_1\, h_{cr}\, \epsilon_m$. The reinforced and unreinforced combination becomes:

$$\boldsymbol{w} = \left(\boldsymbol{K_1\, c + K_2\, \frac{\emptyset}{\rho}}\right)\boldsymbol{\epsilon_m} = \boldsymbol{K_1\, h_{cr}\, \epsilon_m} \quad (20)$$

Where K_2 = 0. Implying bond is not relevant for the limiting case.

- The maximum crack width (w_{lim}) in flexure is for the unreinforced case.

The Ferry-Borges equation was thereby extended for flexural situations to the following:

$$\boldsymbol{w} = \left(\boldsymbol{K_1\, c + K_{2,1}\, fn\, \left(\frac{c}{h_{cr}}\right)}\right)\boldsymbol{\epsilon_m} \quad (21)$$

Experiments further showed the behaviour of cracks close and further away from the rebar were influenced differently (Allen, 1988):

- Directly over the rebar the extension of Ferry-Borges for flexural situations was valid.
- Further away from the bar, behaviour of the unreinforced flexural section was more relevant.

Where the crack position on the concrete surface was defined by a_{cr}, the distance from the surface to the nearest longitudinal bar, the following hyperbolic relationship was developed:

$$\boldsymbol{w} = \left(\frac{\boldsymbol{a_{cr} w_o w_{lim} \epsilon_m}}{\boldsymbol{c w_{lim} + (a_{cr} - c) w_o}}\right) \quad (22)$$

Where:

$w_k = the\ design\ crack\ width$

$w_o = crack\ width\ directly\ above\ the\ rebar$: $S_m = K_1\, c + K_2\, \frac{\emptyset}{\rho}$ (Ferry-Borges)

$w_{lim} = crack\ controlled\ by\ the\ crack\ height$: $S_m = K_1\, h_{cr}$

$c = concrete\ cover$

The application of this hyperbolic formula was simplified further as follows:

The design procedure in the British code assumed that characteristic loads have a 5% chance of occurring during design life. A crack this rare was unlikely to have a serious impact on durability. Therefore, while applying characteristic loads in the formula, the chance of the crack value being exceeded was increased to 20%, thereby providing a less conservative value.

- The Ferry-Borges equation was simplified to:

$$\boldsymbol{w_0 = 3\, c\, \epsilon_m} \quad (23)$$

The following reasons were considered:

The design width will mostly occur at the maximum distance away from a bar. The variable controlling crack width above a bar is the cover and to a lesser degree $\frac{\emptyset}{\rho}$. This ratio is then ignored. The coefficient K_1 is increased to approximate these secondary influencing factors.

- The equation for crack width away from the rebar was simplified to:

$$\boldsymbol{w_{lim} = 1,5\, (h - x)\, \epsilon_m} \quad (24)$$

The crack height h_{cr} is assumed to be proportional to $(h - x)$. A 20% probability of being exceeded was also incorporated.

When w_0 and w_{lim} are substituted into the orginal hyperbolic formula, the following expression is obtained:

$$\boldsymbol{w} = \left(\frac{3 a_{cr} \epsilon_m}{1 + 2\frac{(a_{cr} - c)}{(h - x)}}\right) \quad (25)$$

Section 3.8.1 of BS8110 states this formula should be used with caution in members subjected mainly to axial tension.

3.1.2 Estimating effective cracking strain

An assumption was made that the tensile stress between cracks at the tension face equals $\frac{2}{3}\ MPa$ (Allen, 1988). This equates to a stiffening force for concrete in tension equal to the following:

$F_{stiff} = \frac{b_1(h-x)}{3}$; this results in an effective value for strain reduction equal to,

$\Delta\varepsilon_s = \frac{b_1(h-x)}{3\ E_s A_s}$; since strain equals $\frac{F}{E_s A_s}$

The average value for steel strain thereby equals:

$$\boldsymbol{\varepsilon_{sm} = \varepsilon_s - \frac{b_1(h-x)}{3\ E_s A_s}} \qquad (26)$$

When considering a position on the concrete surface a distance α' from the compression face, the average value of strain here equals:

$$\varepsilon_m = \frac{(\alpha' - x)}{(d-x)}\ \text{x}\ \varepsilon_{sm}$$

$$= \boldsymbol{\varepsilon_s\ \text{x}\ \frac{(\alpha'-x)}{(d-x)} - \frac{b_1(h-x)}{3\ E_s A_s}\ \text{x}\ \frac{(\alpha'-x)}{(d-x)} = \varepsilon_1 - \varepsilon_2} \qquad (27)$$

The variables can be understood from Figure 3-1 where:

ϵ_m $= is\ the\ average\ strain\ at\ the\ level\ where\ the\ cracking\ is\ being\ considered$

ϵ_1 $= is\ the\ the\ strain\ at\ the\ level\ considered\ calculated\ on\ the\ basis\ of\ a\ cracked\ section$

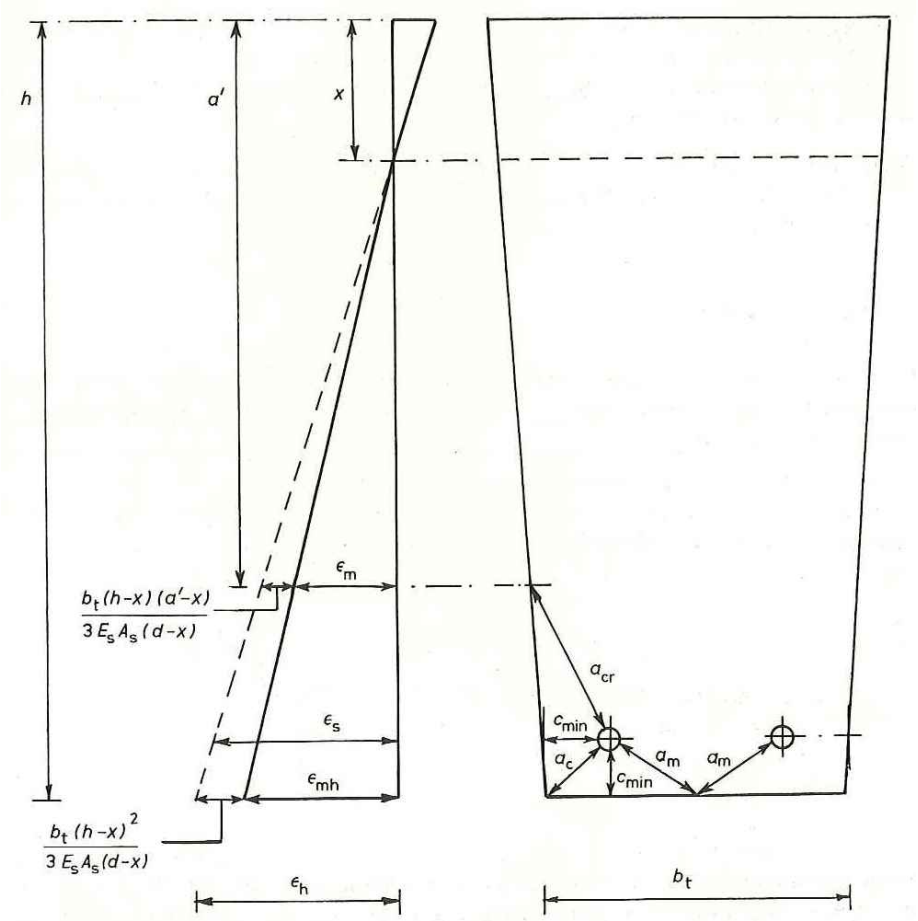

Figure 3-1: Variables influencing crack width formula (Allen, 1988)

The formula for reduction of tension stiffening in BS5400 is more closely related to the general formulation in section 2.6.2 (Eq. 18). The factor for stiffening effect of the concrete in the tension zone is increased to from 1.2 to 3.8.

3.2 South African codes

The investigation of formulas in the BS8110/BS8007 code is relevant to the South African SABS 0100-1 as the formulas are identical.

3.3 Eurocodes 1992 (EC 2)

The Eurocode 2 set of design standards was developed by the Commission of European communities and based on the Volume II: CEB-Fib Model code for concrete structures.

The standard comprises the volumes related to concrete design:

- EN1992-1-1:2004, Eurocode 2: Design of concrete structures – Part 1-1: General rules and rules for buildings
- EN1992-2:2005, Eurocode 2: Design of concrete structures – Concrete bridges design and detailing rules
- EN1992-3:2006, Eurocode 2: Design of concrete structures – Liquid retaining and containment structures

3.3.1 Estimating crack spacing

When all cracks are formed, as described by the fundamental theory, the crack width is obtained from the following compatibility statement (Beeby & Narayanan, 2005).

$$\boldsymbol{w} \quad = \boldsymbol{S_{rm}\epsilon_m} \tag{28}$$

Where:

$w \quad = the\ crack\ width$

$s_{rm} \ = the\ average\ crack\ spacing$

$\epsilon_m \ = the\ average\ strain$

The variable that defines the minimum crack spacing is the transfer length S_0. The maximum spacing is $2S_0$. The average crack spacing S_{rm}, as per the theory, is between S_0 and $2S_0$.

The distance S_0 is dependant on the rate of stress transfer from reinforcement to the encasing concrete. The bond stress is considered constant along the length S_0. The tensile strength will just be reached at the surface again at distance S_0 from the crack, forming the following relationship:

$$\boldsymbol{\tau\pi\emptyset S_0 \ = A_c f_{ct}} \tag{29}$$

Where:

$\tau \ = bond\ stress$

$A_c \ = Area\ of\ concrete \ \left[{\pi\emptyset^2}/{4\rho}\right]$

$f_{ct} \ = Tensile\ strength\ of\ concrete$

$\emptyset \ = bar\ diameter$

Through rearrangement the following is obtained:

$$\boldsymbol{S_0 = \left[{f_{ct}}/{4\tau}\right] {\emptyset}/{\rho}} \tag{30}$$

and from this: $S_{rm} = \ 0.25\ k\ {\emptyset}/{\rho}$

As in Ferry-Borges, the constant k represents the bond properties of the rebar (Beeby & Narayanan, 2005)

The non-slip component was included as in the fundamental theory to form what appears as a different form of Ferry-Borges.

$$\boldsymbol{S_{rm} = kc + 0.25\, k_1\, {\emptyset}/{\rho}} \qquad (31)$$

- k_1 accounts for the bond properties of the reinforcement, 0,8 is for high bond bars and 1,6 for smooth bars.
- The reinforcement factor ${\emptyset}/{\rho}$ was retained and effective reinforcement ratio ρ_{eff} was defined to account for stress distribution in the tension zone.
- Bending is accounted for with an additional coefficient k_2, being dependant on the form of stress distribution. 0,5 is for bending and 1 for pure tension

k_2 and ρ_{eff} are derived from empirical testing, resulting in the following formula (Beeby & Narayanan, 2005):

$$\boldsymbol{S_{rm} = 2c + 0.25\, k_1 k_2\, {\emptyset}/{\rho_{eff}}} \qquad (32)$$

EC2 refers to the characteristic crack width, defined as a width with a 5% probability of exceedance. Experiments showed the characteristic crack width to be approximately 1,7 times the average width (Beeby & Narayanan, 2005). The maximum spacing is therefore used as a design width.

The formula for average spacing is modified to obtain the design spacing as follows (Beeby & Narayanan, 2005):

$$\boldsymbol{s_{r,max} = 3.4c + 0.425 k_1 k_2 \frac{\phi}{\rho_{p,eff}}} \qquad (33)$$

$s_{r,max} = the\ maximum\ crack\ spacing$

3.3.2 Estimating effective cracking strain

The sum of all crack widths per unit length of a reinforced concrete member, at a depth "y" from the neutral axis, is equal to the overall extension of the member (Mosley, et al., 2012). The entire change in length under bending is contained in the total cracks formed, with reduced tension strain between cracks.

The strain ϵ_1 (extension per unit length) of the member at level y is illustrated in Figure 3-2.

$$\epsilon_1 = \frac{y}{(d - x)}\,\epsilon_s$$

$$= \sum w$$

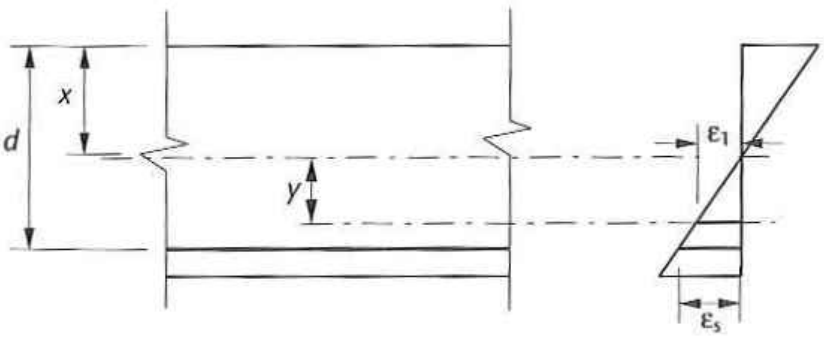

Figure 3-2: EC2 relationship of total strain in reinforced concrete member (Mosley, et al., 2012)

To define this resultant extension, the Eurocode crack model considers the following:

- The effect of the tension strain in the reinforcement at the crack position.
- The tension stiffening between adjacent cracks.
- The mean tension strain in the concrete due to shrinkage.

Average strain as before, is the rebar strain accounting for tension stiffening ϵ_{sm}. Eurocode further reduces this strain with the average strain in the concrete at the surface ϵ_{cm}.

The final formula in EN 1992-1-1 for maximum crack width is therefore.

$$\boldsymbol{w} \quad = \boldsymbol{S_{r,max}(\epsilon_{sm} - \epsilon_{cm})} \qquad (34)$$

The graph of strain variation over unit length in Figure 3-3 , as derived by E Kruger (Kruger, 2018), illustrates this relationship.

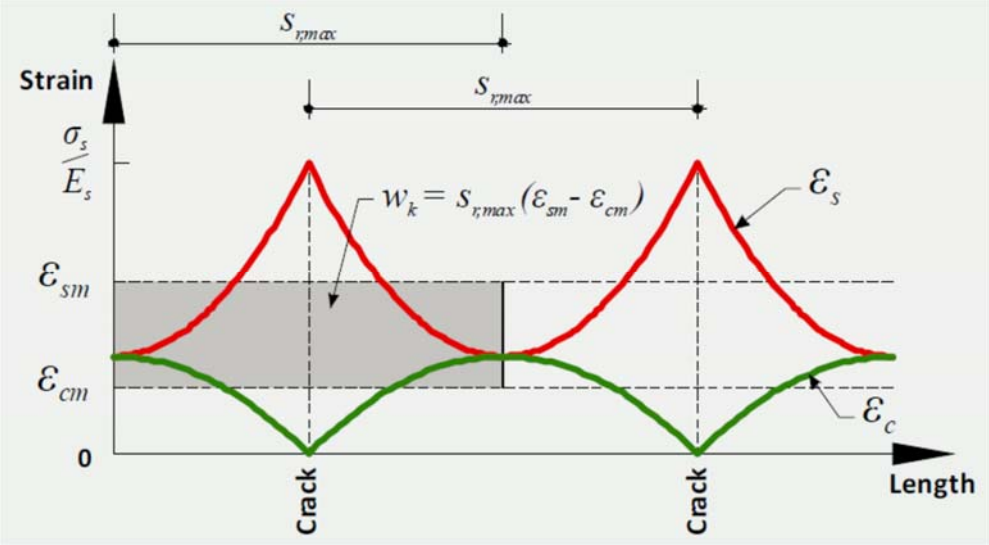

Figure 3-3: EC2 relationship of strain below neutral axis and crack width (Kruger, 2018)

Member strain reaches peaks at the crack positions, the points of maximum and zero strain. The red lines are the strain in steel and green lines the concrete. The concrete fails locally in tension resulting in a crack where concrete tensile capacity is exceeded (peak positions).

The region of bond transfer is in the shaded area between the mean strain lines.

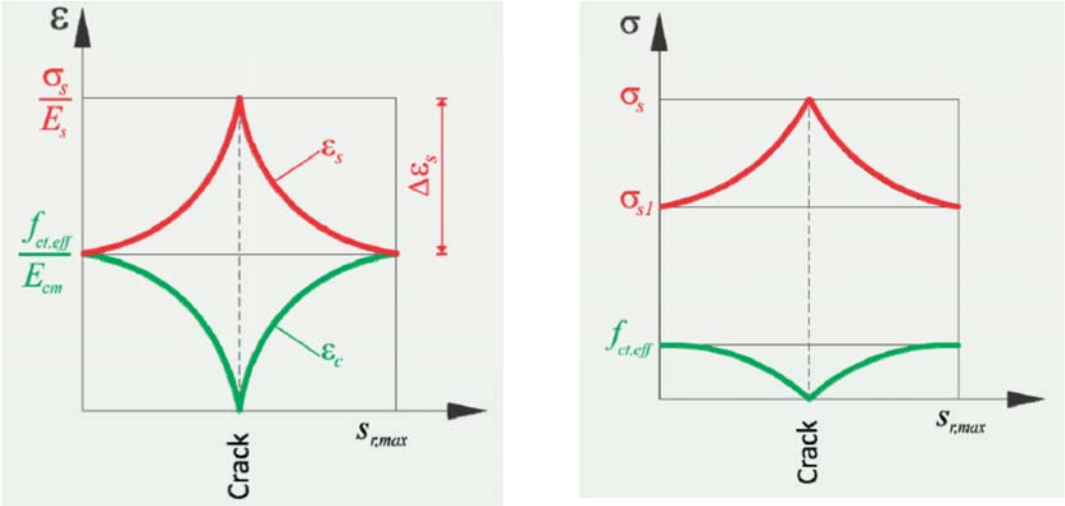

Figure 3-4: The mean strain curve (left) and stress curve (right) at crack position according (Kruger, 2018)

The tension force T, from elastic analysis, at any level below the neutral axis is expressed as a function of the flexural stresses along the length of the element:

- The length between adjacent cracks (transfer length), where the concrete has tension capacity:

  $$\boldsymbol{T = f_{ct,eff}\left(A_{c,eff} - A_s\right) + \sigma_{s1}A_s} \quad (35)$$

  $T = sum\ of\ tension\ force\ in\ rebar\ and\ tension\ of\ net\ tension\ concrete\ area$

  $f_{ct,eff} = effective\ concrete\ tension\ strength$

  $A_{c,eff} = effective\ tension\ concrete\ area$

  $A_s = tension\ steel\ area$

  $\sigma_{s1} = stress\ in\ tension\ steel\ between\ cracks$

- At the crack position where the concrete has no tension capacity:

  $$\boldsymbol{T = \sigma_s A_s} \quad (36)$$

  $T = tension\ force\ in\ steel$

  $\sigma_s = stress\ in\ tension\ steel\ at\ crack$

The rebar carries all the flexural tension force inside the crack width as the concrete has failed locally.

The flexural tension force is the same along the length, therefore following can be deduced:

$$\boldsymbol{\sigma_s A_s = f_{ct,eff}\left(A_{c,eff} - A_s\right) + \sigma_{s1} A_s} \quad (37)$$

$$(\sigma_s - \sigma_{s1})A_s = f_{ct,eff}\left(A_{c,eff} - A_s\right)$$

Where the concrete has not failed, most of the tension force is carried by the concrete and there is also no force in the rebar yet. The expressions are then simplified.

$$(\sigma_s - \sigma_{s1})A_s = f_{ct,eff}\, A_{c,eff}$$

$$(\sigma_s - \sigma_{s1}) = \frac{f_{ct,eff}\, A_{c,eff}}{A_s}$$

$$\frac{\sigma_s - \sigma_{s1}}{E_s} = \frac{f_{ct,eff}\, A_{c,eff}}{E_s A_s}$$

$E_s = modulus\ of\ elasticity\ of\ steel$

The effective reinforcement ratio is given by the expression; $\rho_{p,eff} = \frac{A_s}{A_{c,eff}}$

Therefore, the reduction due to tension stiffening is given by:

$$\boldsymbol{\Delta\varepsilon_s = \frac{f_{ct,eff}}{\rho_{p,eff} E_s}} \quad (38)$$

The three strain parameters for determining effective strain along with their formulations are tabulated in Table 3-3. In Table 3-3 k represents the constants for the shapes of the strain curve and is dependent on load duration.

The shapes are a function of the bond relationships between the rebar surface and concrete.

Table 3-3: Expressions for the parameters to predict effective strain according to EC2 (EC for Standardization, 2005).

PARAMETER	FORMULA	GRAPH
The tension strain in the reinforcement	$\frac{\sigma_s}{E_s}$	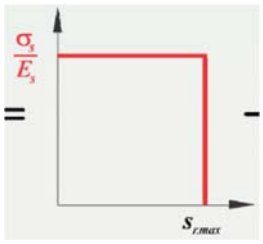
The tension stiffening effect resulting from concrete between adjacent cracks	$k_t \Delta\varepsilon_s$	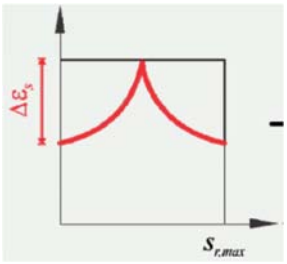
The mean tension strain in the concrete	$\frac{k_t f_{ct,eff}}{E_{cm}}$	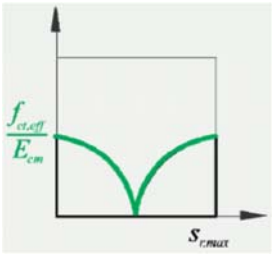

The values of the three expressions are inserted into the compatibility equation for crack width:

$$w_k = s_{r,max}\left\{\underbrace{\frac{\sigma_s}{E_s} - k_t\Delta\varepsilon_s}_{(\epsilon_{sm}} - \underbrace{\frac{k_t f_{ct,eff}}{E_{cm}}}_{\epsilon_{cm})}\right\}$$

The mathematical form allows subtraction by obtaining a common denominator, E_s:

$$w_k = s_{r,max}\left\{\left[\frac{\sigma_s}{E_s} - \frac{k_t\frac{f_{ct,eff}}{\rho_{p,eff}}}{E_s}\right] - \frac{k_t f_{ct,eff} E_s}{E_{cm} E_s}\right\}$$

Adjustment to the final term is done by inserting the fraction for modular ratio:

$$w_k = s_{r,max}\left\{\left[\frac{\sigma_s}{E_s} - \frac{k_t\frac{f_{ct,eff}}{\rho_{p,eff}}}{E_s}\right] - \frac{k_t\alpha_e f_{ct,eff}}{E_s}\right\} \quad (39)$$

Simplified further, the apparent strain can be written as follows:

$$\epsilon_{sm} - \epsilon_{cm} = \frac{\sigma_s - k_t\frac{f_{ct,eff}}{\rho_{p,eff}}(1+\alpha_e\rho_{p,eff})}{E_s} \geq 0.6\frac{\sigma_s}{E_s} \quad (40)$$

(EN1992-1-1: Clause 7.3.4 Equation 7.9)

$\epsilon_{sm} = mean\ strain\ in\ reinforcing\ steel$

$\epsilon_{cm} = mean\ strain\ in\ concrete\ between\ cracks$

3.4 American codes (ACI series)

The main concrete design codes used in the United States are following three documents:

- Building code requirements for structural concrete (ACI318-14).
- ACI 350
- Aashto LRFD

The ACI building code was first issued in 1910 and is updated on average every 6 years to include latest research.

3.4.1 Estimating crack spacing

The compatibility equation for crack width was adapted by Brom's (Lapi, et al., 2018), where maximum crack spacing equalled twice the distance between concrete surface and centroid of rebar:

$$w_m = s_m\ \epsilon_{sm} = \left[2.0\ \mathrm{x}\ \left(c + \frac{\emptyset}{2}\right)\right]\frac{\sigma_{s2}}{E_s} \quad (41)$$

This was found to be true when the rebar stress exceeded 138 - 207 MPa with a cover between 32mm and 76mm.

When an effective cover thickness t_e was used, a better prediction of crack spacing was found when rebar was spaced more than 4 to 5 times cover.

$$w_m = s_m\ \epsilon_{sm} = (2.0\ \mathrm{x}\ t_e)\frac{\sigma_{s2}}{E_s} \quad (42)$$

$$t_e = \sqrt{\left(\frac{a}{4}\right)^2 + (h-d)^2}$$

The research of Gergely and Lutz (Allam, et al., 2012) identified the following parameters influencing crack width:

- The stress in the rebar was the most important variable.
- The bar diameter is not a major variable.
- The area of concrete around each bar and the concrete cover is important geometric variables.
- The ratio of crack width at the concrete surface to that at the reinforcement level is proportional to the ratio of nominal strain at the concrete surface and the reinforcement strain.

By using the steel stress and the effective concrete area surrounding each bar, an alternative formula was obtained through extensive statistical analysis.

The Gergely-Lutz equation was proposed for bottom crack widths:

$$w_b = 0.091\sqrt[3]{t_b A}\,\beta\,(f_s - 5) \times 10^{-3}$$

A simplification led to the following equation, adopted in ACI 318 until 1995:

$$\boldsymbol{w = 0.076\beta f_s \sqrt[3]{d_b A} \times 10^{-3}} \quad (43)$$

(ACI 318 -95 McCormac and Brown)

Where:

$w = the\ most\ probable\ maximum\ crack\ width\ (inches)$

$\beta_h = ratio\ of\ the\ distance\ between\ the\ neutral\ axis\ and\ concrete\ tension\ face$

$to\ distance\ between\ neutral\ axis\ and\ centroid\ of\ the\ tensile\ steel$

$f_s = computed\ tensile\ stress\ at\ service\ load$

$d_c = the\ clear\ cover\ from\ the\ nearest\ conrete\ surface\ in\ tension$

$to\ the\ centroid\ of\ the\ closest\ rebar$

$A = effective\ tension\ area\ of\ concrete\ around\ the\ main\ reinforcement,$

$with\ the\ same\ centroid\ as\ this\ reinforcement$

$divided\ by\ the\ number\ of\ bars\ in\ the\ tension\ area$

This equation was found not to be reliable when thicker concrete covers were used.

Frosch developed a crack model independent of actual concrete cover based on the following parameters:

- The crack width remains a direct function of the strain in the reinforcement multiplied by the crack spacing.

- The maximum crack spacing is estimated to be twice the controlling cover distance by the expression $d' = \sqrt{{d_c}^2 + (0.5s)^2}$
- The concrete between the cracks does not resist any tension.

The following formula was proposed:

$$w_c = 2\frac{f_s}{E_s}\beta\sqrt{(d_c)^2 + \left(\frac{s}{2}\right)^2} \quad (44)$$

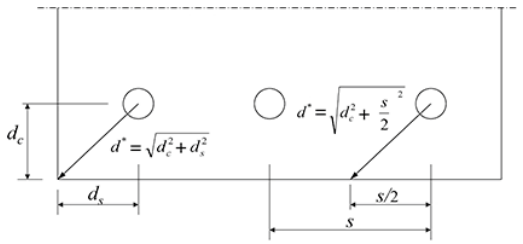

Figure 3-5: Controlling cover dimensions of crack model (Frosch, 2014)

Where:

$w_c = crack\ width\ (inches)$

$f_s = stress\ in\ steel\ reinforcement\ (ksi)$

$E_s = the\ modulus\ of\ elasticity\ of\ steel\ reinforcement\ (ksi)$

$\beta = factor\ relating\ the\ strain\ at\ the\ tension\ face\ to\ the\ strain\ at\ the\ reinforcement\ layer$

$d_c = distance\ from\ the\ tension\ face\ to\ centroid\ of\ the\ nearest\ reinforment\ layer\ (inch)$

$s = reinforcement\ bar\ spacing\ (inch)$

The equation can be rearranged to obtain the maximum permitted spacing of the reinforcement for a limiting crack width:

$$s = 2\sqrt{\left(\frac{w_c E_s}{2 f_s \beta}\right)^2 - (d_c)^2} \quad (45)$$

The ACI committee stated with the inherent variability of concrete it is not possible to accurately calculate crack widths (ACI committee 224, 2001). The code requirements therefore only prescribe maximum rebar spacing.

Frosch equation is therefore simplified to obtain a maximum permitted reinforcement spacing based on working elastic steel strain.

3.4.2 Estimating effective cracking strain

Based on the Frosch model, the ACI 318 code does not currently include an allowance for tension stiffening effects.

3.5 The fib Model code for concrete structures (MC2010)

The purpose of this Model code is to serve as a basic set of technical standards that countries can make use of to develop national standards (Borosnyoi & Balazs, 2005).

3.5.1 Estimating crack spacing

The model calculates the width based on the deformation of a prismatic reinforced concrete bar under axial tension, with the compatibility equation arranged as follows:

$$\boldsymbol{w_d = 2l_{s,max}(\epsilon_{sm} - \epsilon_{cm} - \epsilon_{cs})} \qquad (46)$$

The fib model requires the following expressions to be met:

$w_d \leq w_{lim}$ $\quad where:$

$w_d = the\ design\ crack\ width$

$w_{lim} = the\ nominal\ limit\ value\ of\ crack\ width$

The influence distance of bond stress transfer, adjacent to the crack position is given by $l_{s,max}$. The length $l_{s,max}$ is determined from the following expression:

$$\boldsymbol{l_{s,max} = kc + \frac{1}{4} \text{ x } \frac{f_{ctm}}{\tau_{bms}} \text{ x } \frac{\emptyset_s}{\rho_{s,ef}}} \qquad (47)$$

(Fib Modelcode 2010: Clause 7.6.4.4, equation7.6-4)

where:

$k = empirical\ factor\ for\ the\ influence\ of\ concrete\ cover$

$f_{ctm} = mean\ tensile\ strength\ of\ concrete$

$\tau_{bms} = mean\ bond\ strength\ between\ rebar\ and\ concrete,$

$\rho_{s,ef} = \dfrac{A_s}{A_{c,ef}}$

$A_{c,ef} = effective\ area\ of\ concrete\ in\ tension$

$\emptyset_s = nominal\ diameter\ of\ the\ reinforcing\ bars$

The method requires the stage of cracking to be identified before the design crack width can be determined.

Under increasing applied tension strain, four stages of response are distinguished.

1. The uncracked stage
2. The crack formation stage
3. The stabilised cracking stage
4. The steel yielding stage

The cracking load, N_r, is estimated from the following expression:

$$\boldsymbol{N_r = A_c f_{ctm}(1 - \alpha_e \rho_{s,ef})} \quad (48)$$

where:

$\alpha_e = modular\ ratio\ \frac{E_s}{E_c}$

The maximum crack width during crack formation is obtained when the tensile force reaches and exceeds the cracking load N_r.

When the applied tension load N exceeds crack load N_r stabilised crack stage (crack propagation phase) applies.

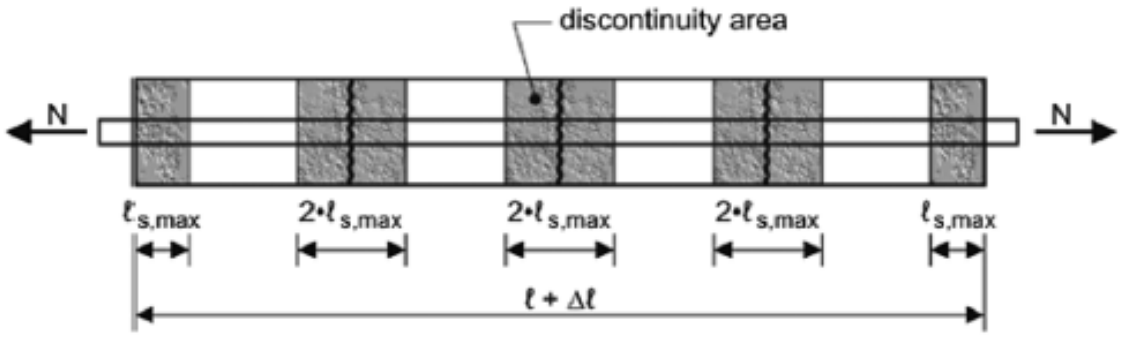

Figure 3-6: Illustration of reinforced prismatic bar subject to deformation (Balazs, 2013)

Each new crack that forms reduces the unshaded portion of the member in Figure 3-6.

When the boundaries of $2l_{s,max}$ overlap, no new cracks will appear, and the stabilised crack stage is initiated. The existing cracks propagate and widen.

3.5.2 Estimating effective cracking strain

The model distinguishes between bond, mean strain and shrinkage factors to differentiate the stages of cracking.

$$\boldsymbol{\epsilon_{sm} - \epsilon_{cm} - \epsilon_{cs} = \frac{\sigma_s - \beta\,\sigma_{sr}}{E_s} - \eta_r\,\epsilon_{sh}} \quad (49)$$

Where:

$\sigma_s = steel\ stress\ in\ a\ crack$

$\sigma_{sr} = the\ maximum\ steel\ stress\ in\ a\ crack\ at\ the\ crack\ formation\ stage, for\ pure\ tension$

$\sigma_{sr} = \frac{f_{ctm}}{\rho_{s,ef}}\left(1 + \alpha_e \rho_{s,ef}\right)$

$$\rho_{s,ef} = \frac{A_s}{A_{c,ef}}$$

$$A_{c,ef} = effective\ area\ of\ concrete\ in\ tension$$

$$\alpha_e = modular\ ratio\ \frac{E_s}{E_c}$$

$$\beta = empirically\ obtained\ coefficient\ to\ assess\ the\ mean\ strain\ over\ l_{s,max}\ depending\ on\ the\ type\ of\ loading\ (short - term\ or\ long - term)$$

$$\eta_r = a\ coefficient\ for\ considering\ the\ shrinkage\ contribution$$

$$\epsilon_{sh} = free\ shrinkage\ strain$$

	Crack formation stage	Stabilized cracking stage
Short-term, instantaneous loading	$\tau_{bms} = 1.8 \cdot f_{ctm}(t)$ $\beta = 0.6$ $\eta_r = 0$	$\tau_{bms} = 1.8 \cdot f_{ctm}(t)$ $\beta = 0.6$ $\eta_r = 0$
Long-term, repeated loading	$\tau_{bms} = 1.35 \cdot f_{ctm}(t)$ $\beta = 0.6$ $\eta_r = 0$	$\tau_{bms} = 1.8 \cdot f_{ctm}(t)$ $\beta = 0.4$ $\eta_r = 1$

Figure 3-7: Values for τ_{bms}, β & η_r for deformed reinforcing bars (Balazs, 2013)

4. EXAMINATION OF NUMERICAL MODELS

There are various concepts and modelling techniques in existence that have been proposed by researchers. The most notable of these are as follows:

- Microplane theory – Bazant and Ozbolt (1990)
- The particule model – Bazant et al (1990)
- Lattice model – Mier (1997)

Literature indicates (Shi, 2009) there are two generally accepted computational theories for crack analysis in concrete fracture mechanics using the finite element method. These are referred to as the discrete model and smeared crack approaches (Shi, 2009).

4.1 Discrete crack model

The crack itself is considered an element with defined geometry. The fracture process zone (FPZ), the cohesive forces acting on the crack surface and the geometric shapes in the mix form the boundaries of the crack element. This allows the physical reality of the cracked concrete to be closely simulated. (Shi, 2009). The analysis evolves as follows:

- A crack forms at the interface between two fictional elements, being the two opposite faces of the crack.
- When the crack opens, the boundary conditions change, the fracture properties being described by constitutive law.
- As the crack grows and propagates, refinement of the mesh near the crack tip through constant re-meshing, is continually performed.

The discrete crack model is particularly suited for analysing massive concrete structures such as dams (Balazs, 2013). The fictitious crack model, proposed by Hillerborg, is widely accepted as one of the simplest and the most accurate nonlinear discrete fracture mechanics models for concrete (Shi, 2009).

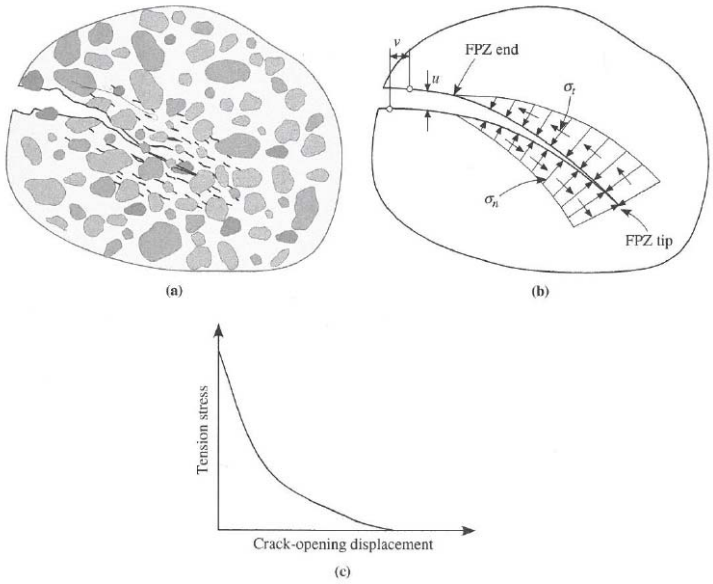

Figure 4-1: An actual crack in concrete with its fictitious crack model after Hillerborg et al. Tension softening is shown in the graph above, 1976 (Shi, 2009)

4.2 Smeared crack approach

The smeared crack approach considers the cracked solid as a continuum. Cracks are represented by changing the constitutive relations of the finite elements. The problem is subdivided into elements, analysing the problem through these elements and reassembling these elements into the whole to obtain a global solution. The stress-strain relations of the elements can be altered to reflect the effects of the cracking. This approach is convenient for static as well as dynamic crack analysis (Shi, 2009).

A crack is represented by orthotropic damage to concrete within the area of the crack element. The damage is described by the fracture energy required to open a discrete crack. The crack opening constitutive law is defined by three parameters (Shi, 2009):

- Tensile strength
- Fracture energy
- Shape of the stress softening function

In the FEM model, the crack is represented by a smeared crack associated with one finite element. The fracture energy is distributed in the FEM volume by smeared cracks. The model is suitable where many cracks occur in plain and reinforced concrete. The application is dependent on sufficiently fine finite element meshes. RC beams with 6 to 8 finite elements per depth has been shown to give sufficiently accurate results (Shi, 2009).

The upper limit for acceptable element size is controlled by the fracture energy of the concrete. With large elements, the energy released after exceeding tensile strength can be larger than the resisting fracture energy, and a stable strain localisation is not possible (Balazs, 2013).

4.3 :Numerical models for bond

To determine the various bond-slip relations, tension pull-out experiments are carried out. The advantage of analysing bond-slip through numerical simulations are real boundary conditions are set, since the bond-slip behaviour is modelled on actual experimental data instead of assumptions as in code-based models.

To analyse global bond-slip behaviour, a macroscopic model such as the smeared crack or discrete crack models can be used. (Mier, 1997). The following bond models have been proposed in literature (Mier, 1997).

- BS8110 model for bond (Bangash, 2001)
  The BS8110 model considers plain and deformed bar types. Two types of bond are recognised, namely anchorage and local bond.
  The anchorage bond stress for simple pull-out is obtained from the following equation:

$$\boldsymbol{\sigma_b} = {}^{\boldsymbol{\sigma_s \emptyset}}\!/_{\boldsymbol{4L}} \qquad (50)$$

  The bond resistance at ultimate bar strength is obtained as follows:

$$\boldsymbol{\sigma_b} = {}^{\boldsymbol{0,87\sigma_{yt}\pi\emptyset^2}}\!/_{\boldsymbol{4\pi\emptyset L^2}} \qquad (51)$$

  In both these equations the following variables apply:

  $\boldsymbol{\sigma_b} = \ bond\ stress$

  $\boldsymbol{\sigma} \ = \ stress\ in\ reinforcing\ steel$

  $\emptyset = \ diameter\ of\ reinforcing\ steel$

  $L = \ length\ or\ developement\ length\ of\ embedded\ reinforcing\ steel$

  $\boldsymbol{\sigma_b} = \boldsymbol{\sigma_{yt}}\ yield\ strength\ of\ the\ reinforcing\ steel$

  For local (flexural) bond the bond stress is based on ultimate shear and for a beam of uniform depth is given by:

$$\boldsymbol{\sigma_b} = {}^{\boldsymbol{V}}\!/_{\boldsymbol{d\,\Sigma O}} \qquad (52)$$

  $V = \ the\ ultimate\ shear$

  $d = \ the\ depth\ of\ the\ beam$

  $\boldsymbol{\Sigma O} = \ the\ sum\ of\ the\ effective\ parameters\ of\ the\ bars\ in\ tension$

- Brice, Salinger and Wastlund models (Bangash, 2001)

  It is assumed the section between 2 consecutive cracks has constant bending moment. At the cracks the tension stress in concrete (σ_t) equals zero and in the bars (σ_{yt}) the maximum stress is reached. Away from the cracks an increasing amount of the total tensile force is transferred from the bars to the concrete through the bond between concrete and steel.

  At a position x along the length, the bond between steel and concrete is given by:

  $$\Sigma O \int_0^x \sigma f\left(x/L\right) dx \qquad (53)$$

  The following approximations apply here:

  $$\sigma_{bx} = \sigma_b f\left(x/L\right) \qquad (54)$$

  $$\sigma_t, \sigma_s = \sigma_{yt} - \left(p/A\right) \sigma_b \int_0^x f\left(x/L\right) dx \qquad (55)$$

  The moment at the position x:

  $$M_x = \sigma_x A_s z + \sigma_t z_c \qquad (56)$$

  From equation 55:

  $$\sigma_t = \left(p\sigma_b Z/z_c\right) \int_0^x f\left(x/L\right) dx$$

  $z_c = section\ modulus$

  $z \quad = lever\ arm$

  The maximum stress σ_{cu} in the concrete occurs at L/2 when cracking takes place. This will occur when σ_t equals σ_{tu}. Then at L/2 the length of development is given as follows:

  $$L = B_1 \frac{1}{p} \frac{z_c}{z} \frac{\sigma_{tu}}{\sigma_b} \qquad (57)$$

- Somayaji and Shah model (Bangash, 2001)

  The model accounts for the relationship between σ_{bx} and the second derivative of the local slip S_x. An exponential bond stress distribution function is also assumed. The local slip is determined from the following equation:

  $$S_x = Ae^x + Be^{-x} + C\frac{x^2}{2} + Dx + E \qquad (58)$$

  Where A-E are constants.

5. COMPARISON OF MODELS

The formulation of available analytical and numerical models has been examined. This section compares the application of the fundamental theories for each approach.

5.1 Semi-analytical models

These models analyse the tension area of concrete (see Figure 2-10) by modelling the bond-slip relationship around the tension reinforcement. The effective tension area for tie action and crack growth over cover depth is simulated.

Two fundamental theories underlying the analytical models of flexural crack analysis in reinforced concrete has been identified:

- No slip theory – the concrete at the perimeter of the rebar does not shift relative to the length of bar. A crack forming at the tension surface, widens over the cover depth, and ceases at the bar surface.
- Slip theory – movement occurs between the rebar and the surrounding concrete. This split widens towards the tension surface.

The average crack width on the tension face is represented by the compatibility relationship of crack spacing multiplied by effective tensile cracking strain.

5.1.1 Crack spacing

As can be deduced from the discussions in section 3, where the derivations used for crack spacing in each crack model was presented, the following items are important variables in estimating average crack spacing.

- Bar diameter and reinforcement ratio $\frac{\emptyset}{\rho}$ – represents the influence of ultimate bond strength between rebar and concrete. Based on the behaviour of bond failure of an axial tie.
- Concrete cover – equals the distance from a surface crack to the point where tension stress is no longer influenced by the crack. Based on the bending of a beam where no bond failure has occurred at the rebar surface.

The above is contained in the Ferry-Borges equation, discussed in section 2.6.1, where:

$S_m = K_1\, c + K_2\, \frac{\emptyset}{\rho}$; where K_1 represents influence of cover depth and K_2 represents bond strength.

The application of this equation varies. The codes can be grouped according to their emphasis.

a) British code (South African code) and American code

The British standards effectively ignores the influence of bond strength by assuming the ratio $\frac{\emptyset}{\rho}$ (Figure 2-46) to be zero. To compensate for any weaknesses in bond, the effect of cover failure under bending action is doubled as described in section 3.1.1.

A further term added is for the bending effect of an unreinforced element, with the assumption the crack reduces stress over a length equal to the tension depth. This results in the maximum depth being the factored tension height represented by the term; $w_{lim} = 1{,}5\ (h - x)\ \epsilon_m$.

The maximum crack spacing in the American code is simply twice the controlling cover distance, which is twice the furthest distance from the concrete face to edge of rebar (Figure 3-5).

In summary, these codes only consider the effect of cover and concrete thickness in estimating the tension stress distribution on a concrete face. The width of crack where no bond slip occurs is calculated here and the influence of bond failure (slip) is ignored.

b) Eurocode and Fib model

These European models consider the full Ferry-Borges formula in estimating crack spacing. These can be compared as follows:

Table 5-1: Crack spacing formulas in the European codes (Eq. 33 & 47)

Eurocode 2	Fib MC2010
$S_{rm} = 3.4c + 0.425k_1k_2\frac{\phi}{\rho_{p,eff}}$	$l_{s,max} = kc + \frac{1}{4}\ \mathrm{x}\ \frac{f_{ctm}}{\tau_{bms}}\ \mathrm{x}\ \frac{\emptyset_s}{\rho_{s,ef}}$

It is evident both formulas consider all the terms in Ferry-Borges, therefore the calculation of crack spacing includes the state of bond failure. Different influencing factors are used:

The factor k for cover is 1 in the fib code, whereas Eurocode estimates a wider cover influencing zone denoted by the factor 3,4. The mean bond strength in the fib code does not differentiate between bending and pure tension, it considers long and short duration loads (Figure 3-7). There is no identifiable bond distribution factor in the formulation. The Eurocode has factors for stress type (bending or pure tension) and bond distribution for bar type. The estimation of the effective concrete area in tension is the same between the codes. The ratio 0.25 is the same for EC 2 formula when no probability of exceedance is considered (see 3.3.1).

In summary, these codes are heavily influenced by bond strength due to the second portion of the Ferry-Borges equation (2.6.1 a).

5.1.2 Effective cracking strain

The ACI 318 code does not reduce the tensile strain at the reinforcement level with the tension stiffening between cracks.

The British codes reduce the elastic crack strain with an allowance for tension stiffening. The European codes include this allowance, with a different formulation as noted earlier. The EC2 and Fib further reduces the strain with a mean tension strain in the concrete due to shrinkage.

a) British code (South African code)

The tension stiffening is the result of the tensile stress at the tension face between cracks, with an assumed value of $\frac{2}{3}\ MPa$. The resultant force due to this stress is estimated, through strain proportionality, a distance away from the compression face, based on the tension depth to the neutral axis.

Fluctuating live load, a characteristic of traffic loading, increases fatigue strain which reduces the effect of tension stiffening. Higher tension stress in steel has a similar effect. Consequently, due to the nature of loading, the BS5400 bridge code considers diminishing tension stiffening effects as applied load increases.

The does not include strain reduction due to tension stiffening if more than half the total applied moment is attributable to live load.

b) Eurocode and Fib model

The Eurocode limits the reduction of the elastic strain to maximum 40% of the steel strain. The Fib model has no such allowance as seen in Table 5-2.

Table 5-2: Formulas for effective strain in the European codes (Eq. 40 & 49)

Eurocode 2	Fib MC2010
$\epsilon_{sm} - \epsilon_{cm} = \frac{\sigma_s - k_t \frac{f_{ct,eff}}{\rho_{p,eff}} \left(1 + \alpha_e \rho_{p,eff}\right)}{E_s} \geq 0.6 \frac{\sigma_s}{E_s}$	$\epsilon_{sm} - \epsilon_{cm} - \epsilon_{cs} = \frac{\sigma_s - \beta\, \sigma_{sr}}{E_s} - \eta_r\, \epsilon_{sh}$

The Eurocode considers the difference between the full tension strain at the crack and the small amount of steel strain between the cracks as a function of the actual concrete tension strength at the time of cracking. This value often above 2MPa, since flexural cracking is normally initiated after 28days. The resultant stiffening force is based on an effective tension area around the steel, whereby a tie is simulated. It considers the effects of bond stress distribution due to load duration.

The Fib model makes a similar approximation as the Eurocode in identifying a resultant stiffening force. In both cases the effects of bond stress distribution are considered based on load duration.

In summary, these codes are heavily influenced by duration of applied stress.

5.2 Numerical models

Numerical models are energy methods where crack behaviour is quantified by considering the fracture energy in the entire section. More in depth understanding of material physics is required to apply the fracture theory.

Material interface properties are modelled at all observation levels within the concrete member. Accounting for the stress concentrations around flaws allows the size effect to be modelled in the design. To analyse the entire member, a finite element model (FEM) is created.

This contrasts with analytical methods where only the tension zone of the section is analysed. Numerical methods therefore provide a more comprehensive means of crack analysis (Bazant & Planas, 1997). The size effect property of concrete has been identified in numerous research studies. The larger the concrete member the lower the nominal strength as more flaws are present in the microstructure. Through modelling of appropriate stiffness's within the hardened concrete, numerical models can consider the size effect. As the analysis in analytical methods focus on the tension regions only, size effect cannot be included.

- The discrete crack approach (Hillerborg et al 1976) - From a macroscopic perspective this provides the most accurate physical material model to study cracks (Shi, 2009). The complete geometry of a single crack can be physically estimated including the crack propagation path and critical mouth opening displacement (CMOD).
- The smeared crack approach (Rashid 1968) – this is the more computationally convenient method of the two, due to its continuum assumption for cracked concrete materials.

Due to the continuum assumption for cracked concrete materials, the smeared crack approach is computationally more convenient than the discrete crack approach. It is accepted in practice as one of the most effective means for crack analysis in concrete structures for predicting general structural behaviour (Shi, 2009). It can only however predict cracking behaviour approximately (Shi, 2009).

Fracture energy is influenced by the bond relationships between aggregate, hardened cement paste and the reinforcement (Bažant, 2002). Literature shows the input variables for these micro and meso relationships are also obtained numerically, based on bond theories.

The Fib model and ACI codes provide methods to estimate stiffness parameters, which are based on empirical derivations. The material stiffness properties are modelled as a mesh through FEM. With appropriate stiffness parameters for each phase in the matrix, a crack model for reinforced or mass concrete can be analysed.

5.3 Desktop comparison

The choice between numerical methods or analytical code-based methods for a crack analysis depend on two factors:

- The size of the concrete element being assessed
- The proximity of the tensile rebar to the tension surface

The benefits of numerical methods of analysis are more apparent in large members. The work of Alam, et al., and other similar investigations, should be used as a guide to asses which modelling method is suitable to a problem.

To compare the models for the five concrete codes discussed, a desktop analysis was performed on a one way spanning simply supported element. The analysis involved computing each formulation in spreadsheet format.

A master spreadsheet was created with common inputs for beam geometry, number of bars at the flexural face, cover, concrete and steel classes. The equations for the codes are linked to the master input. The same member characteristics are computed into each code formula for comparison.

The applied live service moment was increased from zero in increments equivalent to 10% of the dead service moment of the member. The maximum live moment value was increased to 50% above the dead moment value. The following sections were analysed and compared:

Table 5-3: Member configurations for crack model comparison

SECTION SIZE	Case 1 (C1)	Case 2 (C2)
1000x250	Y12 @ 150mm c/c	Y16 @ 300mm c/c
1000x500	Y12 @ 150mm c/c	Y16 @ 230mm c/c
1000x750	Y16 @ 150mm c/c	Y20 @ 230mm c/c
1000x1000	Y16 @ 150mm c/c	Y20 @ 300mm c/c
1000x1500	Y16 @ 150mm c/c	Y20 @ 230mm c/c
500x1500	Y20 @ 140mm c/c	Y25 @ 270mm c/c
500x2000	Y25 @ 140mm c/c	Y32 @ 270mm c/c

The following ratios were plotted on line graphs to obtain results for critical comparison of the crack models:

1. The increase in crack width against increasing applied live moment:
   - The values of E were estimated by the analytical methods for Young's modulus proposed by the specific code, including the effects of long-term creep.
2. The increase in crack width against increasing applied live moment:
   - The second comparison is like the 1st but ignores the effect of tension stiffening.
3. The increase in crack width against increasing applied live moment, for constant modular ratio of 15:
   - The models across the design codes are compared ignoring the influence of varying E values between codes. Literature shows a modular ratio of 15 is acceptable to estimate crack widths under long term loading, in absence of detailed creep approximations.
4. The increase in crack width against increasing steel strain, due to applied live load.
   - E values determined as in 1 & 2.
   - The bond conditions were varied where the models included a variable for bond, which is applicable to the Eurocode and Fib model code. The bonded strength started at the recommended for ribbed bars and worsened in 50% increments.

6. ANALYSIS

The graphs for shallow and deep members are presented and analysed in this section. The formulas applicable to these graphs are tabulated in Appendix 10.1. The relationship between increasing applied live moment and the resulting widening crack width is generally linear. The maximum allowable steel stress for applying the analytical formulas is 0,8fy (Table 3-2).

The trend lines show tension stiffening effect and cover has the most significant influence on crack width values. Their degree of influence is determined by the member depth. The influence of member depth varies across codes due to the difference in analytical formulation. The bond conditions between rebar surface and concrete are also significant.

At the transition between crack formation and crack propagation, an abrupt change in trend is noted in the fib code. This results from the table of variables in Figure 3-7, where the denominator for bond factor in the cracking spacing formula increases from 1,35 during crack formation to 1,8 in crack propagation. In the strain reduction formula, the numerator for load duration decreases from 0,6 to 0,4.

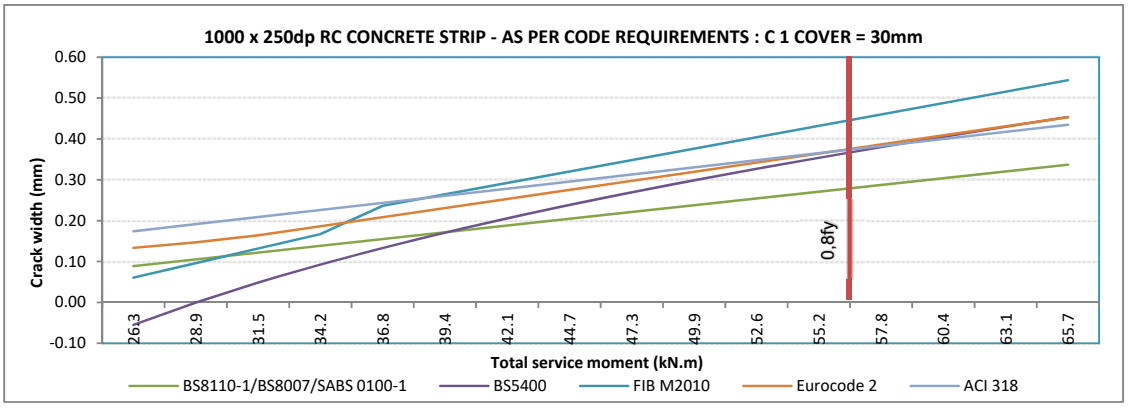
1000 x 250dp RC CONCRETE STRIP - AS PER CODE REQUIREMENTS : C 1 COVER = 30mm
Crack width (mm)
0.60
0.50
0.40
0.30
0.20
0.10
0.00
-0.10
0,8fy
26.3
28.9
31.5
34.2
36.8
39.4
42.1
44.7
47.3
49.9
52.6
55.2
57.8
60.4
63.1
65.7
Total service moment (kN.m)
BS8110-1/BS8007/SABS 0100-1
BS5400
FIB M2010
Eurocode 2
ACI 318

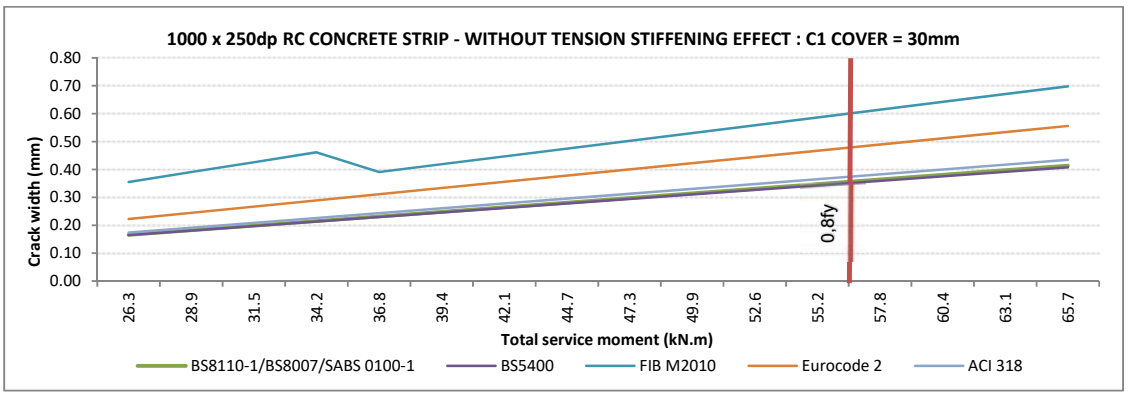
1000 x 250dp RC CONCRETE STRIP - WITHOUT TENSION STIFFENING EFFECT : C1 COVER = 30mm
Crack width (mm)
0.80
0.70
0.60
0.50
0.40
0.30
0.20
0.10
0.00
0,8fy
26.3
28.9
31.5
34.2
36.8
39.4
42.1
44.7
47.3
49.9
52.6
55.2
57.8
60.4
63.1
65.7
Total service moment (kN.m)
BS8110-1/BS8007/SABS 0100-1
BS5400
FIB M2010
Eurocode 2
ACI 318

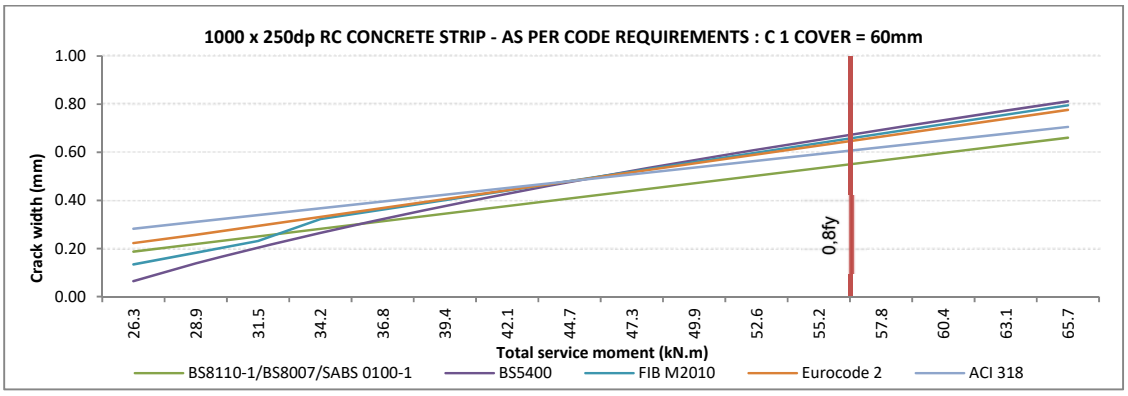
1000 x 250dp RC CONCRETE STRIP - AS PER CODE REQUIREMENTS : C 1 COVER = 60mm
Crack width (mm)
1.00
0.80
0.60
0.40
0.20
0.00
0,8fy
26.3
28.9
31.5
34.2
36.8
39.4
42.1
44.7
47.3
49.9
52.6
55.2
57.8
60.4
63.1
65.7
Total service moment (kN.m)
BS8110-1/BS8007/SABS 0100-1
BS5400
FIB M2010
Eurocode 2
ACI 318

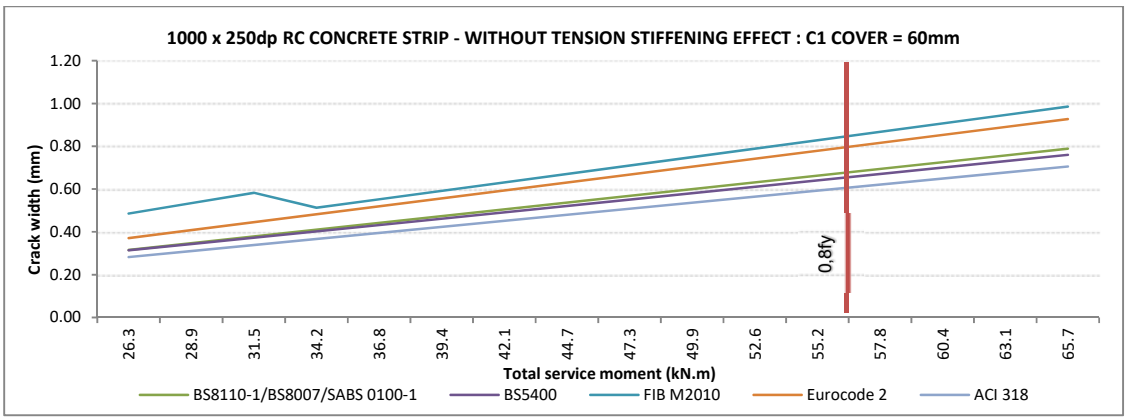
1000 x 250dp RC CONCRETE STRIP - WITHOUT TENSION STIFFENING EFFECT : C1 COVER = 60mm
Crack width (mm)
1.20
1.00
0.80
0.60
0.40
0.20
0.00
0,8fy
26.3
28.9
31.5
34.2
36.8
39.4
42.1
44.7
47.3
49.9
52.6
55.2
57.8
60.4
63.1
65.7
Total service moment (kN.m)
BS8110-1/BS8007/SABS 0100-1
BS5400
FIB M2010
Eurocode 2
ACI 318

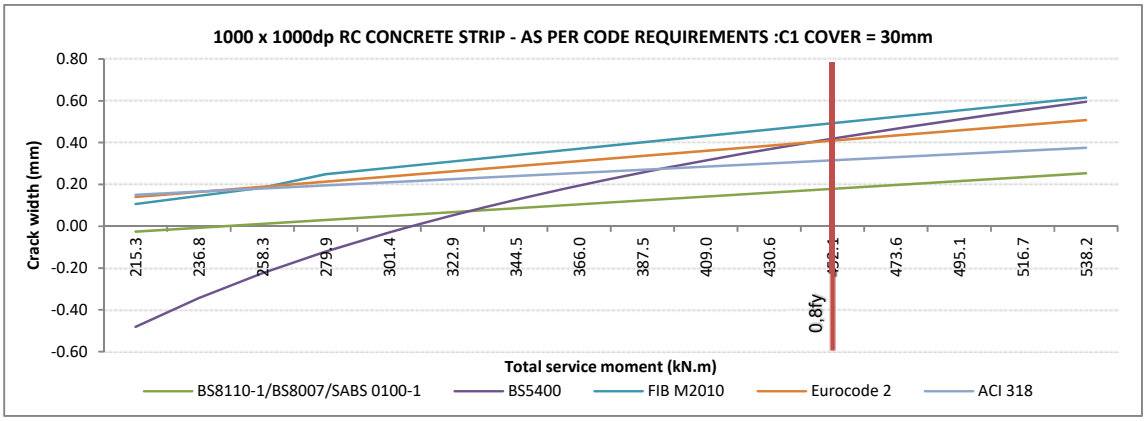
1000 x 1000dp RC CONCRETE STRIP - AS PER CODE REQUIREMENTS :C1 COVER = 30mm
Crack width (mm)
0.80
0.60
0.40
0.20
0.00
-0.20
-0.40
-0.60
215.3
236.8
258.3
279.9
301.4
322.9
344.5
366.0
387.5
409.0
430.6
452.1
473.6
495.1
516.7
538.2
0,8fy
Total service moment (kN.m)
BS8110-1/BS8007/SABS 0100-1
BS5400
FIB M2010
Eurocode 2
ACI 318

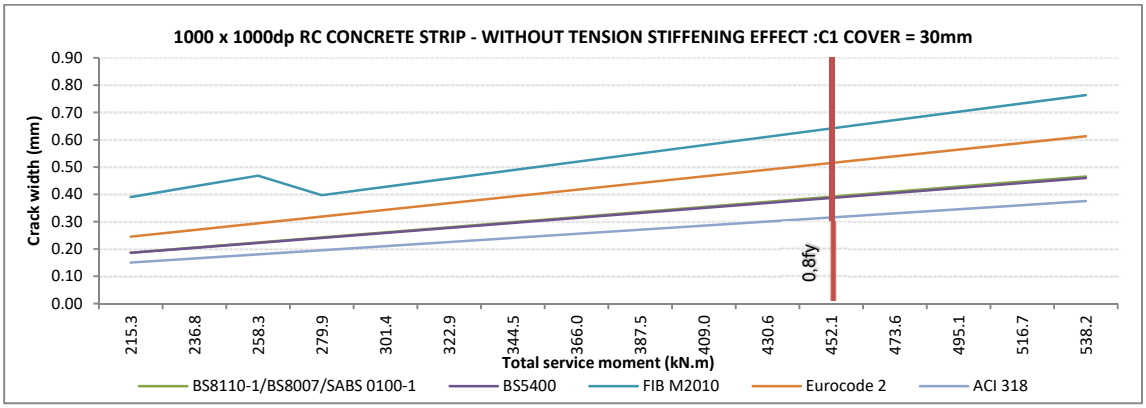
1000 x 1000dp RC CONCRETE STRIP - WITHOUT TENSION STIFFENING EFFECT :C1 COVER = 30mm
Crack width (mm)
0.90
0.80
0.70
0.60
0.50
0.40
0.30
0.20
0.10
0.00
215.3
236.8
258.3
279.9
301.4
322.9
344.5
366.0
387.5
409.0
430.6
452.1
473.6
495.1
516.7
538.2
0,8fy
Total service moment (kN.m)
BS8110-1/BS8007/SABS 0100-1
BS5400
FIB M2010
Eurocode 2
ACI 318

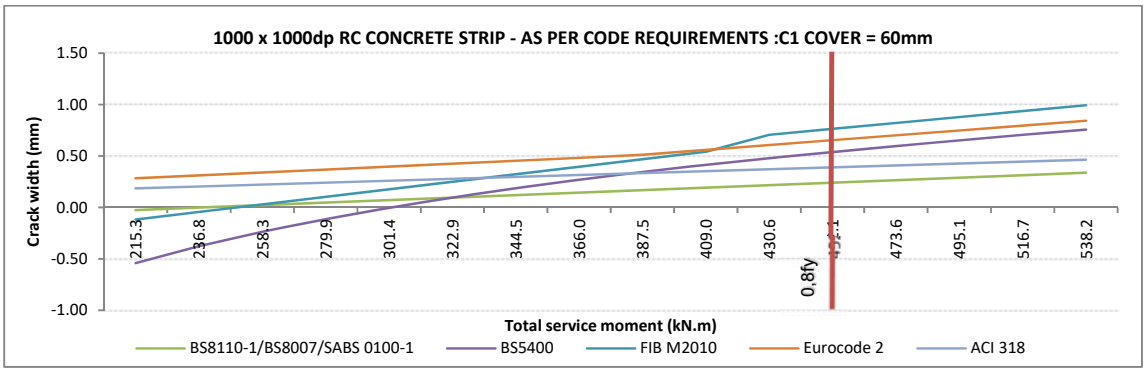
1000 x 1000dp RC CONCRETE STRIP - AS PER CODE REQUIREMENTS :C1 COVER = 60mm
Crack width (mm)
1.50
1.00
0.50
0.00
-0.50
-1.00
215.3
236.8
258.3
279.9
301.4
322.9
344.5
366.0
387.5
409.0
430.6
473.6
495.1
516.7
538.2
0,8fy
Total service moment (kN.m)
BS8110-1/BS8007/SABS 0100-1
BS5400
FIB M2010
Eurocode 2
ACI 318

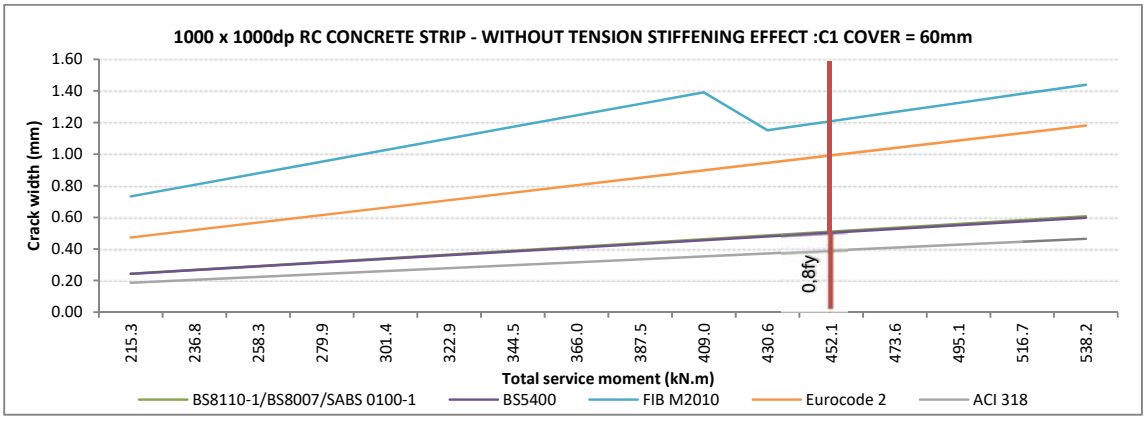
1000 x 1000dp RC CONCRETE STRIP - WITHOUT TENSION STIFFENING EFFECT :C1 COVER = 60mm
Crack width (mm)
1.60
1.40
1.20
1.00
0.80
0.60
0.40
0.20
0.00
215.3
236.8
258.3
279.9
301.4
322.9
344.5
366.0
387.5
409.0
430.6
452.1
473.6
495.1
516.7
538.2
0,8fy
Total service moment (kN.m)
BS8110-1/BS8007/SABS 0100-1
BS5400
FIB M2010
Eurocode 2
ACI 318

6.1 Influence of tension stiffening

All codes except the ACI allows for the reduction of elastic strain with the tension stiffening effect to determine an effective cracking strain. ACI 318 does not reduce strain, therefore higher crack widths should be expected.

Estimated crack spacing in ACI however gives the lowest values, noted in the graphs without tension stiffening effect. Where the cover distance is doubled, the crack spacing is lower than by the remaining codes. These lower results from ACI is expected, as it only considers the first term of the Ferry-Borges expression (section 2.6.1c). When the elastic strain is reduced by tension stiffening as required by the codes, the ACI's final crack widths are in similar range to the other final values.

When the elastic strain is not reduced by tension stiffening, straight-line plots are noted. When included, the graphs have lower values. The BS 5400 bridge code also has a curved shape. The curve is due to the multiplication of the value for strain reduction $\Delta\varepsilon_s$, by the complement to the fraction of live to dead service moments. This is seen in the effective strain formula of BS5400:

$$\epsilon_m = \epsilon_1 - \left[\frac{3.8 b_t h (a' - d_c)}{\epsilon_s A_s (h - d_c)}\right] \mathbf{x} \left[\left(1 - \frac{M_q}{M_g}\right) 10^{-9}\right] \quad (59)$$

(BS5400-4: Clause 5.8.8.2 Equation 25)

Where Mq is the live service moment and Mg the dead.

The curved shape is more pronounced at lower tension, flattening at higher moments, thereby modelling the diminishing tension stiffening effect under increased stress, in line with crack theory (section 2.4.3). The BS5400 code is unique in this aspect as the other codes do not consider the reduction of tension stiffening effect under increasing stress. At low live moment (starting at 0 kN.m live), BS5400 predicts values of zero and below and a drastic drop is noticed in the deeper members.

As seen in section 5.1, the British codes assume a stiffening stress much lower than the European codes, while basing the stiffening force on the full depth from the neutral axis. The graphs show the tension stiffening in the British code has a greater reduction effect in deeper members. In shallower members, the reduction remains similar across the codes. This indicates basing the concrete tension stress capacity, on the full tension depth from the neutral axis (3.1.2) results in higher strain reductions. Consequently, the British code will give lower crack widths in larger sections.

The Fib model formulation gives a slightly larger decrease in strain compared to the Eurocode. This is due to the larger coefficient for mean strain over the transfer length during crack formation, under long term loading (sections 3.3.2 and 3.5.2).

6.2 Influence of cover

Examination of the crack formulas in section 3, and the comparison in section 5.1, showed the significant influence cover had on crack spacing in the fundamental theory.

The influence of cover originates from no slip theory where the transfer length (described in 2.2.2 and 2.4.3) either side of a crack equals the cover distance. Crack spacing is a function of cover due to shear deformation, this is contained in Ferry-Borges fundamental formula for a crack appearing above reinforcement (2.6.1).

The British formulas consider only no-slip theory, adding a maximum limit to crack width based on the depth of a crack in an unreinforced section (5.1.1a). The distance on the tension face influenced by this crack equals twice the crack depth (3.1.1).

Eurocode and fib include the influence of both cover and bond effects as its formulas account for both no-slip and slip theory (5.1.1b). Like the British codes, the examination of the ACI 318 model shows this code also adopts no slip theory.

As cover depth influences crack spacing, the tension stiffening effect was ignored to directly compare results from the formulas.

The crack width is graphically compared at constant moments with cover distances varying from 20mm to 60mm. To amplify the influence of cover, the loading arrangement was changed. Firstly the applied service moment is the sum of dead moment and a live moment equal to half the dead. In the second instance, the applied service moment is the sum of dead moment and a live moment equal to the dead. These comparisons were done for a shallow and deep member.

The fib model and Eurocode predict the highest widths overall. This is expected since the final crack width in these codes is a function of both non-slip and slip behaviour. The British and American codes only consider the initial non-slip stage (5.1.1a). The result is evident as the lowest results are predicted where only deformation from non-slip behaviour is noted. In shallow members, an identical trend exists across all the codes. The crack widths increase proportionally with increasing cover. The load intensity does not alter the relationship.

In deep members, the codes considering no slip and slip behaviour still show a constant increase in crack width with thickening cover. The trend differs in the British and ACI code, where no increase in crack width occurs with increasing cover. The British code has a higher crack width, due to its formulation adding the unreinforced effect (3.1.1) to its cover allowance.

The theory however indicates cracks widen over thicker cover widths (2.2.2). This analysis shows relating cover to crack width in Ferry-Borges (2.6.1) does not provide reliable results in deeper members.

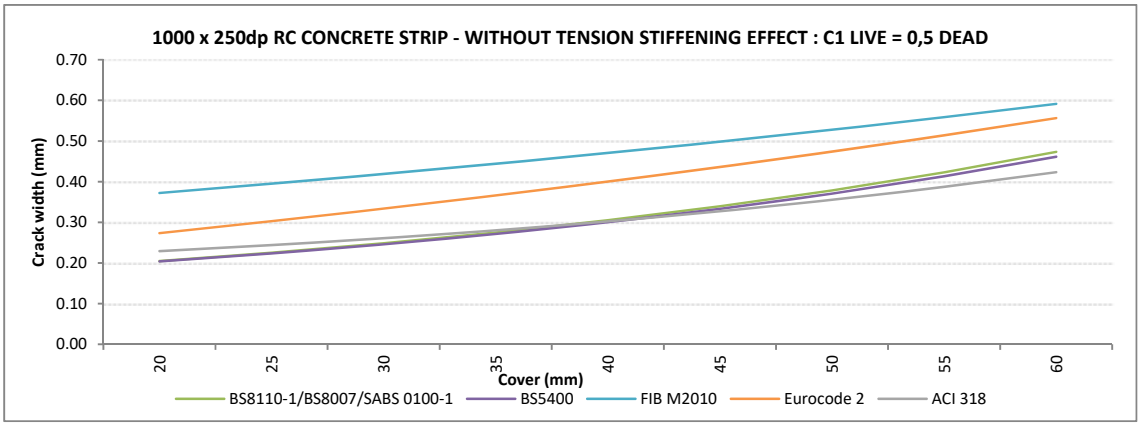
1000 x 250dp RC CONCRETE STRIP - WITHOUT TENSION STIFFENING EFFECT : C1 LIVE = 0,5 DEAD
Crack width (mm)
0.70
0.60
0.50
0.40
0.30
0.20
0.10
0.00
20
25
30
35
40
45
50
55
60
Cover (mm)
BS8110-1/BS8007/SABS 0100-1
BS5400
FIB M2010
Eurocode 2
ACI 318

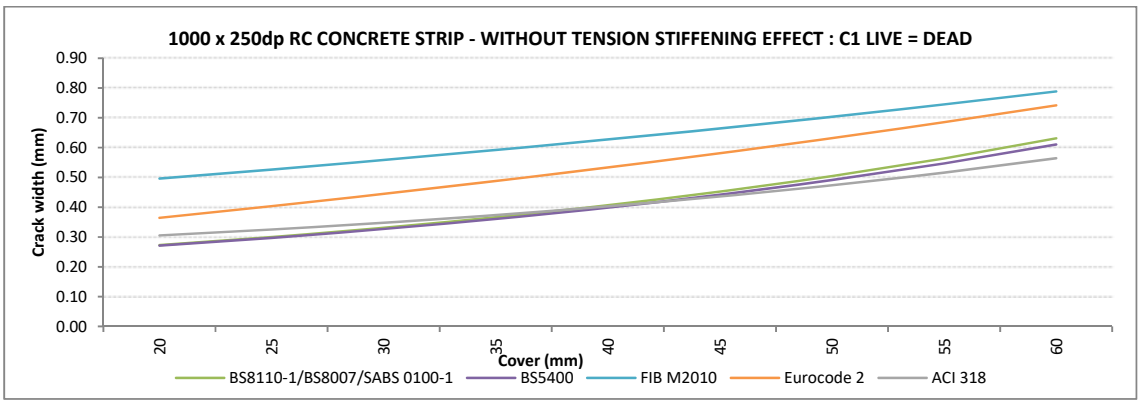
1000 x 250dp RC CONCRETE STRIP - WITHOUT TENSION STIFFENING EFFECT : C1 LIVE = DEAD
Crack width (mm)
0.90
0.80
0.70
0.60
0.50
0.40
0.30
0.20
0.10
0.00
20
25
30
35
40
45
50
55
60
Cover (mm)
BS8110-1/BS8007/SABS 0100-1
BS5400
FIB M2010
Eurocode 2
ACI 318

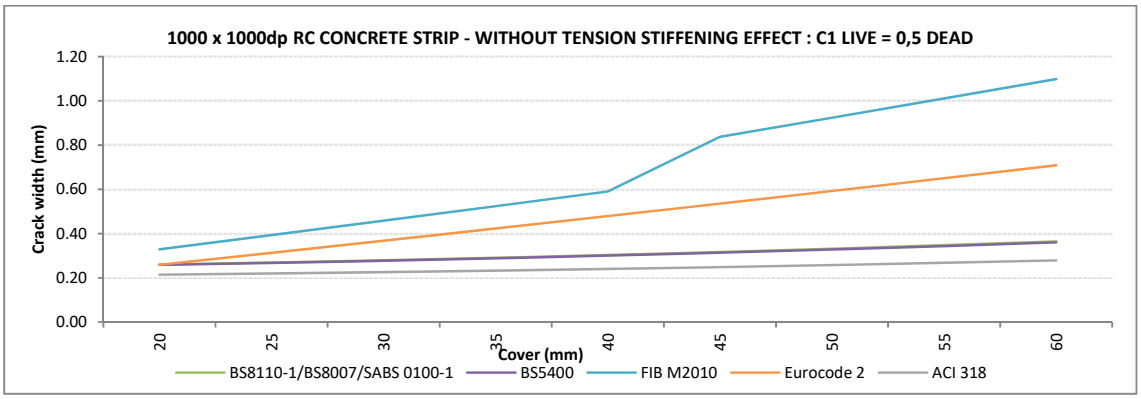
1000 x 1000dp RC CONCRETE STRIP - WITHOUT TENSION STIFFENING EFFECT : C1 LIVE = 0,5 DEAD
Crack width (mm)
1.20
1.00
0.80
0.60
0.40
0.20
0.00
20
25
30
35
40
45
50
55
60
Cover (mm)
BS8110-1/BS8007/SABS 0100-1
BS5400
FIB M2010
Eurocode 2
ACI 318

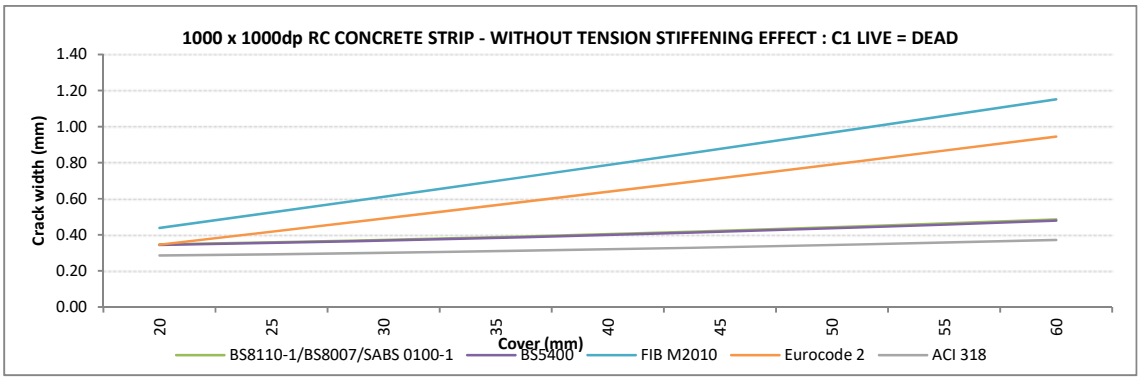
1000 x 1000dp RC CONCRETE STRIP - WITHOUT TENSION STIFFENING EFFECT : C1 LIVE = DEAD
Crack width (mm)
1.40
1.20
1.00
0.80
0.60
0.40
0.20
0.00
20
25
30
35
40
45
50
55
60
Cover (mm)
BS8110-1/BS8007/SABS 0100-1
BS5400
FIB M2010
Eurocode 2
ACI 318

6.3 Modelling bond effects

The British code ignores the reinforcement ratio $\frac{\emptyset}{\rho}$ (section 3.1.1), and thereby ignores the influence of bond from the fundamental Ferry-Borges equation (section 2.6.1a). The same applies to the Frosch model in ACI 318. Consequently, these codes estimate lower crack width values versus the codes that additionally consider the bond term. This is also seen in the earlier graphs ignoring tension stiffening.

The Eurocode and Fib code includes the fundamental term for bond (section 5.1.1), approximating bond failure with an empirical variable for bond strength. The Fib model code calculates the bond strength by multiplying $\frac{\emptyset}{\rho}$ with the ratio of concrete tensile strength and bond stress. Here bond stress is an empirical value for crack stage and load duration (Figure 3-7). In the Eurocode, empirical factors for bond and stress type (bending or tension stress), are multiplied by the ratio $\frac{\emptyset}{\rho}$. This models the following fundamental theory:

- The distribution of bond stresses around the rebar is dependent on the type of stress (section 2.6.1) - accounted for by Eurocode only.
- The bond between rebar and concrete reduces with load duration (section 2.4.3) - accounted for by Fib only.

The factors in the Eurocode accounting for the bond properties in reinforcement are 0,8 for high bond bar and 1,6 for smooth bars. To assess the influence bond has on the formulas, graphs were plotted where the effect of bond loss was increased in increments of 30% from 0,8.

The bond stress in the Fib model code is obtained by factoring the tensile strength of the concrete. To assess the impact of bond here, the factor of 1,8 was reduced incrementally by 30% to weaken the bond strength.

The resulting graphs show a constant rate of widening crack width for a constant strain increase due to the loading described in section 5.3. Cover does not influence the impact of varying bond.
This indicates the impact of bond on crack width in the fundamental Ferry-Borges formula is much greater than the contribution of cover effects. With weaker bond, the rate of crack width increase is greater.

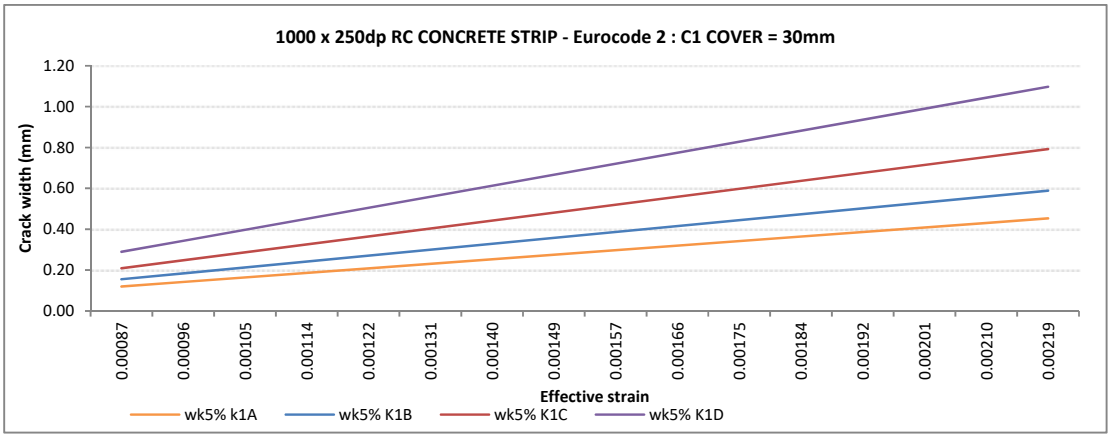
1000 x 250dp RC CONCRETE STRIP - Eurocode 2 : C1 COVER = 30mm
Crack width (mm)
1.20
1.00
0.80
0.60
0.40
0.20
0.00
0.00087
0.00096
0.00105
0.00114
0.00122
0.00131
0.00140
0.00149
0.00157
0.00166
0.00175
0.00184
0.00192
0.00201
0.00210
0.00219
Effective strain
wk5% k1A
wk5% K1B
wk5% K1C
wk5% K1D

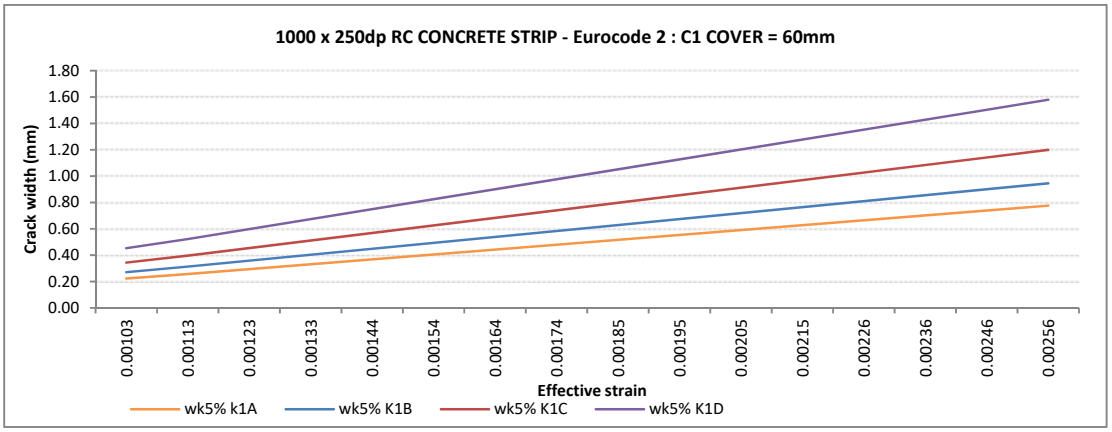
1000 x 250dp RC CONCRETE STRIP - Eurocode 2 : C1 COVER = 60mm
Crack width (mm)
1.80
1.60
1.40
1.20
1.00
0.80
0.60
0.40
0.20
0.00
0.00103
0.00113
0.00123
0.00133
0.00144
0.00154
0.00164
0.00174
0.00185
0.00195
0.00205
0.00215
0.00226
0.00236
0.00246
0.00256
Effective strain
wk5% k1A
wk5% K1B
wk5% K1C
wk5% K1D

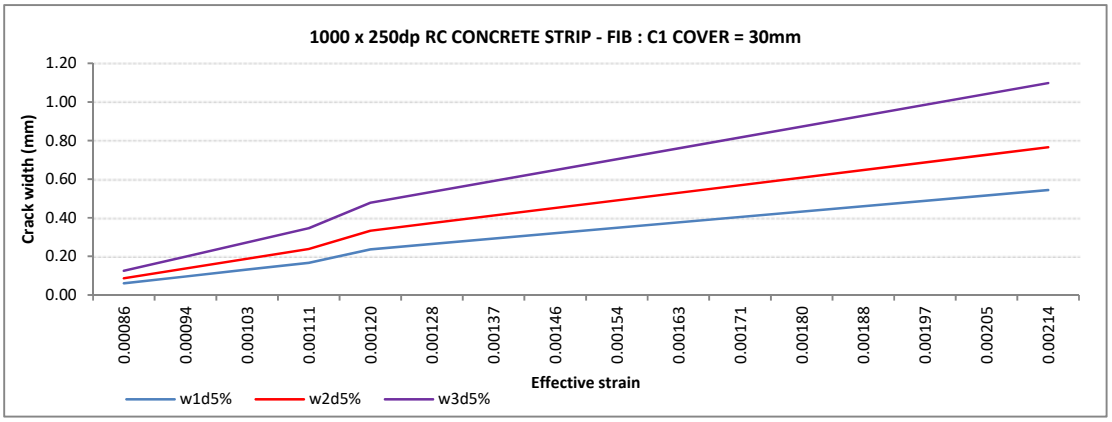
1000 x 250dp RC CONCRETE STRIP - FIB : C1 COVER = 30mm
Crack width (mm)
1.20
1.00
0.80
0.60
0.40
0.20
0.00
0.00086
0.00094
0.00103
0.00111
0.00120
0.00128
0.00137
0.00146
0.00154
0.00163
0.00171
0.00180
0.00188
0.00197
0.00205
0.00214
Effective strain
w1d5%
w2d5%
w3d5%

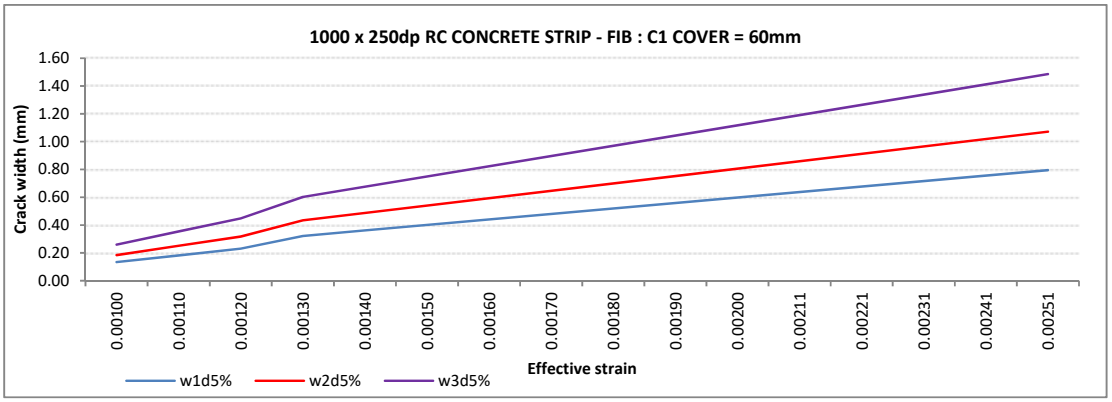
1000 x 250dp RC CONCRETE STRIP - FIB : C1 COVER = 60mm
Crack width (mm)
1.60
1.40
1.20
1.00
0.80
0.60
0.40
0.20
0.00
0.00100
0.00110
0.00120
0.00130
0.00140
0.00150
0.00160
0.00170
0.00180
0.00190
0.00200
0.00211
0.00221
0.00231
0.00241
0.00251
Effective strain
w1d5%
w2d5%
w3d5%

6.4 Secondary cracking

Where the spacing of cracks equals twice the transfer length, the cracks formed to this point are called the primary cracks (section 2.2.2). This is the end of the crack formation stage and during the propagation stage the primary cracks widen. As described in section 2.2.2, new cracks in the form of secondary cracking can still form while the primary cracks widen. These result from the tension stresses in the individual bars.

A larger bar transfers more stress to the surrounding concrete than a smaller. With a higher stress in the encasing concrete, a larger amount of secondary cracking is expected (section 2.6.1). The extent and width of secondary cracks are therefore directly affected by rebar detailing, as the use of smaller bars will result in less tension stress in the encasing concrete.

The case C2 uses larger bars at wider spacings for each of the scenarios previously analysed (refer to section 5.3).

In the shallow members, an increase in crack width is noted for the larger bars at wider spacings equating to the same area of steel. The least impact is seen in the Eurocode and British code. The largest is noted in the remaining codes with the largest increase in the ACI code.

In the deeper members the trend is similar, with the Eurocode remaining the most constant. The codes considering only the cover term in Ferry-Borges estimate crack widths closer to Eurocode. The increase in ACI is not as substantial as in shallow members. When comparing the differences in bond for increasing steel stress, the increase in the crack widths are not as substantial.

These graphs show the influence of tension rebar layout is greater in the codes that only consider the effect of cover. Theory indicates bar configuration influences the stress around the rebar, increasing breakage and loss of bond strength (section 2.6.1). This theory indicates a greater impact should be seen in the codes considering bond failure.

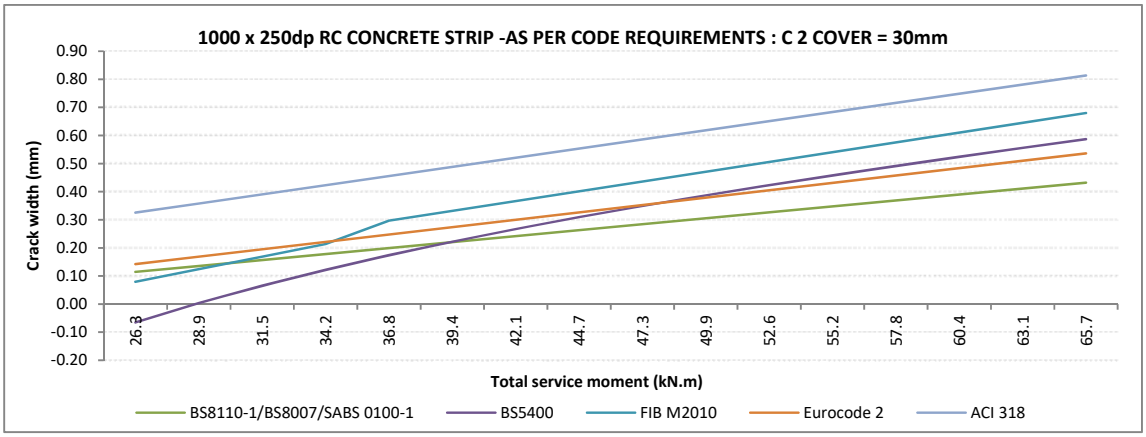
1000 x 250dp RC CONCRETE STRIP -AS PER CODE REQUIREMENTS : C 2 COVER = 30mm
Crack width (mm)
0.90
0.80
0.70
0.60
0.50
0.40
0.30
0.20
0.10
0.00
-0.10
-0.20
26.3
28.9
31.5
34.2
36.8
39.4
42.1
44.7
47.3
49.9
52.6
55.2
57.8
60.4
63.1
65.7
Total service moment (kN.m)
BS8110-1/BS8007/SABS 0100-1
BS5400
FIB M2010
Eurocode 2
ACI 318

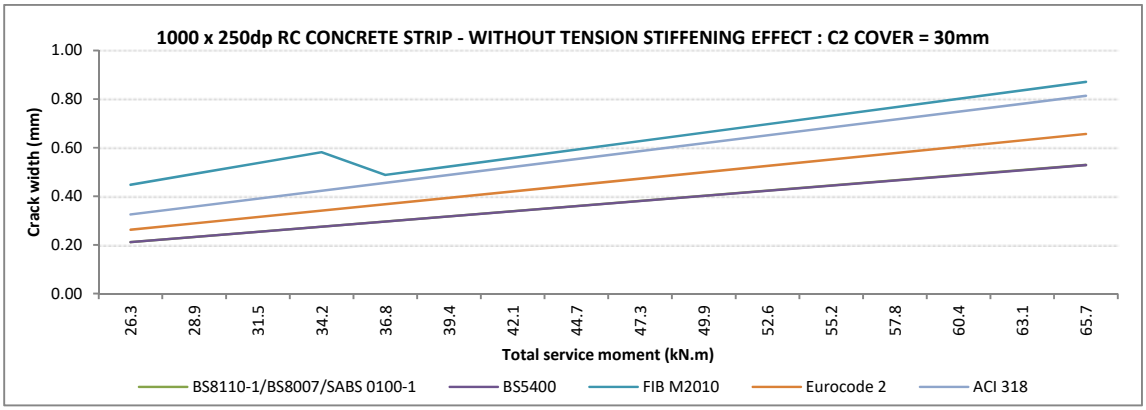
1000 x 250dp RC CONCRETE STRIP - WITHOUT TENSION STIFFENING EFFECT : C2 COVER = 30mm
Crack width (mm)
1.00
0.80
0.60
0.40
0.20
0.00
26.3
28.9
31.5
34.2
36.8
39.4
42.1
44.7
47.3
49.9
52.6
55.2
57.8
60.4
63.1
65.7
Total service moment (kN.m)
BS8110-1/BS8007/SABS 0100-1
BS5400
FIB M2010
Eurocode 2
ACI 318

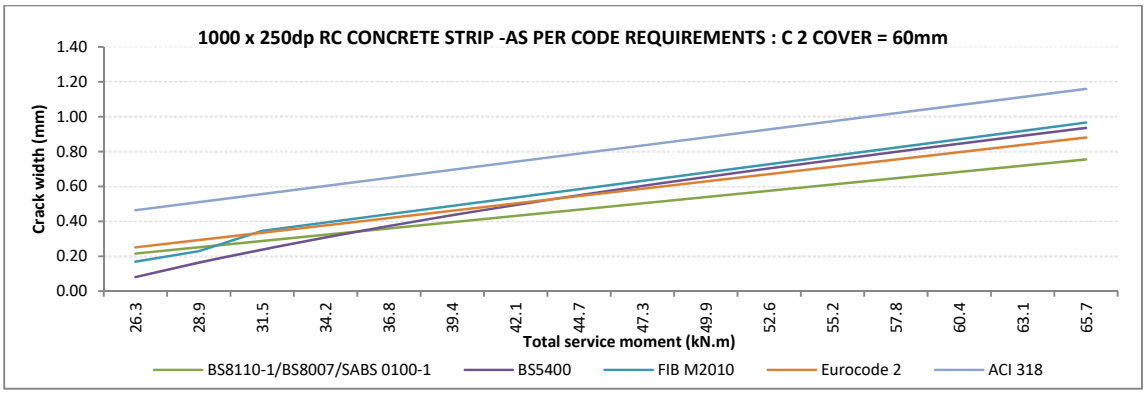
1000 x 250dp RC CONCRETE STRIP -AS PER CODE REQUIREMENTS : C 2 COVER = 60mm
Crack width (mm)
1.40
1.20
1.00
0.80
0.60
0.40
0.20
0.00
26.3
28.9
31.5
34.2
36.8
39.4
42.1
44.7
47.3
49.9
52.6
55.2
57.8
60.4
63.1
65.7
Total service moment (kN.m)
BS8110-1/BS8007/SABS 0100-1
BS5400
FIB M2010
Eurocode 2
ACI 318

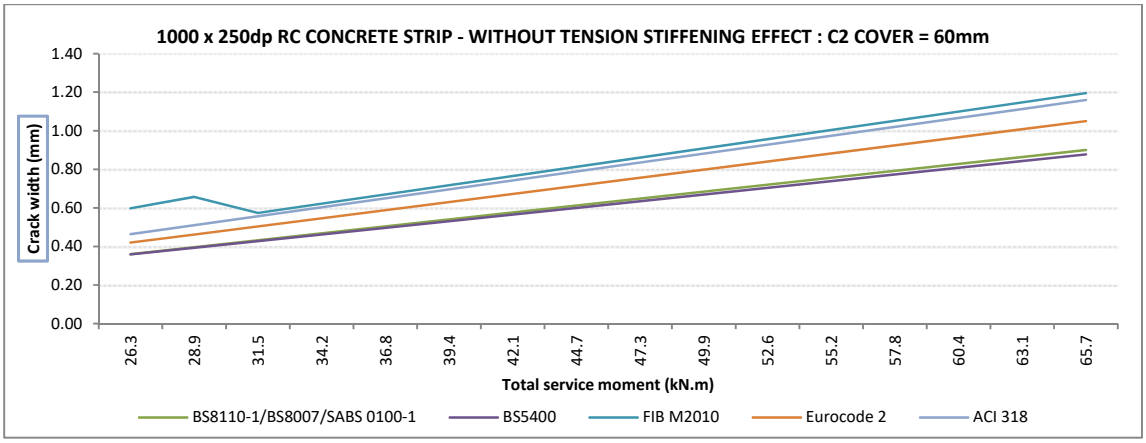
1000 x 250dp RC CONCRETE STRIP - WITHOUT TENSION STIFFENING EFFECT : C2 COVER = 60mm
Crack width (mm)
1.40
1.20
1.00
0.80
0.60
0.40
0.20
0.00
26.3
28.9
31.5
34.2
36.8
39.4
42.1
44.7
47.3
49.9
52.6
55.2
57.8
60.4
63.1
65.7
Total service moment (kN.m)
BS8110-1/BS8007/SABS 0100-1
BS5400
FIB M2010
Eurocode 2
ACI 318

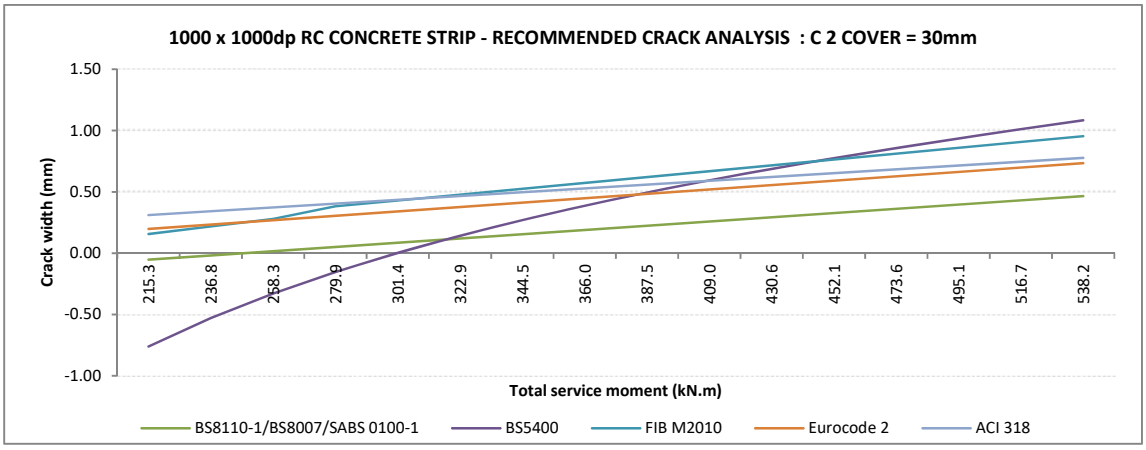
1000 x 1000dp RC CONCRETE STRIP - RECOMMENDED CRACK ANALYSIS : C 2 COVER = 30mm
Crack width (mm)
1.50
1.00
0.50
0.00
-0.50
-1.00
215.3
236.8
258.3
279.9
301.4
322.9
344.5
366.0
387.5
409.0
430.6
452.1
473.6
495.1
516.7
538.2
Total service moment (kN.m)
BS8110-1/BS8007/SABS 0100-1
BS5400
FIB M2010
Eurocode 2
ACI 318

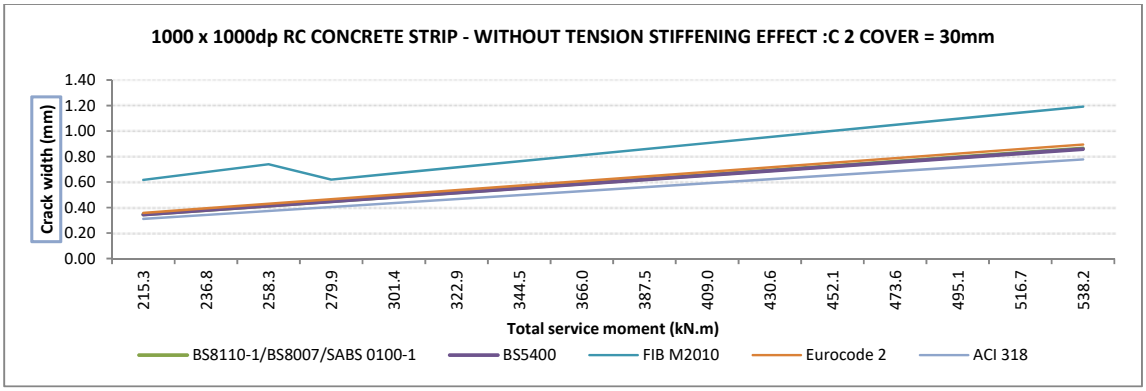
1000 x 1000dp RC CONCRETE STRIP - WITHOUT TENSION STIFFENING EFFECT :C 2 COVER = 30mm
Crack width (mm)
1.40
1.20
1.00
0.80
0.60
0.40
0.20
0.00
215.3
236.8
258.3
279.9
301.4
322.9
344.5
366.0
387.5
409.0
430.6
452.1
473.6
495.1
516.7
538.2
Total service moment (kN.m)
BS8110-1/BS8007/SABS 0100-1
BS5400
FIB M2010
Eurocode 2
ACI 318

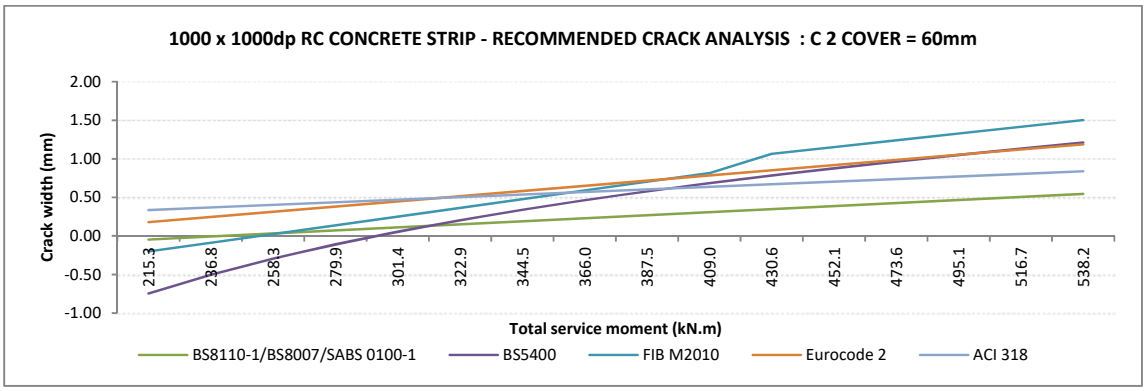
1000 x 1000dp RC CONCRETE STRIP - RECOMMENDED CRACK ANALYSIS : C 2 COVER = 60mm
Crack width (mm)
2.00
1.50
1.00
0.50
0.00
-0.50
-1.00
215.3
236.8
258.3
279.9
301.4
322.9
344.5
366.0
387.5
409.0
430.6
452.1
473.6
495.1
516.7
538.2
Total service moment (kN.m)
BS8110-1/BS8007/SABS 0100-1
BS5400
FIB M2010
Eurocode 2
ACI 318

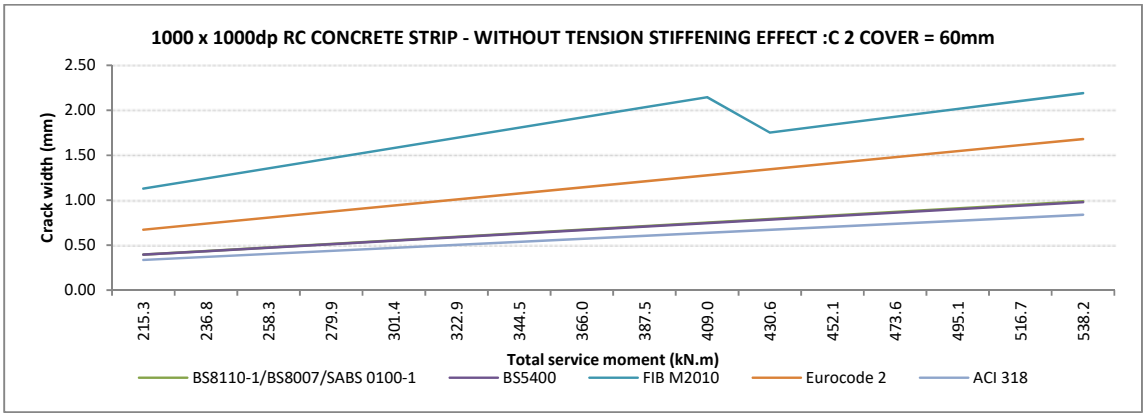
1000 x 1000dp RC CONCRETE STRIP - WITHOUT TENSION STIFFENING EFFECT :C 2 COVER = 60mm
Crack width (mm)
2.50
2.00
1.50
1.00
0.50
0.00
215.3
236.8
258.3
279.9
301.4
322.9
344.5
366.0
387.5
409.0
430.6
452.1
473.6
495.1
516.7
538.2
Total service moment (kN.m)
BS8110-1/BS8007/SABS 0100-1
BS5400
FIB M2010
Eurocode 2
ACI 318

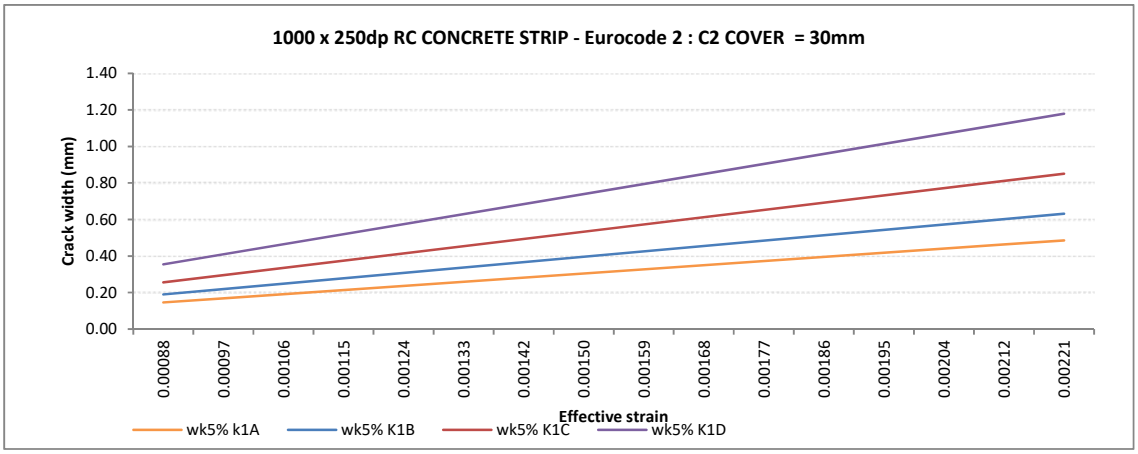
1000 x 250dp RC CONCRETE STRIP - Eurocode 2 : C2 COVER = 30mm
Crack width (mm)
1.40
1.20
1.00
0.80
0.60
0.40
0.20
0.00
0.00088
0.00097
0.00106
0.00115
0.00124
0.00133
0.00142
0.00150
0.00159
0.00168
0.00177
0.00186
0.00195
0.00204
0.00212
0.00221
Effective strain
wk5% k1A
wk5% K1B
wk5% K1C
wk5% K1D

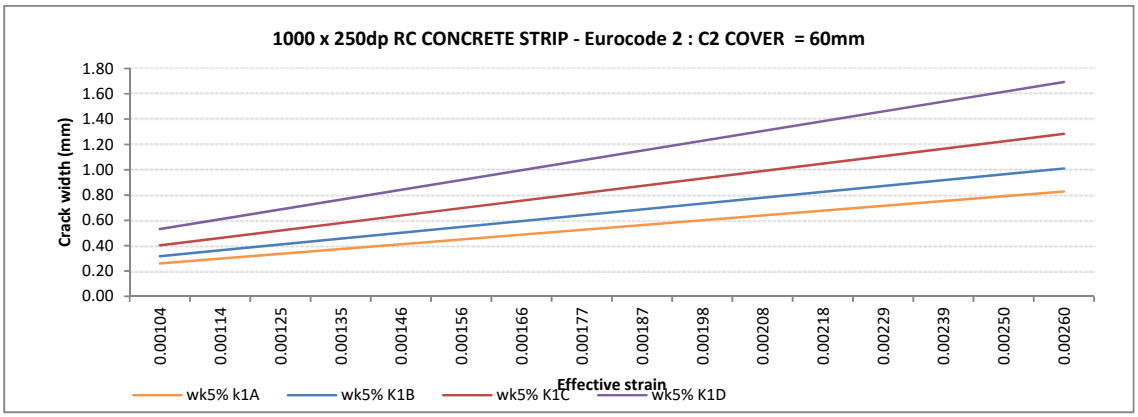
1000 x 250dp RC CONCRETE STRIP - Eurocode 2 : C2 COVER = 60mm
Crack width (mm)
1.80
1.60
1.40
1.20
1.00
0.80
0.60
0.40
0.20
0.00
0.00104
0.00114
0.00125
0.00135
0.00146
0.00156
0.00166
0.00177
0.00187
0.00198
0.00208
0.00218
0.00229
0.00239
0.00250
0.00260
Effective strain
wk5% k1A
wk5% K1B
wk5% K1C
wk5% K1D

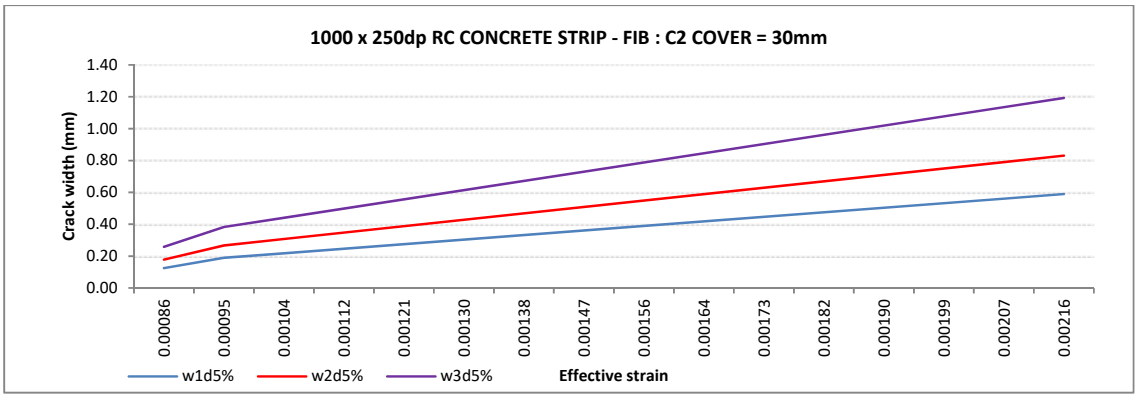
1000 x 250dp RC CONCRETE STRIP - FIB : C2 COVER = 30mm
Crack width (mm)
1.40
1.20
1.00
0.80
0.60
0.40
0.20
0.00
0.00086
0.00095
0.00104
0.00112
0.00121
0.00130
0.00138
0.00147
0.00156
0.00164
0.00173
0.00182
0.00190
0.00199
0.00207
0.00216
w1d5%
w2d5%
w3d5%
Effective strain

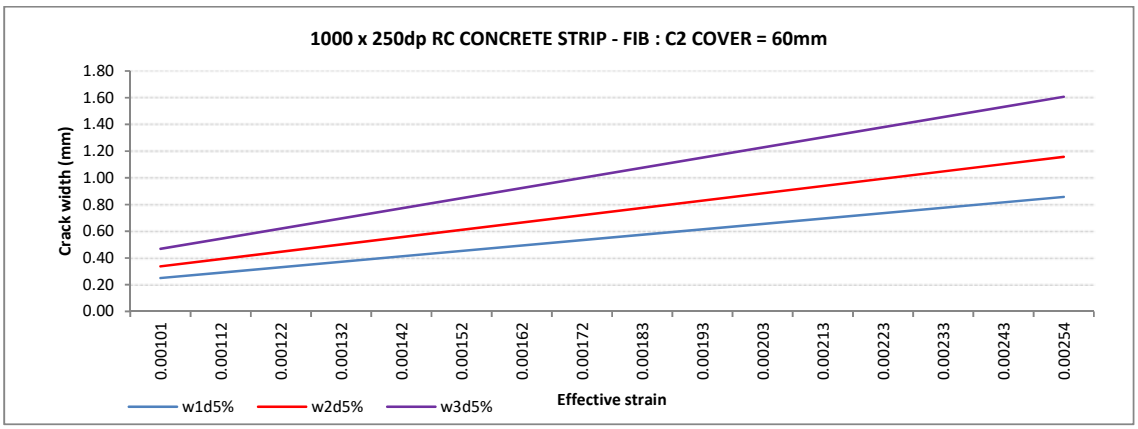
1000 x 250dp RC CONCRETE STRIP - FIB : C2 COVER = 60mm
Crack width (mm)
1.80
1.60
1.40
1.20
1.00
0.80
0.60
0.40
0.20
0.00
0.00101
0.00112
0.00122
0.00132
0.00142
0.00152
0.00162
0.00172
0.00183
0.00193
0.00203
0.00213
0.00223
0.00233
0.00243
0.00254
w1d5%
w2d5%
w3d5%
Effective strain

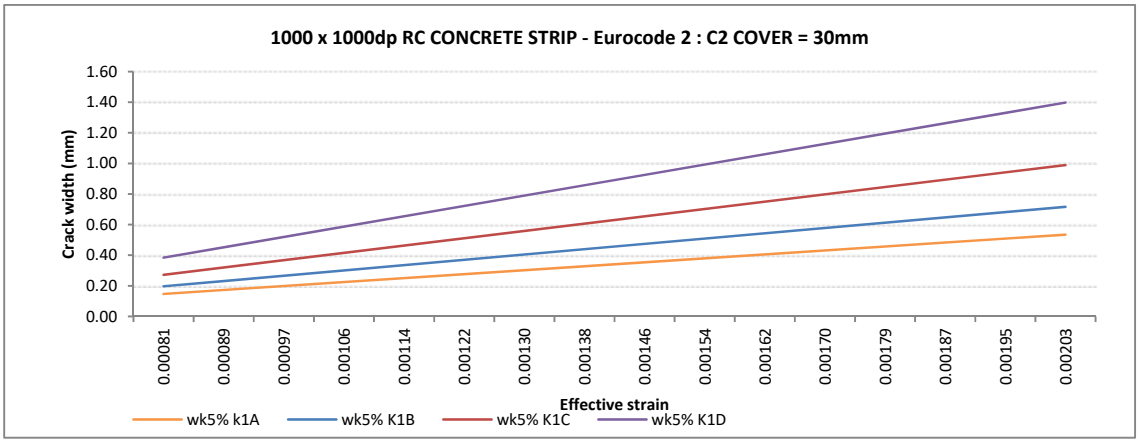
1000 x 1000dp RC CONCRETE STRIP - Eurocode 2 : C2 COVER = 30mm
Crack width (mm)
1.60
1.40
1.20
1.00
0.80
0.60
0.40
0.20
0.00
0.00081
0.00089
0.00097
0.00106
0.00114
0.00122
0.00130
0.00138
0.00146
0.00154
0.00162
0.00170
0.00179
0.00187
0.00195
0.00203
Effective strain
wk5% k1A
wk5% K1B
wk5% K1C
wk5% K1D

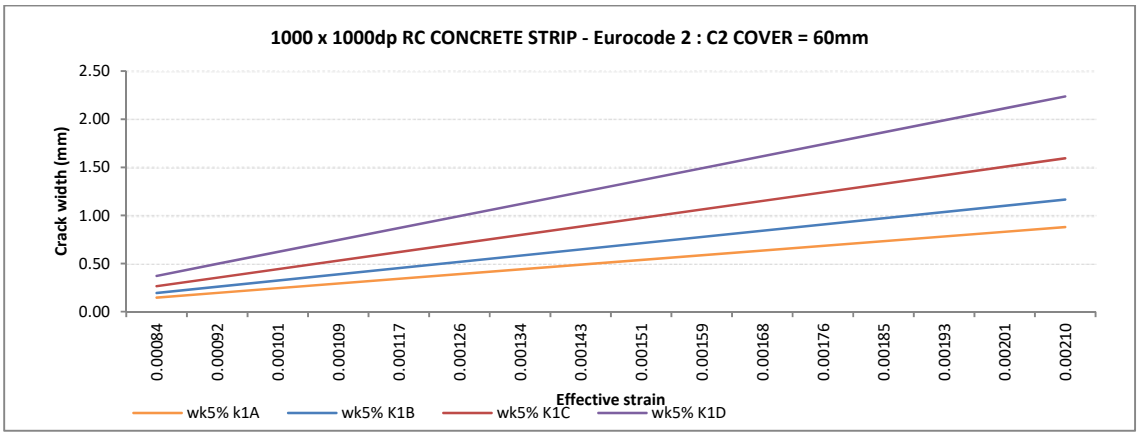
1000 x 1000dp RC CONCRETE STRIP - Eurocode 2 : C2 COVER = 60mm
Crack width (mm)
2.50
2.00
1.50
1.00
0.50
0.00
0.00084
0.00092
0.00101
0.00109
0.00117
0.00126
0.00134
0.00143
0.00151
0.00159
0.00168
0.00176
0.00185
0.00193
0.00201
0.00210
Effective strain
wk5% k1A
wk5% K1B
wk5% K1C
wk5% K1D

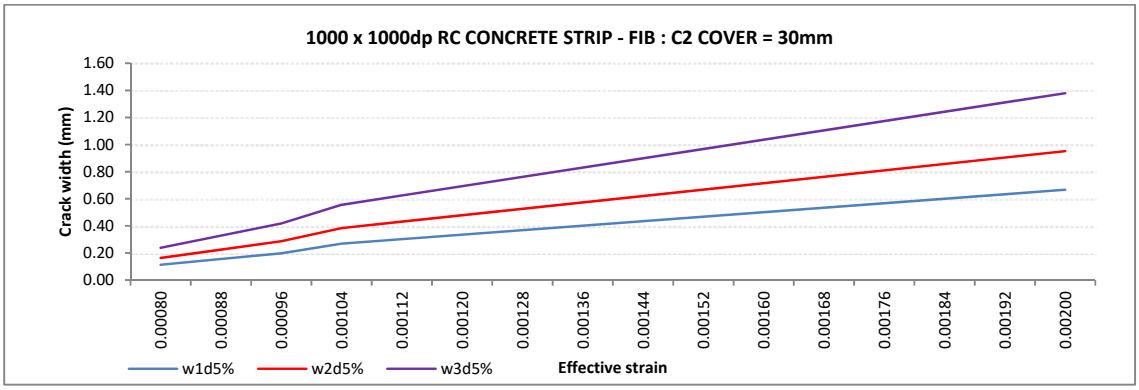
1000 x 1000dp RC CONCRETE STRIP - FIB : C2 COVER = 30mm
Crack width (mm)
1.60
1.40
1.20
1.00
0.80
0.60
0.40
0.20
0.00
0.00080
0.00088
0.00096
0.00104
0.00112
0.00120
0.00128
0.00136
0.00144
0.00152
0.00160
0.00168
0.00176
0.00184
0.00192
0.00200
w1d5%
w2d5%
w3d5%
Effective strain

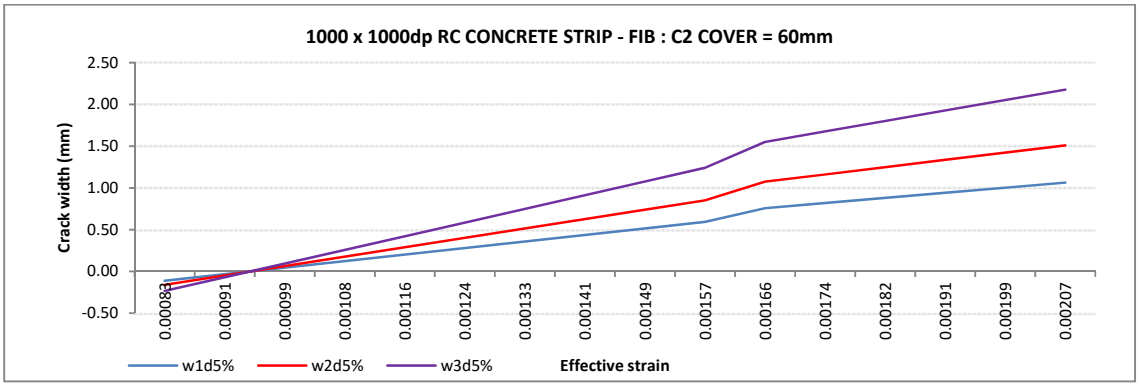
1000 x 1000dp RC CONCRETE STRIP - FIB : C2 COVER = 60mm
Crack width (mm)
2.50
2.00
1.50
1.00
0.50
0.00
-0.50
0.00083
0.00091
0.00099
0.00108
0.00116
0.00124
0.00133
0.00141
0.00149
0.00157
0.00166
0.00174
0.00182
0.00191
0.00199
0.00207
w1d5%
w2d5%
w3d5%
Effective strain

7. DISCUSSION

According to Fantilli, Vallini and Mihashi (section 2.2.2), the crack profile in reinforced concrete members is determined by the following factors:

- Bond slip mechanisms
- Fracture mechanics of concrete
- Shear deformability of concrete

This study has examined how the analytical and numerical crack models simulate these three crack mechanisms to estimate average crack widths.

The numerical methods presented provide the most accurate physical model to for crack analysis. They create models of reinforced concrete which simulate the available fracture energy based on principles of fracture mechanics. Additionally, the methods allow numerical approximations for bond slip and shear deformability.

Simpler, more convenient methods for practitioners are available through analytical approaches, based on approximations for shear deformability and bond slip. Crack width calculation in reinforced concrete design codes are based on analytical methods (see section 3). The methods use elastic beam analysis to estimate tension strain in the section. Tension softening (2.4.3) occurring before RC beam failure, due to the elastic mismatch of steel and concrete, creates local cracks. This maintains the elastic rule of strain compatibility over the depth of the beam section.

Based on this examination, the numerical and analytical methods presented can be categorised according to their theoretical focus:

- Discrete and smeared crack approaches (Numerical) - Fracture mechanics, Shear deformability, Bond slip mechanisms
- Eurocode and Fib concrete design codes (Analytical) - Shear deformability, Bond slip mechanisms
- British codes and ACI 318 concrete design codes (Analytical) - Shear deformability

Concrete in the immediate vicinity of reinforcement bonds to the steel surface, resisting strain deformation. The bond exists through the adhesion, friction and mechanical interlock of the steel to the concrete (section 2.4.1). For the matrix to split by crack formation, the concrete around the steel reinforcement needs to slide relative. The resulting surface crack widths can differ considerably from the primary cracks' widths at the steel surface (section 2.2.2).

7.1 Numerical theorems

Fracture is the breaking down of a solid under applied stress. The fracture of a solid body is related to its deformation response as depicted by the stress and strain response curves (see section 2.3). The curves fit the three response categories of ductile, brittle and quasi-brittle. The behaviour is unique to its categorisation in these deformation responses. Fracture energy of a material equals the area under the plot of these response curves. The area thereby equals the energy required to reach a point towards ultimate failure.

Fracture energy measures toughness and brittleness, where the larger the energy, the more work required towards failure i.e. less brittle.

In section 2.1.1, the influence of the characteristics of the concrete matrix on fracture energy was examined. Concretes quasi-brittle nature is attributed to its heterogenous material constituents. The constituents form different phases in the mixture related to its deformation response. The aggregates are brittle, and the cement paste is liquid transforming into a brittle with hardening. The microphases form the quasi-brittle body with characteristics determined at the micro-level interface. Soundness of this interface is the primary factor determining the bodies material fracture energy as described in 2.3.4.

7.2 Analytical theorems

The study showed the theoretical basis for analytical crack modelling is the typical action of a centrally reinforced concrete tie (sections 2.5.2 and 2.6.1a). The fundamental theory also includes an estimate of cracking resulting from shear deformability (section 2.6.1b), as examined in section 2.2.2.

When applied to beam action, shear deformability and slip action overlap (section 2.6.1).

These contributing factors lead to the contrasting crack theorems of non-slip and slip behaviour (section 2.2.2), relevant once surface cracks form (after localised tension softening has occurred) (section 2.4.3):

- Non-slip action - cracking in a reinforced concrete beam under flexural tension begins at the tension surface through bending deformation. (failure after tension softening)
- Slip action - at higher levels of reinforcement stress, relative slip occurs between the reinforcement and encasing concrete, thereby exposing the steel surface (influenced by adjacent tension stiffening).

These two theorems led to the fundamental crack theorem of Ferry-Borges, combining the influence of both theories to estimate crack spacing (section 2.6.1c).

The compatibility equation for average crack width is the crack spacing multiplied by the effective cracking strain (section 2.6). The effective crack strain is the elastic strain, from beam theory, at the level of tension steel, less allowances for tension stiffening (section 2.2.2). The transfer of tension stress from steel to concrete over the transfer length, increases the stiffness of the steel.

In reinforced concrete ties under axial tension, cracks occur at the meso level interface, at the rebar surface. The tension strain in concrete is higher than the steel and the concrete slides relative, indicating local failure. The steel away from the crack is stiffened, reducing the cracking strain from the steel. The stiffening effect diminishes under large stress, repetitive and long-term loading (section 2.4.3). With the uncertainty of the stress level where tension stiffening is no longer effective, commentary on the BS5400 recommends it might be prudent to ignore the effect. The ACI 318 code ignores the effect completely (section 3.4.2).

7.3 Application of models

The examination of the theories behind the crack models allows the reliability of each approach to be explained.

7.3.1 Numerical methods

The smeared-crack approach is the preferred numerical method for crack analysis of reinforced concrete members (section 5.2). It models the concrete member in its entirety, not only the localised failure, as in the discrete crack approach and analytical methods.

The fracture energy within a body is a function of the amount of inelastic strain in a material before ultimate failure (section 2.3). Concrete in its hardened form has quasi-brittle behaviour under applied stress as it undergoes inelastic strain, not seen in brittle deformation, before failure (section 2.3.3). The extent of this inelastic strain, and hence delayed failure, has been shown (section 2.1.1) to be a function of aggregate shape, aggregate volume in the mix, nominal aggregate size and the condition of the interfacial transition zone.

After tension softening wears off and the concrete fails locally, all the stress at failure transfers to the steel present in the concrete matrix. This transfer occurs through the bond stress, a function of the bond between the steel and concrete. The incompatibility of strains causes bond slip to occur between the steel and concrete. Mesh sequences representing the micro and meso level relationships contributing to facture energy, provides a model of the fracture characteristics of the concrete body. This mesh includes energy transfer simulation of bond stresses (bond-slip model). The mesh sequence in the smeared crack approach uses finite element analysis, a universally accepted form of reinforced concrete analysis.

7.3.2 Analytical methods

The comparison of the crack models (section 5.1) grouped each according to their application of the fundamental Ferry-Borges equation.

The Eurocode and fib code accounts for all terms in this formula to estimate crack spacing. These models factor the shear deformability over cover distance and the bond slip failure at the rebar perimeter. It therefore also has variables for bond strength. Based on experimental results (section 3.1.1), these methods determine the crack width directly above the tension bar.

The ACI 318 and the British codes include an estimate for shear deformability, by assuming a reduction in tension stress on the concrete surface related to the cover depth. The British formulation assumes the worst crack width to be furthest from the rebar. The term for bond stress distribution is ignored (second term in Ferry-Borges), as the widths closest to tension rebar is assumed to be much less (section 3.1.1.). The British code adds a further factor assuming an unreinforced member in bending, with tension reduction on the concrete surface being equal to the crack height formed. With this approach, the code only considers the rebar with regards to its spacing and ignores bond stresses, while still including a tension stiffening effect. An increase in the factor for shear deformability over cover is considered to account for any additional influence of bond failure. The ACI code ignores the tension stiffening effects, completely avoiding bond considerations.

Considering the fundamental theory, Eurocode and the Fib code would likely predict higher average crack widths. The British code should estimate slightly higher values than ACI, as it includes a factor for an unreinforced member. This is confirmed by the analysis in section 6.

A comparison of the crack width values without the reduction for tension stiffening, shows under the same loading and configuration the Fib code and Eurocode provides the highest estimates of crack width. Thus, by retaining the bond slip factor, wider crack values are predicted. The approach of the British code to ignore the reinforcement ratio and compensate by increasing the shear deformability factor (section 3.1.1), does not sufficiently account for bond-slip failure. Similarly, the same deduction applies to the ACI 318 code, where the lowest crack widths are predicted.

These outcomes are further emphasised by the graphs comparing crack widths over increasing cover (section 6.2). The crack widths remain the lowest for the British and ACI code. The graphs of 60mm cover with increasing load, show at lower loads these codes provide estimates closer relative to the European models. The increase in cover does increase the shear deformability factor on which British and ACI code places emphasis. The influence of cover on the crack width values is less than the influence of bond-slip. This is further proved

in the graphs of increasing cover, where the rate of crack width increase is constant. In the deeper members, increasing cover does not increase crack width, which does not correlate with basic theory.

The hypothesis underlying the British codes, where the largest crack width occurs furthest from the tension steel, ignores the crack at the rebar. The potential for corrosion is effectively ignored since this originates from bond slip. Above the rebar, bond slip will expose the naked steel to corrosive effects. Where water tightness between bars is a requirement, the no-bond slip equations are therefore more relevant.

The inclusion of the tension stiffening effect to determine the final crack values, changes the trend. The low values from the ACI 318, which does not consider tension stiffening in the final crack width value, are in comparable range with the rest of the codes. Although the tension stiffening reduces the crack widths throughout, the effect should taper off at higher applied loads (section 2.6.2). This does not occur since in the graphs, the widening crack width trend increases past the point of 0,87fy. The tension stiffening estimate under higher stresses is therefore inaccurate.

The final values for BS5400 is questionable as the inclusion of the stiffening effect results in a curved line, which is negative under low applied moments. In deeper members, the negative value further decreases. The values appear acceptable from about a third of the yield stress.

BS8110 uses an assumed stiffening stress $\left(\frac{2}{3}\ MPa\right)$over the full depth of the tension area to estimate the effective stiffening force (section 5.1.2a). Eurocode and Fib applies an assumed stress of 2MPa over an effective area around the tension steel (section 5.1.2b). The BS 8110 therefore has a higher tension stiffening value, and resultant lower crack width estimate, in larger sections. The European codes will have a greater decrease with larger cover.

Closer examination of the Fib model code across all cases in this examination, show that before the tensile force is reached, the crack width widens drastically. The rapid increase in crack width during crack formation across all configurations does not correlate with the flatter trend line in crack propagation. This flatter trend line is more comparable with the slope of the lines for the other codes. The fib code states during crack formation stage the crack widths do not widen until the constant tensile cracking force is exceeded. The increasing crack width in the graphs indicate the predicted values in the Fib crack model during formation are possibly not reliable. Under lower stresses the Fib model should be used with caution, however this is not a critical crack stage in any case. The crack width values above the constant tensile cracking force can be considered more reliable crack estimation by the Fib model code.

Bond strength between rebar and concrete, has a significant impact on crack width, at both the bar and concrete surfaces (section 2.4.1). This has been shown where the codes that allow for bond-slip predict higher crack values. Changes in bond conditions have a significant impact on crack width. Crack widths widen at higher stresses when the bond weakens (graphs in section 6.3). The BS and ACI would underestimate crack width, especially where wider bar spacing is used. By considering the combination of all influencing factors discussed in this section, it is clear the British standard has the highest potential to underestimate crack widths. In deep members this reduction can be greatly magnified, due to the larger effective tension area of the British codes.

7.4 Crack width and service life prediction

Analytical models determine slip lengths at rebar surfaces from the relative strain differences that exist between bonded rebar and the surrounding concrete. The rigorous formulation of slip lengths, obtained by the integration of actual strains, is simplified by the formulas for average design crack width. The bond of steel and concrete resists the relative sliding behaviour that leads to steel exposure. Corrosion of rebar was examined in section 2.2.3. Corrosion initiation is caused by the degradation of the passivation layer around the rebar when the steel is exposed.

A two-stage crack formation process is identified by the no-slip and slip theories. Under low steel stress the bond stresses (section 2.4.1) are not overcome and cracking will remain in the cover depth. This explains the observations of Fantilli in section 2.2.2, where crack widths at the surface does not always indicate the rebar surface is exposed. This is the no-slip period.

Therefore, the appearance of cracks regardless of width on the tension surface does not imply that loss of service life will follow. Surface cracking that will cause corrosion, ultimately leading to loss of service life (Figure 2-15), must have the following characteristics:

- Extend the full cover depth to the rebar surface.
- Open pathway in the concrete matrix to a slip surface where the steel is exposed.

When these scenarios exist, alkalis can reach the steel surface resulting in depassivation and corrosion initiation. Reduced design life results from corrosion propagation. Corrosion initiated locally will only grow to harmful levels when oxygen can move over the length of the rebar surface. The rate of corrosion propagation depends on the following:

- Time taken for alkali's and chlorides to reach the reinforcement – accelerated by crack width and depth.
- Freedom of movement of oxygen in the matrix over the rebar length - accelerated by concrete permeability.

Cracks appearing on a concrete surface is only detrimental to service life when the following exists simultaneously:

- The cracks extend to the rebar surface – this occurs when steel stress is high enough to overcome the bond stresses resulting in slip.
- Microcracking occurs in the concrete around the rebar increasing permeability – this occurs under increasing steel stress. Microcracking also increases when larger bars are used.

Since the British and ACI codes calculate crack widths midway between the tension steel (sections 3.1.1 and 3.4.1), the crack width here is directly related to rebar spacing. As established previously, bond failure is not considered a significant contributing factor by these models. Wide cracks calculated by these codes would then therefore not necessarily indicate harmful rebar exposure or service life loss. Cracks calculated by these codes should not be used in design for durability. These codes are more relevant where leakage is to be avoided.

Durability design requires limiting crack widths in the region of the rebar, therefore the bond slip models of Eurocode and Fib are more applicable. The limiting of crack width on its own by onerous application of these methods does also not guarantee limiting corrosion propagation. Due to shear deformability, a wider crack width can exist with deeper cover. However, this does not indicate the conditions exists for corrosion propagation over the length of the rebar. For a wide crack to contribute to reduced service life, the tension steel between adjacent cracks need a degree of exposure. This exposure occurs when the concrete between cracks is damaged through microcracking and breakage from high steel strains (section 2.2.3).

Therefore, the important factors to limit crack width for service life design in reinforced concrete are the following:

- Limiting tensile rebar stress
- Good quality concrete around rebar.

8. CONCLUSION

Crack width determination using the analytical methods in the design codes provide a convenient method of estimation. The use of elastic beam theory versus fracture mechanics methods is an efficient approach. In large reinforced concrete members, numerical methods should be used as these can include the influence of the size effect. The amount of flaws present impacts the crack and cannot be ignored in larger concrete members. It is not acceptable in large members to only consider the concrete in tension as in the analytical formulations.

The analytical models in design codes can be grouped by the way fundamental theory is applied. The most suited applications can thereby be derived. The no-slip models of the British standard and American codes are more suited for designing for water tightness than reducing service corrosion. Their formulas ignore the reinforcement ratio $\frac{\emptyset}{\rho}$, thus ignoring the bond effect, and estimate its impact by applying a conservative factor to shear deformation.

The European codes are more suited for durability design as bond slip is modelled by accounting for all the factors in the fundamental Ferry-Borges formula. Bond slip is indicative of service life adequacy.

The British standards are more reliable for shallow beam members. In deeper members, the results become unreliable. Narrower bar spacings are important in British and ACI standards as wider bar spacings will give more conservative crack width estimates. Additionally, the BS5400 is more suited for use in higher stressed members, below the maximum of 0,87 fy tension stress. The results are unreliable under low stress.

The Fib model is unreliable under low stress as the values determined do not correlate with crack theory. The spike in the trend line between crack formation and propagation stages, gives less confidence in the results.

The Eurocode appears the most reliable model over those examined in this report. Its consideration of slip and non-slips as well as its consideration for bar stress type means it allows for all variables from fundamental crack theory. Direct comparison of the values obtained by the Eurocode and British code models is not advisable as the codes apply to different regions on the concrete tension face.

The conversion to Eurocode from British standards is recommended for crack width design as serviceability design is more reliable in the Eurocode model. The simplification by the British standard formulas results in an inaccurate estimate of the type of crack that would cause concrete degradation. The standard only considers cracks between the tension rebar; it is therefore largely affected by bar spacing. A crack estimated by this model is not above the

rebar where the steel surface is exposed. The Eurocode model estimates the bond slip directly. The crack is the type that will likely lead to corrosion propagation as the steel is directly exposed.

9. BIBLIOGRAPHY

ACI committee 224, 2001. *Control of cracking in concrete structures: ACI224-R01 ,* s.l.: American concrete institute.

ACI318, Committee, 2014. *Building code requirements for structural concrete ACI318-14.* Farmington hills: American concrete institute.

Addis, B., 2004. *Fundamentals of concrete.* 3 ed. Midrand: Cement and concrete institute.

Alam, S. Y., Lenormand, T., Loukili, A. & Regoin, J. P., 2010. Measuring crack width and spacing in reinforced concrete members. *Fracture mechanics of concrete and concrete structures*, 23-28 May, pp. 377-382.

Alexander, M., 2014. *Concrete: Constituent materials and properties lecture notes distributed in Structural concrete properties and practice CIV5002Z at the University of Cape Town.* Rondebosch , on 17 March 2014.

Allam, S. M., Shoukry, M. S., Rashad, G. E. & Hassan, A. S., 2012. Crack width evaluation for flexural RC members. *Alexandria engineering journal,* Volume 51, pp. 211-220.

Allen, A. H., 1988. *Reinforced concrete design to BS8110: Simply explained.* New York: E & FN Spon.

Balazs, G. L. e. a., 2013. Design for SLS according to fib Model code 2010. *Structural concrete 14,* Issue 2.

Bangash, M., 2001. *Manual of numerical methods in concrete.* London: Thomas Telford.

Bažant, Z. P., 2002. Concrete fracture models: testing & practice. *Engineering fracture mechanics,* 69(2), pp. 165-205.

Bazant, Z. P. & Planas, J., 1997. *Fracture and size effect in concrete and other quasibrittle materials.* s.l.:CRC Press.

Beeby, A. W., 1979. The prediction of crack widths in hardened concrete. *The Structural Engineer,* 57A(1), pp. 9-17.

Beeby, A. W. & Narayanan, R. S., 2005. *Designers guide to Eurocode 2: Design of concrete structures.* London: ICE publishing.

Borosnyoi, A. & Balazs, L. G., 2005. Models for flexural cracking in concrete: the state of the art. *Structural concrete,* 6(2), pp. 53-62.

Borosnyoi, A. & Snobli, I., 2010. Crack width variation within the concrete cover of reinforced concrete members. *Building materials,* 62(3), pp. 70-74.

Carino, N. J. & Clifton, J. R., 1995. *Prediction of cracking in reinforced concrete structures,* Gathersburg: NIST BFRI.

Carreira, D. J. & Chu, K.-H., 1986. Stress-strain relationship for reinforced concrete in tension. *ACI Journal,* 83(1), pp. 21-28.

Clark, L. A., 1983. *Concrete bridge design to BS5400.* New York: Construction Press.

Darwin, D., Manning, D. G. & Hognestad, E., 1985. Debate: Crack width, cover and corrosion. *Concrete International,* 7(5), pp. 20-35.

EC for Standardization, 2005. *EN 1992-1-1 Eurocode 2: Design of concrete structures- Part 1-1 General rules and rules for buildings.* Brussels: CEN.

El-Sayed, K. M. et al., 1998. *Influence of aggregate shape on the fracture behaviour of concrete.* Freiburg, AEDIFICATIO Publishers.

Fantilli, A., Vallini, P. & Mihashi, H., 2007. *Crack widths in reinforced cement-based structures.* Italy, Taylor & Francis.

Faye, P. N., Ye, Y. & Diao, B., 2017. Bond effects between concrete and steel bars using different diameter bars and different initial crack width. *Advances in Civil Engineering.*

Francois, D., 1991. Microcracking and damage in concrete. In: S. P. Shah, ed. *Toughening Mechanisms in Quasi-brittle materials.* Rotterdam: Springer, pp. 53-65.

Frosch, R. J., 2014. *Fundamentals of crack control in reinforced concrete.* [Online] Available at: http://www.concretebridgeviews.com/i77/Article1.php [Accessed 3 February 2018].

Glucklich, J., 1968. *Proceedings of international conference on the structure of concrete.* Slough, Cement and concrete association.

Goto, Y. & Otsuka, K., 1971. Studies on internal cracks formed in concrete around deformed tension bars. *ACI Journal,* 68(4), pp. 244-251.

Gribniak, V. et al., 2016. Effect of arrangement of tensile reinforcement on flexural stiffness and cracking. *Engineering structures,* Volume 124, pp. 418-428.

Han, D., Keuser, M., Zhao, X. & Langer, B., 2011. *Influence of Transverse Reinforcing Bar Spacing on flexural crack spacing on reinforced concrete.* s.l., Elsevier.

Hassanzadeh, M., 1998. *The influence of the type of coarse aggregates on the fracture mechanical properties of high strength concrete.* Freiburg, Germany, AEDIFICATO Publishers.

Hertzberg, R. W., 1996. *Deformation and fracture mechanics of engineering materials.* 4th ed. New York: Wiley.

Holly, I. & Bilcik, J., 2013. *The effects of reinforcement corrosion on bond behaviour.* s.l., Elsevier.

Hughes, B. P., 1976. *Limit state theory for reinforced concrete design.* 2nd ed. London: Pitman Publishing Ltd.

Ingraffea, A., Gerstle, W., Gergely, P. & Saouma, V., 1984. Fracture mechanics of bond in reinforced concrete. *Journal of structural engineering,* 110(4), pp. 871-890.

Jokubaitis, V., Juknevicius, L. & Salna, R., 2013. *Conditions for failure of normal sections in flexural reinforced concrete beams of rectangular cross-section.* s.l., Elsevier.

Kaklauskas, G., 2017. Crack model for reinforced concrete members based on compatibility of stress-transfer and mean strain approaches. *Journal of structural engineering,* 143(9).

Karihaloo, B. L. & Huang, X., 1991. Tensile response of quasi-brittle materials. *Pure and applied geophysics,* 137(4), p. 461–487.

Kruger, E., 2018. EC2 Crack width calculation method. course handout, Liquid retaining structures, Stellenbosch University, delivered 13 April 2018.

Lapi, M., Orlando, M. & Spinelli, P., 2018. A review of literature and code formulations for cracking in reinforced concrete members. *Structural concrete,* pp. 1-23.

Lawn, B. R. & Wilshaw, T. R., 1975. *Fracture of brittle solids.* London: Cambridge University Press.

Leonhardt, F., 1988. Cracks and crack control in concrete structures. *PCI Journal,* 33(4), pp. 124-145.

Mahran, U. M., 2013. Theoretical Study for Bond between reinforcement steel and concrete. *International Journal of Sciences: Basic and Applied Research (IJSBAR),* 12(1), pp. 93-102.

Maleque, M. A. & Salit, M. S., 2013. *Materials selection and design.* Singapore: Springer.

McCormac, J. C. & Brown, R. H., 2009. *Design of reinforced concrete.* 8th ed. New Jersey: John Wiley and Sons Inc..

Mehta, P. & Monteiro, P., 2014. *Concrete: Microstructure, properties and materials.* 4th ed. New York: McGraw Hill Education.

Mier, J. G., 1997. *Fracture processes of concrete.* Boca Raton, Florida: CRC Press.

Mindness, S., Young, F. J. & Darwin, D., 2003. *Concrete.* 2nd ed. New Jersey: Prentice Hall, Pearson Education, Inc.

Mosley, B., Bungey, J. & Hulse, R., 2012. *Reinforced concrete design to Eurocode 2.* 7 ed. s.l.:Palgrave & Macmillan.

Mosley, W. H. & Bungey, J. H., 1990. *Reinforced concrete design.* 4 ed. London: Macmillan.

Neville, A. M., 1997. Aggregate bond and modulus of elasticity. *ACI materials journal,* 94(1), pp. 71-74.

NG, P., Lam, J. & Kwan, A., 2011. *Effects of Concrete-to-Reinforcement Bond and Loading Conditions on Tension Stiffening.* Hong Kong, Elsevier.

Owens, G. & Fulton, F. S., 2009. *Fulton's concrete technology.* 9th ed. Midrand: Cement & Concrete Institute.

Parton, V. Z. & Morozov, E. M., 1989. *Mechanics of elastic-plastic fracture.* 2nd ed. New York: Hemisphere Publishing Corporation.

Pinder, G. F. & Herrera, I., 2012. *Mathematical modeling in science and engineering.* Hoboken, New Jersey: John Wiley & Sons.

Regan, P. E. & Yu, C. W., 1973. *Limit state design of structural concrete.* London: Chatto and Windus.

Reynolds, C. E., Steedman, J. C. & Threlfall, A. J., 2008. *Reynolds reinforced concrete designer's handbook.* 11 ed. Boca Raton: Taylor and Francis.

Sagues, A. A. & Kranc, S. C., 2001. *Corrosion forecasting for 75-year durability design of reinforced concrete,* Tallahassee: Florida department of transportation.

Schiessl, P. & Raupach, M., 1997. Laboratory Studies and Calculations on the Influence of Crack Width on Chloride-Induced Corrosion of Steel in Concrete. *ACI Materials journal,* 94(1), pp. 56-61.

Shaikh, F., 2018. Effect of Cracking on Corrosion of Steel in Concrete. *International Journal of Concrete Structures and Materials.*

Shi, Z., 2009. *Crack analysis in structural concrete.* 1st ed. Burlington,MA: Elsevier Ltd.

Tasdemir, M. A. & Karihaloo, B. L., 2001. Effect of type and volume fraction of aggregate on the fracture properties of concrete. In: D. B. e. al, ed. *Fracture Mechanics of concrete structures.* Cardiff: Swets & Zeitlinger, pp. 123-129.

Teo, T. J., Yang, G. & Chen, I.-M., 2014. Compliant Manipulators. In: A. Nee, ed. *Handbook of Manufacturing Engineering and Technology.* s.l.:Springer, pp. 1-64.

University of South Florida, Tampa; Florida Department of Transportation; Federal Highway Administration, 2001. *Corrosion forecasting for 75 year durability design of reinforced concrete,* Springfield, VA: National technical information service.

Velten, K., 2009. *Mathematical Modeling and Simulation.* Weinheim: Wiley-VCH.

Wescott, A., 2010. Eurocodes: The new British standards for structural design. *Proceedings of the Institution of Civil Engineers - Civil Engineering,* 163(1), pp. 9-9.

Wittmann, F. H., 1983. *Fracture Mechanics of Concrete.* Amsterdam: New York: Elsevier Science Publishers.

Xu, L., Nie, X., Zhou, M. & Tao, M., 2017. Whole-process crack width prediction of reinforced concrete structures considering bonding deterioration. *Engineering structures,* Volume 142, pp. 240-254.

Yamato, N., Nakai, H. & Kanakubo, T., 2008. *Prediction method of crack width and spacing in reinforced concrete based on bond analysis.* Beijing, s.n.

Young, J. F., Mindness, S., Gray, R. J. & Bentur, A., 1998. *The science and technology of engineering materials.* New Jersey: Prentice-Hall.

10. APPENDICES

10.1 Table of crack width formulas in concrete design codes

PROPERTY	BS8110/ BS8007	BS5400	ACI 318	Eurocode 2	Fib MC2010
Crack spacing	$\frac{3a_{cr}}{1+\frac{2(a_{cr}-c_{min})}{(h-x)}}$	$\frac{3a_{cr}}{1+\frac{2(a_{cr}-c_{nom})}{(h-d_c)}}$	$2\sqrt{(d_c)^2+\left(\frac{s}{2}\right)^2}$	$3.4c+0.425k_1k_2 \text{ x } \frac{\phi}{\rho_{p,eff}}$	$kc+\frac{1}{4} \text{ x } \frac{f_{ctm}}{\tau_{bms}} \text{ x } \frac{\emptyset_s}{\rho_{s,ef}}$
	a_{cr} = distance to bar from point on surface c_{min}/c_{nom} = cover to tension steel h = overall member depth; d = effective depth x/d_c = depth of neutral axis		d_c = distance from concrete face to centroid of rebar s = rebar spacing	k_1 = Rebar bond k_2 = Stress (bending/tension) c = cover $\rho_{p,eff}=\frac{A_s}{A_{c,eff}}$	f_{ctm} = concrete tension τ_{bms} = bond stress k = cover factor c = cover $\rho_{s,ef}=\frac{A_s}{A_{c,eff}}$
Effective tension strain	$\epsilon_1-\frac{b_t(h-x)(\alpha'-x)}{3E_sA_s(d-x)}$	$\epsilon_1-\left[\frac{3.8b_th(a'-d_c)}{\epsilon_sA_s(h-d_c)}\right] \text{ x } \left[\left(1-\frac{M_q}{M_g}\right)10^{-9}\right]$	$\frac{f_s}{E_s}\beta$ f_s = strain in rebar E_s = E value steel β = factor transferring strain at rebar to concrete surface	$\frac{\sigma_s-k_t\frac{f_{ct,eff}}{\rho_{p,eff}}(1+\alpha_e\rho_{p,eff})}{E_s}$ $\geq 0.6\frac{\sigma_s}{E_s}$ k_t = load duration factor $f_{ct,eff}$ = concrete tension E_s = E value steel σ_s = rebar stress at crack	$\frac{\sigma_s-\beta\,\sigma_{sr}}{E_s}-\eta_r\,\epsilon_{sh}$ σ_s = rebar stress at crack at crack formation E_s = E value steel η_r = shrinkage factor ϵ_{sh} = free shrinkage strain β = load duration factor σ_{sr} = max rebar stress at crack for crack formation
	b_t = width of section at centroid of steel α' = distance from compression edge to crack E_s = E value steel ϵ_s = Elastic strain in rebar ignoring stiffening effects M_q = Live service moment M_g = Dead service moment				

10.2 Fundamental Analytical slip equations

The crack width is obtained by simplifying the bond slip relationship where an average value of bond stress τ_b is adopted. This is illustrated in Figure 10-1.

By using the average distribution of bond stress, the transfer length becomes the following expression:

$$l_{tr} = \frac{\emptyset \, f_{ctm}}{4 \, \tau_b \, \rho_{,ef}}$$

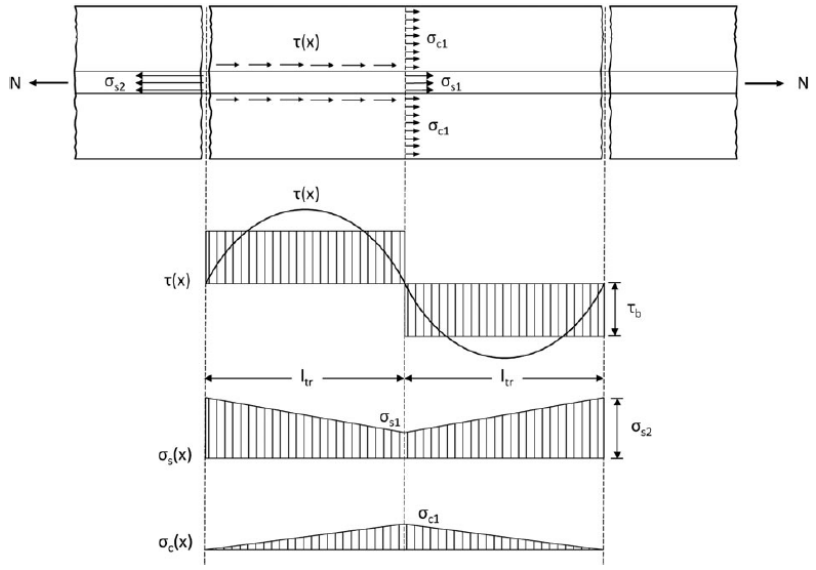

Figure 10-1: Actual and assumed stress distributions accounting for the tension stiffening effect in stabilised cracking phase (Lapi, et al., 2018)

The last formula corresponds to the value provided by Fib Model Code 2010, without the contribution of concrete cover. The transfer length (l_{tr}) is the minimum distance between two consecutive cracks (s_{min}). The maximum crack spacing that could be reached during the cracked phase is equal to twice the transfer length.

$$s_{max} = 2 \, l_{tr} = \frac{\emptyset \, f_{ctm}}{2 \, \tau_b \, \rho_{,ef}}$$

The combination of the integral defining slip and the crack width formula obtained from the substitution of the value $x = l_{tr}$ and considering the equation, the maximum crack width becomes:

$$w_{max} = 2 \, s\left({}^{s_{max}}/_{2}\right) = 2 \int_0^x [\, \epsilon_s(x) - \, \epsilon_c(x)] dx$$

Ignoring the concrete contribution:

$$w_{max} = s_{max}\frac{\sigma_{s2} + \sigma_{s1}}{2E_s} = s_{max}\frac{2\sigma_{s2} + \Delta\sigma_s}{2E_s} = s_{max}\left(\epsilon_{s2} - \frac{\Delta\sigma_s}{2E_s}\right)$$

Through the substitution of $\sigma_{c1} = f_{ct}$ this equation becomes:

$$w_{max} = s_{max}\left(\epsilon_{s2} - \frac{f_{ct}}{2\rho_{ef}E_s}\right) = \frac{\emptyset\, f_{ctm}}{2\,\tau_b\,\rho_{,ef}}\left(\epsilon_{s2} - \frac{f_{ct}}{2\rho_{ef}E_s}\right)$$

The semi-analytical models on which the formulas for crack width determination are based in concrete design codes is like this equation.

10.3 Expressions of basic elastic beam theory

Derivation	Description
Relationships from similar triangles: $\varepsilon_{st}/\varepsilon_{cc} = (d - d_n)/d_n$	$\varepsilon_{st} =$ *the tensile strain in the steel* $\varepsilon_{cc} =$ *maximum compressive strain in concrete* $d =$ *eff depth of the rebar measured from max compression level* $d_n =$ *the depth of the neutral axis measured from* ε_{cc} *level*
Relationships from similar triangles: $f_{st} = E_s\varepsilon_{st} = \boldsymbol{\alpha_e \times f_{ct}}$ Only true under strain compatibility at a given height.	From the basis of compatibility of strain over section height: $\boldsymbol{\varepsilon_{st}}$ ***strain in steel in tension*** $=$ $\boldsymbol{\varepsilon_{ct}}$ ***strain in concrete in tension*** Under this theorem the modular ratio is valid: $\boldsymbol{modular\ ratio\ \alpha_e = \frac{f_{st}}{f_{ct}} = \frac{E_s}{E_c}}$
$f_{st}/f_{cc} = E_s\varepsilon_{st}/E_c\varepsilon_{cc} = \alpha_e(d - d_n)/d_n$	Hooke's law applicable and the strain profile applied.
The assumption of strain compatibility permits the following derivations:	
• $F_c = ½\ f_{cc}bd_n$ • $F_s = f_{st}A_{st} = f_{st}\rho bd$	Resultant compressive and tensile forces in the section for a constant beam width. ρ *the steel ratio* $= A_{st}/bd$
• $F_s = F_c$: • $f_{st}\rho bd = ½\ f_{cc}bd_n$ • $f_{st}/f_{cc} = d_n/2\rho d$	According to equilibrium of the section, the following equations are possible.
• $\alpha_e(d - d_n)/d_n = d_n/2\rho d$ • $(d_n/d)^2 + 2\alpha_e\rho\, d_n/d - 2\alpha_e\rho = 0$	Based on the triangular profiles 2 expressions for f_{st}/f_{cc} are obtained. Equating these provides a quadratic equation, solved through the standard equation: $ax^2 + bx + c$ *where* $x = \frac{-b \pm \sqrt{b^2 - 4ac}}{2a}$
• $d_n/d = -\alpha_e\rho \pm \sqrt{[(\alpha_e\rho)^2 + 2\alpha_e\rho]}$ *where the value of* d_n/d *can only be positive.* • $d_n/d = \left[\sqrt{(1 + 2/\alpha_e\rho)} - 1\right]\alpha_e\rho$	